DESIGN AND DEVELOPMENT OF POLYPEPTIDE MATERIALS DERIVED FROM *N*-CARBOXYANHYDRIDE POLYMERIZATIONS: FROM FUNDAMENTAL INVESTIGATIONS TO NANOMEDICAL APPLICATIONS

A Dissertation

by

JINGWEI FAN

Submitted to the Office of Graduate and Professional Studies of
Texas A&M University
in partial fulfillment of the requirements for the degree of

DOCTOR OF PHILOSOPHY

Chair of Committee,	Karen L. Wooley
Committee Members,	Marcetta Y. Darensbourg
	Lei Fang
	Hung-Jue Sue
Head of Department,	Simon W. North

August 2016

Major Subject: Chemistry

ABSTRACT

Recent decades have witnessed extensive utilization of polypeptide materials in nanomedical applications, such as serving as scaffolds for tissue engineering, matrices for drug and gene delivery, and responsive materials for biosensors, owing to their innate biocompatibility and biodegradability, multiple functionalities and precisely-defined nano- and micro-structures. This dissertation highlights the rational design and development of polypeptide-based materials for simple and easily-controlled preparations toward nanomedical applications, including full characterization studies of the compositions, structures and properties.

With attractive applications in nanomedicine, such as drug and gene delivery systems, polypeptides with well-defined structures are mainly synthesized from controlled *N*-carboxyanhydride (NCA) polymerizations, which can serve to construct polypeptides with versatile functionalities and various molecular topologies, as well as to facilitate investigations of structure-property relationships within polypeptide materials. Therefore, in the first study, a straightforward and readily-adoptable approach to synthesize polypeptides, with controllable polymerization rates, targetable molecular weights and narrow molecular weight distributions, was developed by applying continuous N_2 flow over the reaction mixture during NCA polymerizations. With the establishment of this facile synthetic method, a polypeptide-based versatile and functional nanoparticle platform with reactive and charged functionalities was synthesized from a sequential NCA polymerization and chemical transformation strategy,

and the cationic nanoparticle was further investigated as a gene delivery carrier by electrostatic complexation. In addition to linear polymers, well-defined molecular brushes bearing polypeptides as side chains were constructed *via* a "grafting through" synthetic strategy with two-dimensional control over the brush molecular architectures by integrating NCA polymerizations and ring-opening metathesis polymerizations (ROMPs) to build polypeptide side chains and brush backbones with desirable segment lengths, independently and respectively, in controlled manners. Also, the simple copolymerization of NCAs was utilized to generate copolypeptides having a combination of α-helix and β-sheet secondary structures, which could be controlled by varying the feedstock selections of NCA monomers during polymerization, and were capable of driving mechano-responsive supramolecular gel-to-gel and gel-to-sol transitions reversibly. The revealed structure-property relationships between polymer compositions, supramolecular structures and stimuli-responsive properties, were further applied to construct a polypeptide-based hydrogel system with multi-responsive properties from the statistical copolymerization of various NCA monomers, allowing for control over the release profile of encapsulated naproxen for local delivery.

DEDICATION

To my father, mother and wife

ACKNOWLEDGEMENTS

I would first like to thank my Ph.D. advisor, Professor Karen L. Wooley, for her invaluable support, guidance, advice, patience, and trust throughout my graduate study at Texas A&M University. For the past five years, I have learnt from her not only tremendous knowledge of science and technology, but also, more important, her passion, diligence, and dedication for science and research. She provided me with the freedom to explore the fields of polymer science and nanotechnology, and also gave me helpful advice and suggestion to improve my technique, knowledge and research. She is not only an outstanding advisor in my graduate study, but also a good friend with incredible understanding, support and trust in my daily life, especially when I had family-related issues. I was extremely fortunate to be one of her students, and was able to grow into an independent researcher, presenter and collaborator with critical thinking. Without her, I would not have been able to accomplish what I have accomplished today, and she will always be my great mentor and friend.

I would also like to thank my committee members, Professor Tadhg P. Begley, Professor Marcetta Y. Darensbourg, Professor Lei Fang, and Professor Hung-Jue Sue for their time, support, guidance and advice throughout the course of this research.

The major work of this dissertation was conducted in collaboration with external collaborators. Therefore, I would like to thank all my collaborators who have contributed to this work, including Dr. Steven L. Brody, Dr. John-Stephen A. Taylor and Dr. Archana Parameswar at Washington University in St. Louis, Dr. Darrin J. Pochan,

Dr. Jiahua Zhu and Dr. Yingchao Chen at the University of Delaware, Mr. Peng Liu, Dr. Hung-Jue Sue, Dr. Tadhg P. Begley, Ms. Yanyan Wang and Dr. Donald J. Darensbourg at Texas A&M University.

Within the Wooley group, I would like to recognize Dr. Jiong Zou for his mentorship, advice and guidance in my research and I have learned many useful research skills and techniques from this talented scientist. I also want to acknowledge Mr. Xun He and Mr. Tan Nguyen, who not only helped me in my research, but also taught me how to be a mentor. I would also like to thank all the past and present members of the Wooley group, Dr. Yannick Borguet, Dr. Yingchao Chen, Dr. Sangho Cho, Ms. Corrie Clark, Mr. Daniel Dobbins, Ms. Mei Dong, Dr. Andrew Dove, Ms. Sussana Elkassih, Dr. Mahmoud F. A. Elsabahy, Ms. Simcha E. Felder, Ms. Jeniree A. Flores, Dr. Marco Giles, Ms. Amelia Gonzales, Dr. Tiffany P. Gustafson, Dr. Gyu Seong Heo, Ms. Jesscia Huang, Mrs. Jennifer Imbesi, Dr. Philip Imbesi, Dr. Ashley Jahnke, Ms. Nari Kang, Ms. Sarosh Khan, Mr. Christopher Komatsu, Ms. Samantha Kristufek, Mr. Tyler Kristufek, Mr. Eric Leonhardt, Dr. Ang Li, Mr. Richen Li, Dr. Soon-Mi Lim, Dr. Young H. Lim, Mr. Yen-Nan Lin, Dr. Yun Lin, Dr. Lauren Link, Mr. Alexander Lonnecker, Ms. Casey McDonald, Mr. Andy Moutray, Dr. Koichiro Mikami, Ms. Audrey Nelson, Dr. Amandine Noel, Dr. Adriana Pavia-Sanders, Dr. Kevin A. Pollack, Mrs. Stephanie Flores Pollack, Mr. Kenton Rauwerdink, Dr. Jeffery E. Raymond, Mr. Joel Russell, Dr. Sandani Samarajeewa, Dr. Kellie Seetho, Dr. Ritu Shrestha, Mr. Justin Smolen, Ms. Yue Song, Mr. Matthew Svach, Dr. Lu Su, Dr. Guorong Sun, Ms. Judy Taylor, Ms. Tara Thompson, Mr. Yi-Yun Tsao, Ms. Ginny Vance, Ms. Mariela Vasquez, Mr. Eric Vavra,

Ms. Brook Versaw, Mr. Kevin Wacker, Ms. Sarah Ward, Mr. Hai Wang, Mrs. Danielle P. Wolf, Mr. Ryan Zentay, Dr. Fuwu Zhang, Dr. Shiyi Zhang, Mrs. Jennifer S. Zigmond, for being such great peers and making the lab environment so enjoyable to be in.

Lastly, I would like to thank my parents, my wife and my parents-in-law for their continued support for my graduate research. Especially, I thank my wife for her understanding, support, patience, trust, and love and I appreciate her standing by my side whatever happens for this incredible journey.

For Chapter II, I gratefully acknowledge financial support from the National Heart Lung and Blood Institute of the National Institutes of Health as a Program of Excellence in Nanotechnology (HHSN268201000046C) and the National Science Foundation under Grant DMR-1105304. The Welch Foundation is gratefully acknowledged for support through the W. T. Doherty-Welch Chair in Chemistry, Grant A-0001.

For Chapter III, I would like to thank Professor Tadhg P. Begley at Texas A&M University for access to the circular dichroism spectrometer. This work is financially supported in part from the National Lung and Blood Institute of the National Institutes of Health as a Program of Excellence in Nanotechnology (HHSN268201000046C), the National Science Foundation (DMR-1105304), and the Welch Foundation through the W. T. Doherty-Welch Chain in Chemistry (Grant no. A-0001). The microscopy & imaging center (MIC) at Texas A&M University is also gratefully acknowledged.

For Chapter IV, I would like to gratefully acknowledge financial support from the National Heart Lung and Blood Institute of the National Institutes of Health as a

Program of Excellence in Nanotechnology (HHSN268201000046C) and the National Science Foundation (DMR-1309724 and DMR-1507429). The Welch Foundation is gratefully acknowledged for support through the W. T. Doherty-Welch Chair in Chemistry, Grant no. A-0001.

For Chapter V, I would like to gratefully acknowledge financial support from the National Heart Lung and Blood Institute of the National Institutes of Health as a Program of Excellence in Nanotechnology (HHSN268201000046C) and the National Science Foundation under grant number DMR-1150304. The Welch Foundation is gratefully acknowledged for support through the W. T. Doherty-Welch Chair in Chemistry, Grant no. A-0001. The microscopy & imaging center (MIC) at Texas A&M University is also gratefully acknowledged.

For Chapter VI, I would like to thank Professor Tadhg P. Begley at Texas A&M University for access to the circular dichroism spectrometer. I would like to gratefully acknowledge Professor Hung-Jue Sue at Texas A&M University for instrumentation necessary for mechanical property characterizations. This work is financially supported from the National Lung and Blood Institute of the National Institutes of Health as a Program of Excellence in Nanotechnology (HHSN268201000046C), the National Science Foundation (DMR-1105304, DMR-1309724, and DMR-1507429), and the Welch Foundation through the W. T. Doherty-Welch Chain in Chemistry (Grant no. A-0001). The microscopy & imaging center (MIC) at Texas A&M University is also gratefully acknowledged.

NOMENCLATURE

AAMMA	Accelerated amine mechanism through monomer activation
AMM	Activated monomer mechanism
ATR-FTIR	Attenuated total reflectance-Fourier transform infrared spectroscopy
BLA	γ-Benzyl-L-aspartate
BLG	γ-Benzyl-L-glutamate
[bdmim][BF_4]	1-Butyl-2,3-dimethylimidazolium tetrafluoroborate
[bmim][BF_4]	1-Butyl-3-methylimidazolium tetrafluoroborate
CD	Circular dichroism
$CDCl_3$	Deuterated chloroform
CD_3OD	Deuterated methanol
CGC	Critical gelation concentration
CMC	Critical micelle concentration
COD	1,5-Cyclooctadiene
COX	Cyclooxygenase
DCM	Dichloromethane
DIC	Differential imaging contrast
DLS	Dynamic light scattering
DMA	Dynamic mechanical analysis
DMEM	Dulbecco's modified eagle medium

DMF	*N,N*-Dimethylformamide
DMPA	2,2-Dimethoxy-2-phenylacetophenone
DMSO	Dimethyl sulfoxide
D_2O	Deuterated oxide
DP_n	Degree of polymerization
DSC	Differential scanning calorimetry
EDC	1-Ethyl-3-(3-dimethylaminopropyl) carbodiimide
EDTA	Ethylenediaminetetraacetic acid
EVE	Ethyl vinyl ether
GPC	Gel permeation chromatography
HVT	High vacuum technology
LMWG	Low-molecular-weight gelator
LSCM	Laser scanning confocal microscopy
M_n	Number-average molecular weight
M_w	Weight-average molecular weight
MW	Molecular weight
MWCO	Molecular weight cutoff
MWD	Molecular weight distribution
NACE	Non-aqueous capillary electrophoresis
NAM	Normal amine mechanism
NB	Norbornene
NCA	*N*-Carboxyanhydride

NMR	Nuclear magnetic resonance spectroscopy
Npx	Naproxen
NSAID	Nonsteroidal anti-inflammatory drug
N-TMS	*N*-Trimethylsilyl
OVCAR-3	Human ovarian adenocarcinoma
PBS	Phosphate buffered saline
PDI	Polydispersity index
PEG	Poly(ethylene glycol)
PEO	Poly(ethylene oxide)
PLG	γ-Propargyl-L-glutamate
PS	Polystyrene
PTA	Phosphotungstic acid
RNAi	Ribonucleic acid interference
ROMP	Ring-opening metathesis polymerization
ROP	Ring-opening polymerization
SEM	Scanning electron microscopy
siRNA	Small interfering ribonucleic acid
SPPS	Solid-phase peptide synthesis
TEM	Transmission electron microscopy
TFA	Trifluoroacetic acid
TFA-D	Deuterated trifluoroacetic acid
T_g	Glass transition temperature

TGA	Thermogravimetric analysis
T_{gel}	Critical gelation temperature
THF	Tetrahydrofuran
TMS-CBM	Trimethylsilyl carbamate
UV	Ultraviolet
WAXS	Wide-angle X-ray scattering

TABLE OF CONTENTS

Page

LIST OF FIGURES

Page

LIST OF TABLES

CHAPTER I

INTRODUCTION

1.1 Polypeptides for nanomedical applications

In the last decades, nanomedicine has emerged as a rapidly growing field and attracted increasing attention from both academia and industry. The main target of nanomedicine is the development of therapeutics and diagnostics with the utilization of nanostructured materials for the diagnosis, treatment and prevention of disease, including drug and gene delivery system, tissue engineering, disease diagnosis and biosensor system.[1-3] Together with these promising applications of nanomedicine, there are several requirements for the materials to be used in nanomedical fields, such as biocompatibility and biodegradability, multiple functionalities and precisely-defined nanostructures.[2,3] Polypeptides consisting of α-amino acids linked covalently, share significant similarities to natural proteins and possess great potential in the nanomedical applications, resulting from the fulfillment of these requirements from their structural characteristics (Figure 1.1).[4-8]

First, the backbones of polypeptide materials are comprised of natural or synthetic α-amino acids, thus innate biocompatibility and biodegradability are expected. With the peptide linkages similar to the chemical structures of natural proteins, low or even no cytotoxicity was observed for polypeptide materials acting as therapeutic delivery systems from over two hundred publications since 2011, of which a dozen has

conducted *in vivo* evaluations.[9-15] Especially, polypeptide-based hydrogels have been extensively investigated to demonstrate the capability of polypeptides to be degraded by certain types of enzymes in both *in vitro* and *in vivo* experiments.[16-19] In addition, the enzymatic degradation of polypeptides has been utilized as the key-sensing component in the design of biosensor for the detection of specific and targeted enzyme with the concentration of enzyme down to μM-scale.[20]

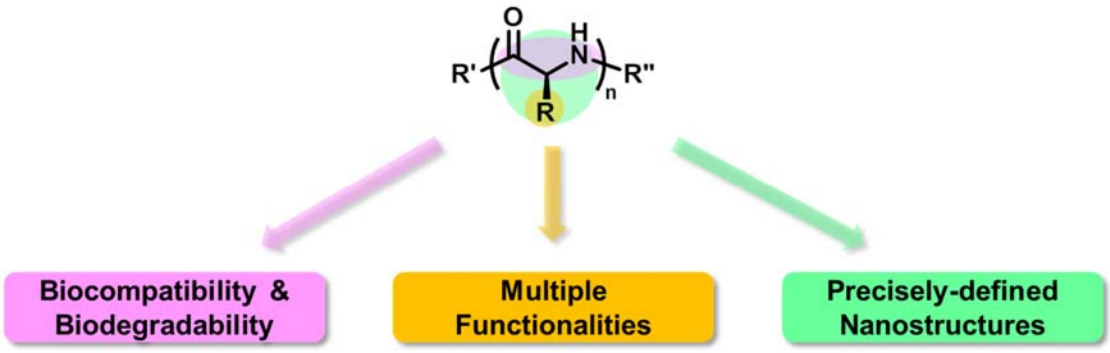

Figure 1.1. Structural characteristics of polypeptides for nanomedical applications.

Second, the side chains of natural or synthetic amino acids can render polypeptides with multiple functionalities with functional groups. Since the mid-1950s, numerous research efforts have been focused on the development of functional polypeptides by expanding the side chain functionalities from natural proteinaceous amino acids, such as hydroxyl, carboxyl, thiol, and amino groups, to synthetic amino acids with more elaborate synthetic schemes, including alkenyl, alkynyl and azido groups *et al.*, which have been widely used to conjugate small molecular drugs, polymers, proteins, peptides, oligosaccharides, polysaccharides, and oligonucleotides

onto polypeptides for broad nanomedical applications.[21-23] With the expectation to mimic protein functions and interact with biological systems, modifications to polypeptides *via* the functional groups of amino acid side chains have been found to affect both functional as well as conformational properties of polypeptides. For example, the hydrophilicity of polypeptides can be largely adjusted by conjugating hydrophilic moieties onto part or whole of side chain functional groups, enabling polypeptides to construct nanosized assemblies with different morphologies, including spheres, rods, fibrils and toroids.[9,22-25]

Third, the backbones of polypeptides, together with the side chains of amino acids can construct well-defined secondary structures, including α-helix and β-sheet, which are difficult to obtain from non-polypeptide-materials.[4,5,7] Especially, due to the significant role of α-helical and β-sheet structures in the formation of three-dimensional protein structures and the regulation of numerous biological activities, their presence in polypeptide-based materials is an attractive property, which can allow polypeptides to further impact biological activities, such as cell adhesion and penetration efficiency.[26-29] For instance, the stabilized helical structure was reported to enhance the delivery efficiency, when polypeptides acted as gene delivery carrier, by triggering pore formation in the cell membrane providing an extra pathway for carried gene to diffuse into the target cell, resulting in the improvement of gene delivery efficiency.[30-32]

1.2 Polypeptides from *N*-carboxyanhydride (NCA) polymerizations

With attractive and promising applications in nanomedicine, polypeptides are

mainly synthesized by protein biosynthesis, solid-phase peptide synthesis (SPPS), and amino acid NCA polymerization. In comparison with conventional protein biosynthesis and SPPS, the ring-opening polymerization (ROP) of NCAs is a more economical and practical synthetic approach for the preparation of polypeptides and peptide hybrid polymeric materials, especially for the synthesis of polypeptides having over 100 repeat units,[7,21,33-36] since the first reports of NCA by Leuchs and co-workers in 1906.[37-39] NCA ROP can be initiated by a range of nucleophiles and bases. Depending on the initiators used in the polymerization, two widely accepted pathways of NCA polymerizations are "normal amine mechanism" (NAM) and "activated monomer mechanism" (AMM) (Figure 1.2).[7,34] In NAM, the polymerization is generally initiated by nonionic initiators, which exhibit more nucleophilicity than basicity, such as primary amines, alcohols and water. During the polymerization, the initiator acts as the nucleophile to attack the carbonyl group at 5-C to open the ring structure of the NCA monomer. After the release of CO_2, the reproduced amine chain end will continue to serve as a nucleophile to attack the carbonyl group of another NCA monomer to propagate the polymer growth. In contrast, AMM involves the initiator acting as a base rather than as a nucleophile, which deprotonates the nitrogen (3-N) in the NCA monomer, resulting in the formation of a corresponding anion. This anion then acts as a nucleophile to attack the carbonyl group at 5-C of another NCA monomer, leading to ring-opening and further chain propagation in the same manner as in NAM. Due to the relatively slower initiation step in comparison with the propagation in AMM, polymerizations following the AMM pathway commonly yield less-controlled and

ill-defined polypeptides.[34] Of course, these two mechanistic treatments are at extremes, with all processes involving equilibria and each in competition.

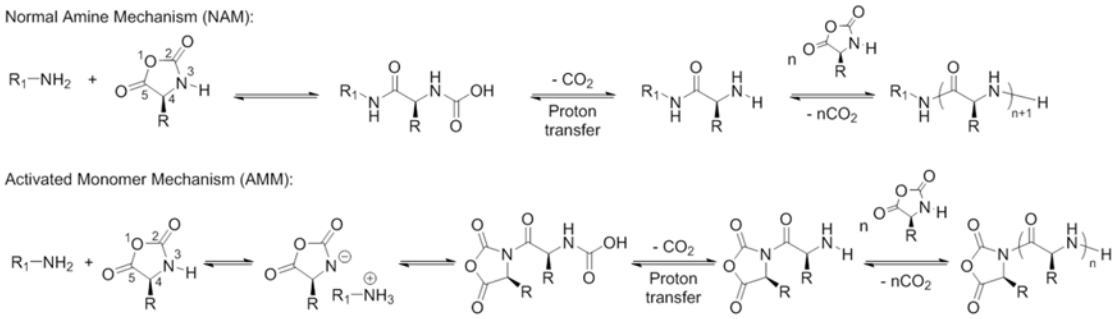

Figure 1.2. NAM and AMM pathways for ring-opening polymerizations of NCAs.

Due to the coexistence of these two polymerization pathways during NCA ROPs, it is often problematic to synthesize high molecular weight polypeptides with controlled structures and varied architectures. Over the past century, significant advances have been made toward NCA ROPs to synthesize well-defined polypeptides, by preventing or at least limiting the AMM pathway during polymerization.[7,40] The AMM pathway can be suppressed by optimization of experimental techniques and reaction conditions while maintaining the utilization of primary amines as initiators (Figure 1.3).[7,41-45] These approaches are attractive because many primary amine initiators are commercially available, and there is no need for the use and removal of catalyst. In 2004, the Hadjichristidis group applied high vacuum technique (HVT) to purify NCA monomers and conduct polymerizations with intermittent removal of CO_2 generated during the reaction.[46] Detailed study of the kinetics indicated rapid and controlled polymerization *via* NAM with efficient inhibition of AMM. The controlled living polymerization under

high vacuum was also confirmed by Messman and co-workers.[47] In 2004, Vayaboury *et al*. reported another innovative approach to eliminate side reactions by systematically studying hexylamine-initiated polymerizations of N^{ε}-trifluoroacetyl-L-lysine NCA as a function of temperature.[48] By lowering the reaction temperature from 20 to 0 °C, the living amine chain-ends increased dramatically from 22% to 99%, which were analyzed by a combination of gel permeation chromatography (GPC) and non-aqueous capillary electrophoresis (NACE). In order to overcome the drawback of long polymerization time at low temperature, the Heise group investigated NCA ROPs of various NCA monomers by combining high vacuum and low temperature techniques, which not only promoted the polymerizations in a controlled manner, but also significantly shortened the polymerization times.[49]

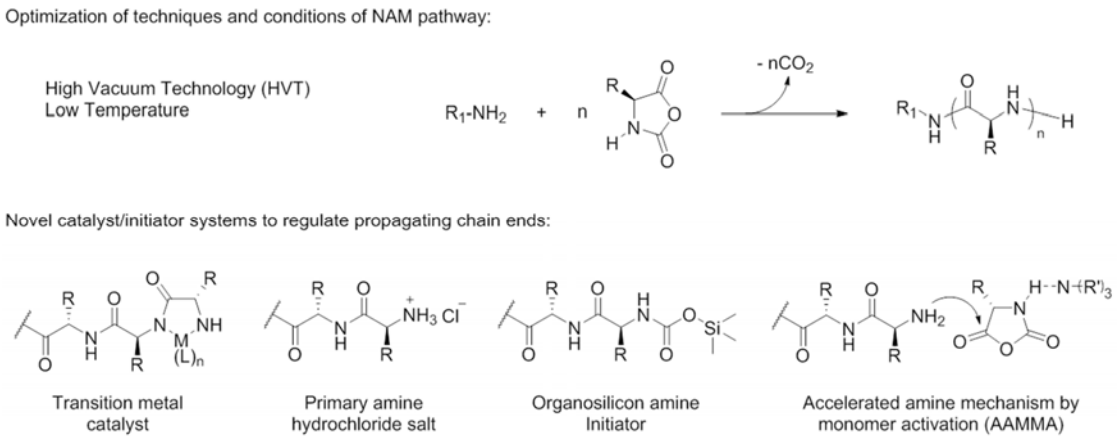

Figure 1.3. Recent advances for controlled ring-opening polymerizations of NCAs, including optimization of techniques and conditions and development of novel catalyst/initiator system.

In addition to the optimization of experimental techniques and reaction conditions, several novel catalyst and initiator systems for regulating propagating chain ends have been developed in the past *ca.* two decades (Figure 1.3).[7,41] In 1997, Deming reported the first living polymerization of NCA monomers by employing transition metal complexes as active species to undergo oxidative addition with NCA monomers, preventing deprotonation of the NCA nitrogen.[50,51] By using zerovalent nickel and cobalt initiators (*i.e.*, $(PMe_3)_4Co$, and bpyNi(COD), where bpy = 2,2'-bipyridine and COD = 1,5-cyclooctadiene), high molecular weight polypeptides with well-defined homo-, di-, tri- and multiblock architectures were obtained. In 2003, another living NCA ROP was reported by using a primary amine hydrochloride salt as the initiator.[52] The primary amine hydrochloride significantly decreased the basicity of the initiator and inhibited the AMM pathway.[53] However, the nucleophilicity of free amines was also reduced in the formation of the hydrochloride salts, resulting in long polymerization times. In 2007, Cheng's group reported organosilicon-mediated living NCA polymerization *via* a group transfer mechanism.[54] This novel initiator significantly reduced polymerization times and afforded precise control over polypeptide structures, resulting from unexpected formation of trimethylsilyl carbamate (TMS-CBM) end groups in both initiation and propagation steps. In a later work, other *N*-trimethylsilyl (N-TMS) amine-based initiators were also developed to introduce functional groups for further modification while maintaining the living features of NCA ROPs.[55,56] Most recently, Zhao *et al*. developed a fast and living NCA polymerization methodology by the incorporation of both primary and secondary or tertiary amines into one initiation

system through an "accelerated amine mechanism through monomer activation" (AAMMA).[57,58] Instead of competition between polymerizations initiated from diverse amines, the secondary or tertiary amines were found to activate NCA monomers *via* hydrogen-bonding to facilitate the initiation and propagation steps of primary amine-initiated polymerizations, resulting in well-defined polypeptides.

1.3 Polypeptide-based organo- and hydrogels

Polypeptide-based organogel and hydrogel systems are of great interest toward nanomedical applications, such as scaffolds for tissue engineering, matrices for controlled therapeutic release and responsive materials for biosensor, due to their innate biocompatibility and biodegradability, versatile functionalities and unique ordered conformations, especially after NCA ROP has emerged as a practical synthetic approach to prepare well-defined polypeptides to facilitate the investigation of the mechanism of sol-gel behaviors.[59-63] Driven by inter- and intramolecular hydrogen-bonding interactions, polypeptides can supramolecularly assemble into nanofibril and/or nanoribbon structures with one-dimensional stacking of polymers or polymer aggregations, including α-helical and β-sheet secondary structures.[19,51,64-67] Stimuli-triggered construction of the nanostructures in polypeptide materials, or change of the conformations between secondary structures, would result in gel formation. Due to the nano- and/or microphase separation derived from supramolecular assembly of polypeptides, a delicate solvophilic-solvophobic balance should be achieved in polypeptide-based gels. Interactions that are strong enough to break this balance would cause either gel breaking into viscous liquid or polymer precipitation.

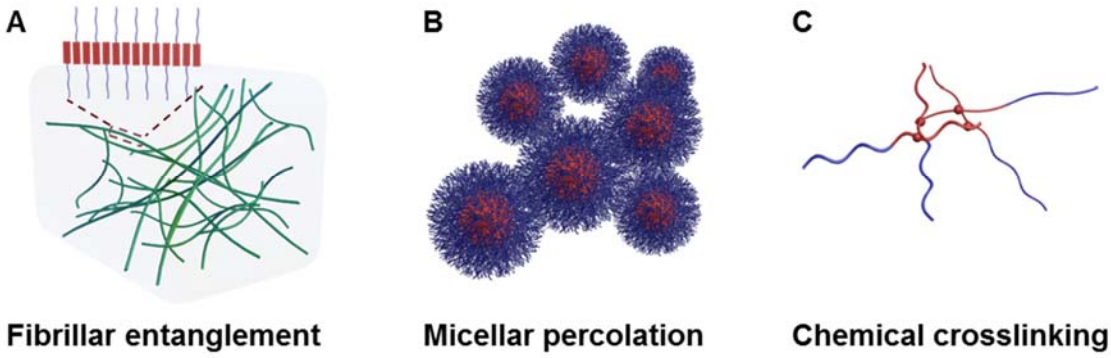

Figure 1.4. Schematic illustrations of polypeptide gelation *via* fibrillar entanglement (a), micellar percolation (b) and chemical crosslinking (c). Adapted from ref. 62. Copyright 2016 Wiley-VCH.

For polypeptide-based gelators that contain at least one polypeptide block segment, secondary structures are considered as one of the remarkable driving forces for gelation. In order to construct supramolecularly assembled gels, the alignment of secondary structures, including α-helixes and β-sheets, into one- dimensional nanofibril or nanoribbon structures have been investigated widely, together with incorporation of another block segment, commonly adopting random coil conformations, to increase the solubility of supramolecular assemblies and balance the solvophilic-solvophobic interactions (Figure 1.4a).[64,66,67] Owing to the significant roles of secondary structures in the gelation process of polypeptide-based materials, the gelation property can be readily tuned by control over the secondary structures *via* structural modifications, such as tuning of stereochemistry of polypeptides, varying block lengths of solvophilic and solvophobic segments, and introducing other moieties that are capable of hydrogen-bonding or other supramolecular interactions into the gelation systems. In the

range of the suitable solvophilic-solvophobic balance, longer solvophobic segments would induce stronger interactions in the nano- and/or microphase domains, which enhanced the gel-forming ability and gel strength.[68,69]

In the last decade, several groups have reported reverse thermal gelation from poly(ethylene glycol) (PEG)-*block*-polypeptide diblock copolymers, which underwent a thermally-induced sol-to-gel transition with an increase of the temperature.[16,17,19,65,70,71] Depending on the secondary structures formed in the polypeptide segment domains, two gelation mechanisms were proposed for this reverse thermal gelation. For polypeptides with β-sheets dominating the secondary structure populations, the polypeptide block segments assembled supramolecularly into nanofibril or nanoribbon structures from one-dimensional stacking of polypeptides, while PEG possessed random coil conformations in aqueous solution.[16,17] With an increase of temperature, dehydration of PEG altered the hydrophilic-hydrophobic balance toward the hydrophobic direction. At the same time, the hydrophobic core was stabilized by strengthening the secondary structures from the polypeptides due to a smaller packing distance from the shrinking of PEG. Also, dehydration of the PEG block upon an increase of the temperature enhanced the physical crosslinking between the hydrophobic domains *via* stronger hydrophobic interactions. On the other side, for polymers with more α-helical components in the polypeptide domains, micellar structures were often observed for amphiphilic block copolymers, in which the polypeptides assembled into the core and PEG constructed the shell domain.[65,72] With an increase of the temperature, dehydration of the PEG enhanced the hydrophobic interactions, and led to aggregation and close packing of micelles for

the creation of percolating gel networks (Figure 1.4b).[73,74] In addition to the above mechanisms that relate to the formation of physically-crosslinked nanofibirl/nanoribbons or aggregated micelles, chemical crosslinkings between functional side chains of polypeptides can also enable gel formation (Figure 1.4c).

1.4 Scope of the thesis

This dissertation is focused on the design and development of polypeptide-based materials derived from NCA polymerizations with emphases on fundamental investigations and nanomedical applications, starting with the development of synthetic methodology for well-defined polypeptides (Chapter II). Then this facile synthetic method was expanded to install functionalities onto diblock copolypeptides for gene delivery application (Chapter III), to construct complex molecular brushes bearing polypeptides as the brush side chains (Chapter IV), and to exert structural control and explore the structure-property relationships in polypeptide-based gel systems (Chapter V). After obtaining an understanding of the gel systems with responsive properties, the structure-property relationships were further utilized to guide the design of controlled release hydrogel for local drug delivery (Chapter VI).

In Chapter II, we investigated a straightforward and readily-adoptable synthetic methodology to prepare polypeptides, with controllable polymerization rates, targetable molecular weights and narrow molecular weight distributions, by applying continuous N_2 flow over the reaction mixture during NCA polymerizations. Detailed kinetic studies revealed that N_2 flow can efficiently remove CO_2 from the reaction system to decarboxylate the carbamic acid intermediate and generate active amine termini for

further chain propagation. This approach is attractive because most of the primary amine initiators are commercially available and there is no need for removal of a catalyst after polymerization, which diminishes potential toxicity issues that may arise in the use of synthetic polypeptide materials for nanomedical applications. With enhanced polymerization rates (6 h *vs* 72 h from traditional method) and controlled features, this economic and easily-operational method can be expanded to build diblock copolypeptides, install chain-end functionalities, and exert structural control for polypeptide materials.

With this facile synthetic approach, in Chapter III, a polypeptide-based versatile and functional nanoparticle platform with reactive, positively- or negatively-charged functionalities was developed from a sequential NCA polymerization and chemical transformation strategy, and the cationic nanoparticle was further investigated as a gene delivery carrier by electrostatic complexation. A facile and straightforward one-pot sequential ROP with accelerated polymerization rate by N_2 flow was applied to synthesize well-defined diblock copolypeptide, poly(γ-benzyl-L-glutamate)-*block*-poly(γ-propargyl-L-glutamate) (PBLG-*b*-PPLG), with the incorporation of the alkyl functional groups allowing for rapid and efficient thiol-yne click-type modifications. Globular nanoparticles were achieved from the self-assembly of the resulting amphiphilic block copolypeptides with helical conformations of polypeptide backbones and distinct surface charges. Minimum cytotoxicity and complete binding efficiency of the obtained cationic nanoparticle to complex small interfering ribonucleic acid (siRNA), together with high efficient cellular uptake of the delivery complex, were demonstrated

in both RAW 264.7 mouse macrophages and human ovarian adenocarcinoma (OVCAR-3) cells. However, low transfection efficiency was observed in OVCAR-3 cells, which drove us to explore polypeptides with more complex molecular topologies to serve as nucleic acids transfection systems for enhanced efficiency.

Driven by the motivation to improve the transfection efficiency of polypeptide-based gene delivery systems, as well as to advance the synthetic methodology for polypeptide materials, we further conducted the investigation to construct polypeptides with more complex molecular topologies. In Chapter IV, well-defined molecular brushes bearing polypeptides as side chains were prepared by a "grafting through" synthetic strategy with two-dimensional control over the brush molecular architectures. By integrating NCA ROPs and ring-opening metathesis polymerizations (ROMPs), desirable segment lengths of polypeptide side chains and brush backbones could be constructed in controlled manners, independently and respectively. A new type of brush-like polymer, poly(norbornene-*graft*-poly(β-benzyl-L-aspartate)) (P(NB-*g*-PBLA)), was synthesized *via* the ROMP of norbornene-terminated polypeptide macromonomers in a mixture of dichloromethane and ionic liquid. The N_2 flow accelerated NCA ROP was utilized to prepare polypeptide macromonomers with different lengths by using norbornene-based primary amine as the initiator. Highly efficient post-polymerization modifications were achieved by aminolyses of PBLA side chains to facilitate installment of functional moieties onto the molecular brushes.

In Chapter V, the simple copolymerization of NCA monomers was utilized to generate copolypeptides having a combination of α-helix and β-sheet secondary structures, which were capable of driving mechano-responsive supramolecular gel-to-gel and gel-to-sol transitions reversibly, which also allowed for injection-based processing and self-healing behaviors. These copolypeptides exhibited tunable secondary structures and resulted in sonication stimulus responsiveness of the organogels with the polypeptide segment variation, controlled by varying the ratio of NCA monomers during the copolymerizations. The supramolecular assembly of β-sheets into nanofibrils constructed the three-dimensional networks within *N,N*-dimethylformamide (DMF). The presence of α-helical components in the copolypeptides enhanced the stability of organogels against sonication, and instantaneous gel-to-gel transitions were observed as *in situ* reconstruction of networks occured within the gelled materials. In marked contrast, the β-sheet-rich gel, exhibited an instant gel-to-sol transition after sonication was applied. The injectability and self-healing capabilities were demonstrated by direct observation of the macroscopic self-healing behavior experiment. These results illustrate the influence of secondary structures on supramolecular assembly of hybrid diblock synthetic polypeptides in the gel state and demonstrate a novel, facile approach to fabricate nanostructures with stimuli-responsive properties.

Based on the structure-properties relationships between polymer compositions, supramolecular structures and stimuli-responsive properties, in Chapter VI, a polypeptide-based hydrogel system, when prepared from a diblock copolymer with polypeptide as one block, exhibited thermo-, mechano- and enzyme-responsive

properties, which were capable to tune the release of Npx from the hydrogel in a controlled manner. With the dominant component of β-sheet secondary structures within the polypeptide segments, this system demonstrated heat-induced sol-to-gel behavior, resulting from supramolecular assembly of β-sheets into nanofibrils for gel formation, and sonication-triggered gel-to-sol transition, which was expected from the structure-property relationships established in organogel systems. Certain enzymes could accelerate the breakdown of the hydrogel by investigating *in vitro* gel weight loss profile. Naproxen (Npx) was loaded in the sol state and entrapped within the hydrogel in the gel state, facilitating this hydrogel as a promising controlled release system for injection-based local delivery of Npx, resulting from the maintenance of sonication-triggered gel-to-sol transition after Npx loaded.

CHAPTER II

A FACILE GLOVEBOX-FREE STRATEGY TO SIGNIFICANTLY ACCELERATE THE SYNTHESES OF WELL-DEFINED POLYPEPTIDES BY *N*-CARBOXYANHYDRIDE RING-OPENING POLYMERIZATIONS[*]

2.1 Introduction

Synthetic polypeptides consisting of α-amino acids linked covalently have significant similarities to natural materials, which have facilitated their utilization extensively in biomedical areas, such as serving as scaffolds for tissue engineering, matrices for drug and gene delivery, and responsive materials for biosensors, and also in technological applications, due to their liquid crystalline characteristics and other properties.[59,75,76] Moreover, their origination from renewable feedstocks and potential biodegradability make polypeptides important materials for environmental purposes. There has been increasing interest, therefore, in developing efficient routes to synthesize well-defined polypeptides. Although Leuchs and coworkers synthesized the first examples of α-amino acid *N*-carboxyanhydrides (NCAs) in 1906,[37-39] significant advances in the concepts of polymer structures and analytical techniques for their characterization were needed before NCA ring-opening polymerization (ROP) emerged as a synthetically straightforward methodology to construct polypeptide materials.[33-35,77]

---

[*] Reprinted (adapted) with permission from "A facile glovebox-free strategy to significantly accelerate the syntheses of well-defined polypeptides by *N*-carboxyanhydride (NCA) ring-opening polymerizations" by Zou J.;[†] Fan, J.;[†] He, X.; Zhang, S.; Wang, H.; Wooley, K. L., *Macromolecules* **2013**, *46*, 4223-4226 ([†]J. Z. and J. F. contributed equally). Copyright 2013 American Chemical Society.

Over the past century,[78] significant advances have been made toward NCA ROPs, with the greatest achievements being realized over only the past *ca.* two decades, to synthesize polypeptides with controlled structures and varied architectures.[49,54,77,79] However, much remains to be understood about the reaction conditions to achieve rapid and reproducible production of well-defined polypeptide materials of controlled degrees of polymerization and sequence.

In the past decade, several groups have developed strategies to achieve well-defined polypeptides with high molecular weights (MWs) and narrow molecular weight distributions (MWDs) by using NCA ROP. For instance, Deming and coworkers developed transition metal complexes as active species to control the addition of NCA monomers and eliminate side reactions in NCA polymerization.[50] Schlaad and coworkers reported primary amine hydrochloride initiated NCA polymerizations, which avoided the formation of NCA anions and inhibited the activated monomer mechanism (AMM) of polymerization.[52] In 2004, the Hadjichristidis group applied high vacuum techniques (HVTs) to purify NCA monomers and conduct polymerizations with intermittent removal of CO_2 generated during the reaction, and effectively promote polymerization *via* the normal amine mechanism (NAM).[46] The controlled living polymerization under high vacuum was also confirmed by Messman and coworkers.[47] Recently, Cheng's group reported organosilicon reagent-mediated living NCA polymerization, which allows for the syntheses of homo, block and brush polypeptides with predictable MWs and narrow MWDs.[55] However, there is still plenty of

opportunity to develop improved methods to achieve efficient and convenient preparation of polypeptides by NCA ROP.

Herein, a straightforward method to enhance the polymerization rate while maintaining the living features of the polymerization by simply using N_2 flow during the NCA ROP was developed. Although the influence of CO_2 in NCA ROP was studied fifty years ago, when it was observed that the immediate removal of CO_2 affected the kinetics of polymerization,[80] the "livingness" of the NCA ROP with removal of CO_2 from the reaction was not demonstrated. With the great impact that polypeptides have been experiencing recently, we chose to re-investigate the influence of CO_2 removal, confirm the advantages of N_2 flow method, and confirm the living characteristics for NCA ROPs by employing γ-benzyl-L-glutamate (BLG) NCA, as a well-studied monomer, and *n*-hexylamine as initiator. Compared to the methods for the preparation of polypeptides from NCAs using primary amines as initiators without catalyst activation, our method had several advantages: 1) promoted polymerization rates, to allow NCA conversions to reach >95% in a matter of hours rather than the multiple day time period that is required typically; 2) glovebox-free operation in a normal fume hood, to increase the convenience, decrease the time and allow for greater variation of the reaction conditions, for instance the temperature; 3) control over the polymerization rate by altering the flow rate of N_2; 4) maintenance of the living features of NCA ROP even at high conversions and high monomer to initiator feed ratios.

2.2 Experimental section

2.2.1 Materials

N,N-Dimethylformamide (DMF, anhydrous, > 99.8%), diethyl ether, dichloromethane (DCM), tetrahydrofuran (THF), *n*-hexane, ethyl acetate, magnesium sulfate ($MgSO_4$, anhydrous, ≥ 99.5%), γ-benzyl-L-glutamate, *n*-hexylamine and bis(trichloromethyl) carbonate were purchased from Sigma-Aldrich company (USA). All other chemicals were used without further purification, unless otherwise noted.

2.2.2 Instrumentation

^{1}H and ^{13}C NMR spectra were recorded on Varian Inova 300 MHz or Varian Mercury 300 MHz spectrometers interfaced to a UNIX computer using VnmrJ software. Chemical shifts were referenced to solvent resonance signals. Attenuated total reflectance-Fourier transform infrared spectroscopy (ATR-FTIR) spectra were recorded on an IR Prestige 21 system (Shimadzu Corp., Japan) and analyzed using IRsolution v. 1.40 software.

N,N-Dimethylformamide-based gel permeation chromatography (DMF GPC) was conducted on a Waters Chromatography, Inc. (Milford, MA) system equipped with an isocratic pump model 1515, a differential refractometer model 2414 and a two-column set of Styragel HR 4 and HR 4E 5 mm DMF 7.8 x 300 mm columns. The system was equilibrated at 70 °C in pre-filtered DMF containing 0.05 M LiBr, which served as polymer solvent and eluent (flow rate set to 1.00 mL/min). Polymer solutions were prepared at concentrations of *ca.* 3 mg/mL and an injection volume of 0.2 mL was used. Data collection and analysis was performed with Empower Pro software. The

system was calibrated with poly(ethylene glycol) (PEG) standards (Polymer Laboratories, Amherst, MA) ranging from 615 to 442,800 Da.

Glass transition temperatures (T_g) were measured by differential scanning calorimetry (DSC) on a Mettler-Toledo DSC822® (Mettler-Toledo, Inc., Columbus, OH), with a heating rate of 10 °C/min. Measurements were analyzed using Mettler-Toledo STAR^e v. 7.01 software. The T_g was taken as the midpoint of the inflection tangent, upon the second heating scan. Thermogravimetric analysis (TGA) was performed under Argon atmosphere using a Mettler-Toledo model TGA/SDTA851^e, with a heating rate of 5 °C/min. Measurements were analyzed by using Mettler-Toledo STAR^e v. 7.01 software.

The control experiments were conducted in the glovebox of SG1200/750TS model, produced by Vigor Gas Purification Technologies Inc. Box pressure was stabilized at 2.70 mbar Argon (> 99%). Oxygen and moisture were lower than 3 ppm. Temperature was stabilized between 28.3 °C and 28.6 °C.

2.2.3 Experimental procedures

Synthesis of γ-benzyl-L-glutamate *N*-carboxyanhydride (BLG NCA) monomer

In a 500 mL three-necked round bottom flask equipped with a magnetic stirrer, condenser and nitrogen inlet, BLG NCA monomer was synthesized from γ-benzyl-L-glutamate (10 g, 42 mmol, 3 equiv) and bis(trichloromethyl) carbonate (4.2 g, 14 mmol, 1 equiv) in 300 mL dry ethyl acetate at 65 °C under N_2 for 4 hours.[81] After cooling to 5 °C, the crude product was extracted with 100 mL 5 °C nanopure water and 100 mL 5 °C 0.5 wt % bicarbonate solution, respectively. The organic layer was dried over $MgSO_4$,

filtrated and concentrated. The resulted solid was further purified by three times recrystallization with ethyl acetate/*n*-hexane 1:1 (v/v), and dried in vacuum to obtain a white crystal (2.6 g, yield: 70%). The product was stored in -20 °C freezer under N_2 atmosphere. ^{1}H NMR (300 MHz, DMSO, ppm): δ 1.99 (m, 2H, C*H*$_2$CH$_2$COOCH$_2$), 2.52 (t, 2H, CH$_2$C*H*$_2$COOCH$_2$), 4.47 (m, 1H, COC*H*NH), 5.10 (s, 2H, COOC*H*$_2$), 7.37 (m, 5H, Ar*H*), 9.10 (br, 1H, COCHN*H*). ^{13}C NMR (75 MHz, DMSO, ppm): δ 26.4, 29.1, 56.2, 65.7, 128.0, 128.1, 128.4, 136.0, 151.9, 171.3, 171.7. FTIR (cm^{-1}): 3331, 3251, 2931, 1859, 1773, 1703, 1250, 1185, 1112, 930. HRMS: calculated [M-H]$^-$ for $C_{13}H_{13}NO_5$: 262.0715, found: 262.0710.

General procedure for the polymerization of BLG NCA

In a 10 mL flame dried Schlenk flask equipped with a magnetic stir bar, BLG NCA (250 mg, 0.960 mmol) was dissolved in dry DMF (5.0 mL). *n*-Hexylamine (0.48 mg, 0.0048 mmol) in a stock solution (40 μL, 0.12 mmol/mL) was added directly into the monomer solution and was stirred under continuous N_2 flow (250 mL/min). The Schlenk flask was capped with a rubber stopper with a needle outlet connected to a tube filled with drying agent. The reaction mixture was stirred at room temperature with a stir rate of 340 rpm, and aliquots were collected by syringe for determination of NCA concentration by measuring the intensity of the NCA anhydride peak at 1788 cm^{-1} using ATR-FTIR. The conversion of NCA monomer was determined by comparing the NCA concentration in the reaction with the initial NCA concentration. All the kinetics studies were conducted at least twice and standard derivations were less than 0.05 for each study. The detailed characterization of one typical polymer, poly(γ-benzyl-L-glutamate)$_{47}$

(PBLG$_{47}$), was conducted. ^{1}H NMR (300 MHz, TFA-D, ppm): δ 0.79 (s, C*H*$_3$CH$_2$CH$_2$), 1.75-2.25 (br, CHC*H*$_2$CH$_2$), 2.28-2.70 (s, br, CH$_2$C*H*$_2$CO), 4.50-4.80 (br, COC*H*NH), 4.90-5.20 (br, COOC*H*$_2$), 7.11-7.27 (br, Ar*H*). ^{13}C NMR (75 MHz, TFA-D, ppm): δ 26.6, 29.8, 53.2, 68.4, 127.9, 128.3, 128.5, 134.1, 173.3, 175.8. FTIR (cm^{-1}): 3292, 3034, 2953, 1728, 1649, 1545, 1452, 1389, 1252, 1121, 966, 741, 694. DSC: T_g = 20 °C. TGA in Argon: 25-280 °C: 0% mass loss, 280-360 °C: 70 % mass loss, 360-500 °C: 8 % mass loss, 22 % mass remaining above 500 °C.

2.3 Results and discussions

The primary amine-initiated *N*-carboxyanhydride (NCA) ring-opening polymerization (ROP) without catalyst is one of the most studied strategies to synthesize polypeptides. By using *n*-hexylamine initiator, the NCA ROP follows the normal amine mechanism (NAM) (Figure 2.1). The primary amine attacks the 5-C=O of the NCA monomer, leading to opening of the ring and proton transfer to form a carbamic acid intermediate. Decarboxylation of the carbamic acid generates a free amino group, which continues to serve as a nucleophile for chain propagation. The loss of CO_2 from the carbamic acid is the rate determining step in NAM, therefore, with the efficient removal of CO_2 from the reaction mixture, the decarboxylation of the carbamic acid continuously shifts the equilibrium to generate active amine for further chain propagation and, thus, first order kinetics are observed.[82,83] However, without removal of CO_2, the carbamic acid dominates and the formation of carbamic acid salt is favored (as shown in Figure 2.1), which reduces the nucleophilicity of the active polymer chain end and presents

different polymerization kinetics.[80,84,85] The polymerization usually requires days to reach high conversion, and in order to minimize potential side reactions induced by water and other impurities, glovebox techniques have been used widely during the process of polymerization to achieve well-defined polypeptides with narrow molecular weight distributions (MWDs).[86] If only freeze-pump-thaw operation is performed to remove water and air, and the polymerization is conducted under sealed conditions, very long reaction times (even one week) are needed and polymers are obtained with relatively broad MWDs. High vacuum techniques can promote the polymerization by removal of the CO_2 during the reaction and produce polypeptides with predictable molecular weights (MWs) and narrow MWDs. However, the polymerizations must be conducted in specially-designed equipment, to avoid loss of monomer, initiator, and solvent, which may experience difficulties with scale up.

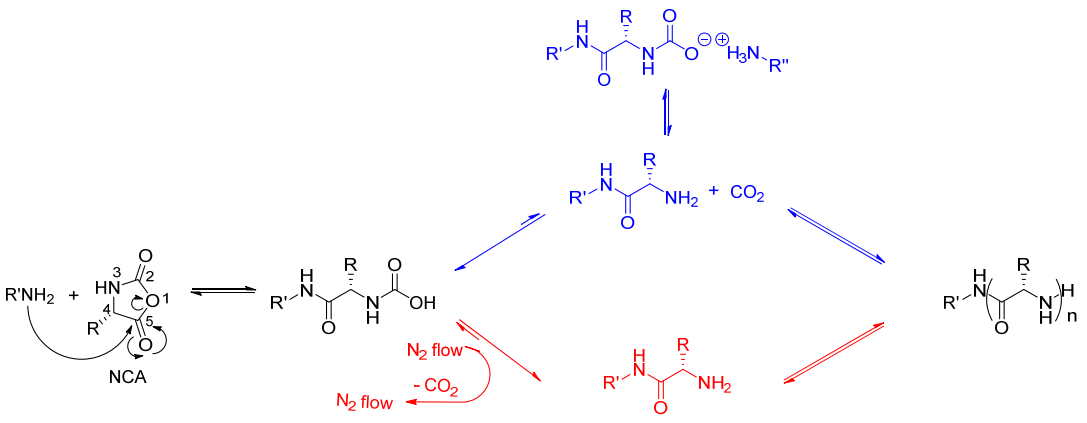

Figure 2.1. NCA ROP under N_2 flow *via* NAM.

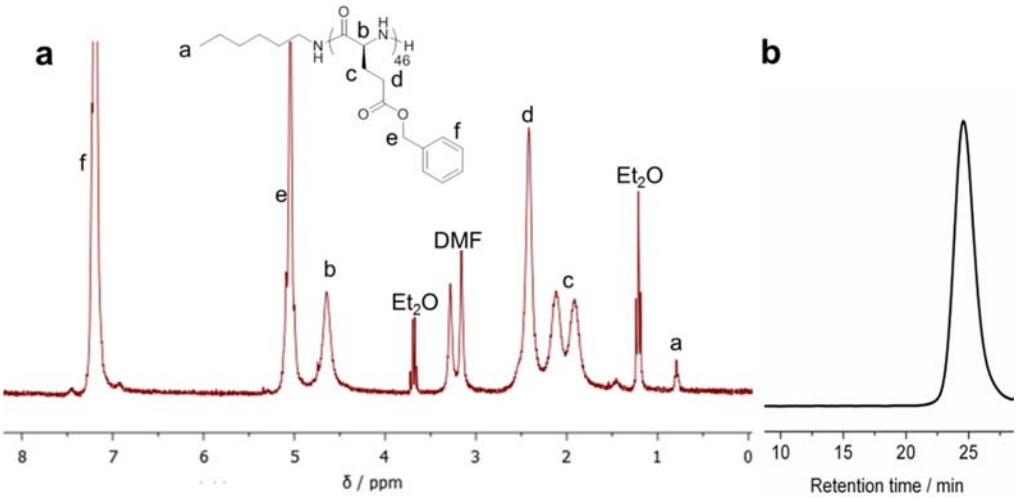

Figure 2.2. (a) ^{1}H NMR spectrum and (b) GPC trace of PBLG$_{46}$.

Fortuitously, it was observed that N_2 flow during the γ-benzyl-L-glutamate (BLG) NCA ROP greatly promoted the polymerization rate, presumably by facilitating the removal of CO_2, so that this effect was explored further. Amino acids were recently reported to behave as efficient CO_2 capture materials *via* the formation of carbamic acids with 1 : 1 stoichiometry of amino acid : CO_2. The highly efficient binding of CO_2 to a variety of amino acids to form stable carbamic acids was confirmed by FTIR, ^{1}H NMR and ^{13}C NMR spectroscopies.[87] It was also reported that the carbamic acids could be efficiently decarboxylated by simply bubbling N_2 through the solution at 40 °C.[87] We, therefore, investigated in detail the effects of N_2 flow during the BLG NCA ROP, by introducing various rates of N_2 flow during the polymerization to alter the efficiency of CO_2 removal from the carbamic acid intermediate and further shift the equilibrium to form active amines on the propagating polymer chain ends. In a general experiment, the polymerization of BLG NCA monomer (recrystallized 3 times from ethyl

acetate/*n*-hexane, 250 mg, 50 eq) was initiated by *n*-hexylamine in dry DMF and allowed to proceed, using standard Schlenk techniques, in which the Schlenk flask was capped with a rubber stopper with a needle outlet connected to a tube filled with drying agent. During an initial polymerization attempt, monitoring of the reaction by attenuated total reflectance-Fourier transform infrared spectroscopy (ATR-FTIR) indicated that the conversion was complete within a few hours, although we had expected much slower progression of the polymerization. Therefore, after only 4 h, the reaction mixture was precipitated into 80 mL dry diethyl ether and a white solid product of poly(γ-benzyl-L-glutamate) (PBLG) was obtained, following centrifugation and drying in vacuum. Gel permeation chromatography (GPC) characterization indicated that the PBLG was well-defined, having a PDI = 1.10 and M_n = 12.0 kDa (Figure 2.2). The degree of polymerization determined by ^{1}H NMR spectroscopy, by comparing the integration values of the terminal methyl protons of the *n*-hexylamido α-chain terminus (0.79 ppm) and the benzyl methylene protons of the repeat units (5.1 ppm) was determined to be 46, which is in agreement with the GPC result. Based upon this finding of relatively rapid polymerization to obtain uniform PBLG material, further experiments to probe the polymerization kinetics and the effects of N_2 flow were performed.

In order to understand how the N_2 flow affected the polymerization rate, the kinetics of NCA ROP were investigated. The typical kinetic study of *n*-hexylamine-initiated BLG NCA ROP was conducted in a 25 mL flame-dried Schlenk flask, the feed ratio of BLG NCA : initiator (I) was fixed at 100 : 1. The initial monomer concentration was 50 mg/mL (0.19 M) with 500 mg BLG NCA dissolved in 10 mL dry

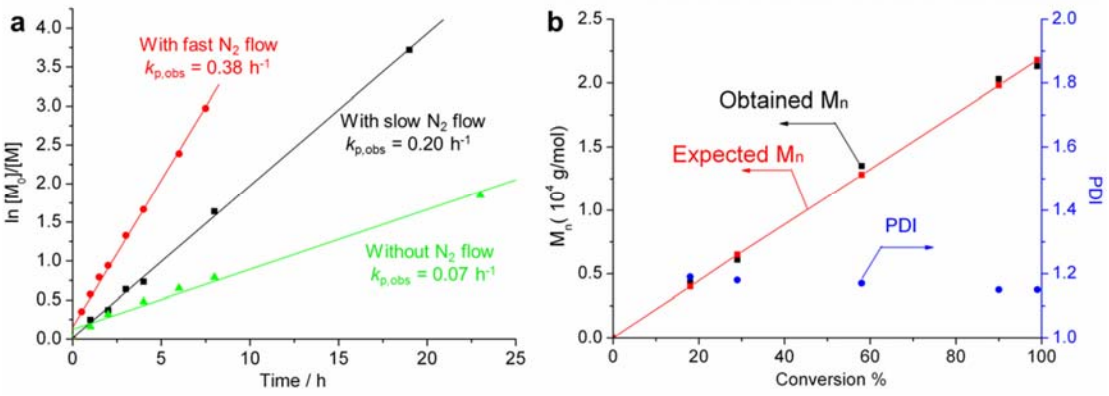

Figure 2.3. (a) Kinetic studies of *n*-hexylamine initiated BLG NCA ROP at room temperature with BLG NCA : I ratio of 100:1. The initial BLG NCA concentration was 50 mg/mL (0.19 M). The N_2 flow rates were 0 mL/min (green line), 100 mL/min (black line) and 250 mL/min (red line). (b) NCA ROP terminated at selected monomer conversion with flow rate of 100 mL/min.

DMF. The polymerization rate was obtained by plotting the natural logarithm of monomer concentration *versus* time and fitting of the data using equation 1.

$$-d[\text{BLG NCA}]/dt = k_p[I][\text{BLG NCA}] \quad (1)$$

$$k_{p.obs} = k_p[I]$$

The conversion was determined by ATR-FTIR using the intensity of BLG NCA anhydride absorption band at 1788 cm^{-1}. The linear fitting of the plot gave $k_{p.obs}$, which reflected the rate of polymerization. With increasing N_2 flow speed (from 0 to 250 mL/min), the $k_{p.obs}$ increased respectively (Figure 2.3a), which indicated that the polymerizations were promoted by N_2 flow. The accelerated rate of polymerization could be attributed to the efficient removal of CO_2 in the reaction system and forcing of the equilibrium to form nucleophilic amine to promote chain propagation. The kinetic studies of a different feed ratio (50 : 1) were conducted and those results also indicated that the N_2 flow promoted polymerization (Figure 2.4). This approach of N_2 flow

method provided an easy way to control the polymerization rate by simply tuning the N_2 flow rate. With higher N_2 flow rate (250 mL/min), a higher $k_{p.obs}$ ($k_{p.obs}$ = 0.38 h^{-1}) was observed than that with low flow rate (100 mL/min, $k_{p.obs}$ = 0.20 h^{-1}). Interestingly, the half-life time ($t_{1/2} = \ln 2/k_{p.obs}$) was 0.91 h for the polymerization with feed ratio of 50 : 1, which is close to the value ($t_{1/2}$ = 0.71 h) obtained by Hadjichristidis using high vacuum technology (HVT).[46] The "living" feature of the NCA ROP under N_2 flow was also supported by the following results: (i) over 95 % monomer conversion was observed in 8 h and the obtained PBLG had M_n = 20.1 kDa, as determined by ^{1}H NMR spectroscopy, which agreed well with the expected PBLG MW (M_n = 20.9 kDa) calculated based upon conversion; (ii) first order kinetic characteristics were observed in BLG NCA ROP; (iii) the obtained polymers had narrow MWDs.

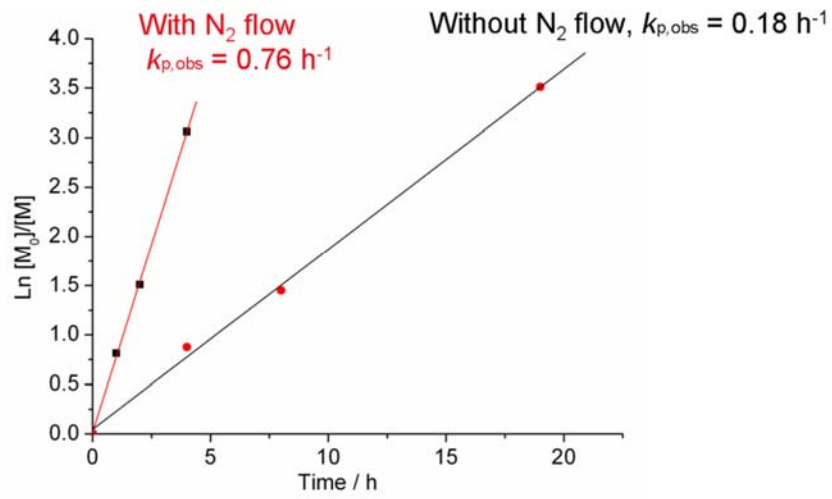

Figure 2.4. Kinetic studies of *n*-hexylamine initiated BLG NCA polymerization at a BLG NCA : I ratio of 50 : 1 at room temperature (the NCA ROP without N_2 flow was conducted in the glovebox). The initial BLG NCA concentration was 50 mg/mL (0.19 M).

Table 2.1. *n*-Hexylamine-initiated BLG NCA ROP with different feed ratios and N_2 flow rates.

Entry	Feed ratio $[M_0] : [I_0]$	Conc. (M)	N_2 flow rate (mL/min)	Time (h)	Conv. (%)	Obtained M_n (kDa)[d]	Expected M_n (kDa)	PDI[e]
1	50 : 1	0.19	250	2	90	9.6	10.0	1.15
2	50 : 1	0.19	100	4	96	10.6	10.6	1.11
3	50 : 1	0.19	0	19	96	13.2	10.6	1.38
4	100 : 1	0.19	250	7.5	95	20.1	20.9	1.18
5	100 : 1	0.19	100	19	99	21.3	21.8	1.12
6	100 : 1	0.19	0	28	81[c]	22.1	17.8	2.19
7	200 : 1	0.19	100	28	75	29.5	33.4	1.14
8	200 : 1	0.19	0[a]	48	75	34.7	33.4	1.18
9	50 : 1	0.19	100[b]	2	99	10.6	11.1	1.19
10	100 : 1	0.19	100[b]	2	45[c]	13.3	10.0	1.23
11	200 : 1	0.19	100[b]	3	37[c]	20.1	16.3	1.48

[a]The reaction was conducted in a glovebox. [b]N_2 was sparged into the reaction mixture. [c]After a certain conversion, the chain propagation halted. [d]Determined by ^{1}H NMR spectroscopy. [e]Determined by GPC characterization.

Chain extension experiments to confirm the livingness of the ω-chain terminus were also performed, by introducing additional aliquots of BLG NCA monomer *via* syringe, sequentially, into the reaction mixture. With the feed ratio of BLG NCA : initiator = 50 : 1, the monomer conversion reached > 99 % after 6 h, monitored by FTIR. The obtained $PBLG_{53}$ had M_n = 11.7 kDa from ^1H NMR and retention time = 24.50 min and PDI = 1.26, as determined by GPC. Another supply of BLG NCA was added into the reaction mixture with the feed ratio of BLG NCA : initiator = 25 : 1. The achieved $PBLG_{74}$, precipitated into diethyl ether after 18 h, was characterized to have a ^1H NMR-determined M_n = 16.3 kDa, retention time = 22.5 min and PDI = 1.26.

To further investigate the best conditions to obtain well-defined polypeptides with minimum polymerization time by using the N_2 flow methods, parameters such as feed ratio, flow rate of N_2 and sparging were screened (Table 2.1). With different feed ratios, accelerated polymerizations were observed in all entries using this N_2 flow method. However, with a moderate flow rate (100 mL/min), the obtained polymers had the narrowest MWDs (Entry 2 and 5 in Table 2.1). When polymerizations were conducted with the venting needle in place and without N_2 flow, the BLG NCA ROP required longer reaction time and had more side reactions, resulting in ill-defined polymers with broad PDIs (Entry 3 and 6 in Table 2.1). Especially, when attempts were made to synthesize polymers with high DP_n under these N_2-flow-free conditions, impurities and moisture in the air caused the polymerization lose the living features and polymers with broader PDIs were produced (Entry 6). When the feed ratio was increased to 200 : 1, the N_2 flow methods continued to afford well-defined PBLG with

narrow PDIs at high conversion (Figure 2.5), while the absence of N_2 flow resulted in dead polymer chains even at low conversion. When sparging N_2 into the reaction mixture, the polymerization rate increased compared to the flow methods (Entry 9 in Table 2.1). However at high feed ratios, termination of the polymerizations was observed (Entries 10 and 11 in Table 2.1).

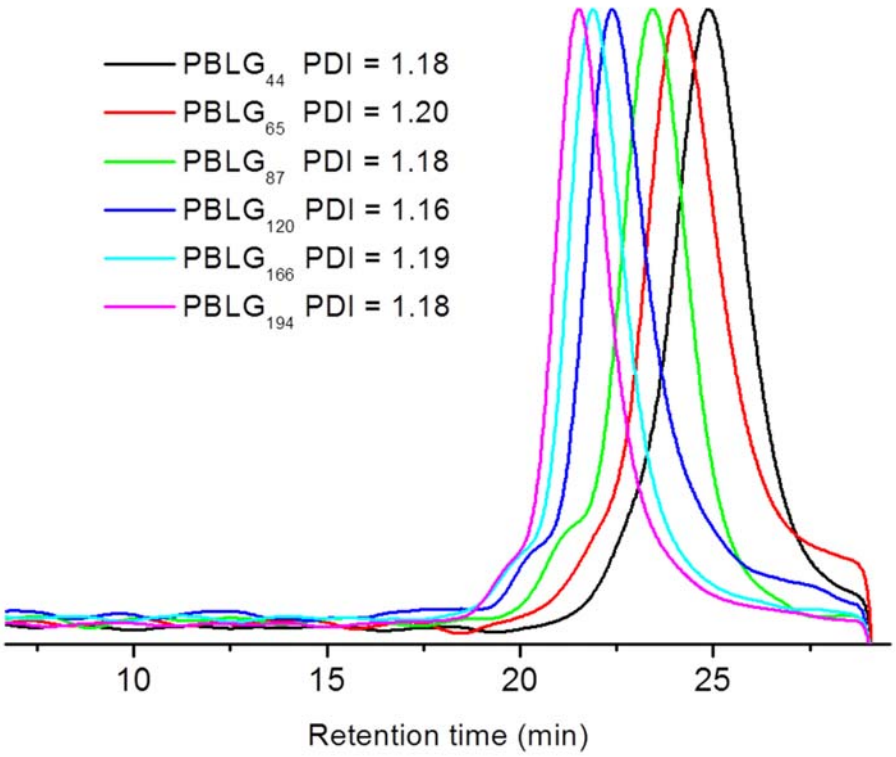

Figure 2.5. The GPC traces of N_2 flow accelerated NCA ROP of BLG quenched at determined time with different degrees of polymerization.

2.4 Conclusions

A N_2 flow accelerated NCA ROP *via* NAM was explored in detail. This easy operational method offers a new approach for the syntheses of polypeptides with controllable polymerization rates, predictable MWs and narrow MWDs. This approach is attractive because most of the initiators are commercially available and there is no need for removal of a catalyst after polymerization. Since no metal catalyst is used, this polymerization strategy diminishes potential toxicity issues that may arise in the use of synthetic polypeptide materials for biomedical applications. The N_2 flow can be easily tuned to balance the polymerization kinetics and structural control in NCA ROP. The significantly accelerated polymerization decreases side reactions that may be introduced by moisture and solvent.[88] In addition to the BLG NCA monomer, the N_2 flow method can also be applied in NCA ROP with varieties of monomers. For instance, expansion of this economic, easily operational and straightforward method is being explored to install chain end functionalities, perform block polypeptide syntheses and exert structural control for materials comprising combinations of different NCA monomers.

CHAPTER III

CONSTRUCTION OF A VERSATILE AND FUNCTIONAL NANOPARTICLE PLATFORM DERIVED FROM A HELICAL DIBLOCK COPOLYPEPTIDE-BASED BIOMIMETIC POLYMER FOR SIRNA DELIVERY*

3.1 Introduction

Small interfering ribonucleic acids (siRNAs) are a class of double-strand RNA molecules that have the capability to selectively knock down gene expression through RNA interference (RNAi) and thus show great promise for therapeutic applications.[89-91] In the last decade, siRNA-based therapeutic research has moved from the academic laboratory to clinical trials for several diseases, such as wet age-related macular degeneration and diabetic macular oedema.[92,93] However, the delivery of siRNA into target cells remains to be a considerable challenge, which stems from their poor stability against hydrolysis by nucleases, ineffective cellular uptake due to their anionic nature and escape into cytoplasm from endosome.[94,95] To circumvent these problems, various natural and synthetic materials, such as lipids, polymers, peptides, proteins/antibodies, aptamers and even small molecules, have been explored as siRNA delivery vectors.[95-100]

---

* Reproduced (adapted) from "Construction of a versatile and functional nanoparticle platform derived from a helical diblock copolypeptide-based biomimetic polymer" by Fan, J.; Li, R.; He, X.; Seetho, K.; Zhang, F.; Zou, J.; Wooley, K. L., *Polym. Chem.* **2014**, *5*, 3977-3981 with permission from The Royal Society of Chemistry. The siRNA complexation and delivery study was in collaboration with Sarosh Khan,[†] Yannick P. Borguet,[†] Mahmoud Elsabahy,[†‡] Jiong Zou,[†] Karen L. Wooley,[†] [†]Departments of Chemistry, Chemical Engineering, Materials Science and Engineering, and Laboratory for Synthetic-Biologic Interactions, Texas A&M University, [‡]Department of Pharmaceutics, Faculty of Pharmacy, Assiut University.

Polymeric nanoparticles with unique physical and chemical properties at the nanoscale have shown great promise for various biomedical applications by acting as a carrier to package and deliver a wide range of therapeutic, diagnostic and theranostic agents, including siRNA, to the desired sites of action.[101-103] In particular, micellar nanoparticles with distinctive core-shell structures have attracted considerable attention due to their tunable sizes and potential modifications in both the core and shell domains by using well-defined and functionalized amphiphilic block copolymers.[104] The development of micellar nanoparticles from non-degradable polymers has been well studied and widely used in nanomedicine, while the undesired side effects such as toxicity and immunogenicity have become an inevitable challenge.[105] In order to overcome the drawbacks of non-degradable polymers, biodegradable synthetic polymers, such as polyesters,[106] polycarbonates,[107] polyphosphoesters,[108] and polypeptides,[109] have been explored as attractive materials to be utilized in biomedical applications due to their intrinsic degradability and low toxicity.[110,111] Compared with other biodegradable synthetic polymers, polypeptides offer additional properties, such as precisely-defined secondary structures derived from chirality and various functionalities introduced by natural and synthetic amino acids that lead to supramolecular hierarchical assemblies, which are often unobtainable from non-polypeptide-based materials.[112]

Polypeptides consisting of α-amino acids with covalent linkages share significant similarities to natural proteins, and recent synthetic methodology developments have facilitated their extensive utilization in biomedical areas, such as serving as scaffolds for tissue engineering, matrices for drug and gene delivery, and responsive materials for

biosensors.[22,59,113] Amphiphilic block copolypeptides, built from polypeptide blocks with different hydrophilicities, have the capability to self-assemble into well-defined nanostructures in aqueous solutions, including micelles, vesicles and helical cylinders, which can serve as versatile material platforms.[75] The most common approach to synthesize block copolypeptides involves sequential ring-opening polymerizations (ROPs) of different amino acid *N*-carboxyanhydride (NCA) monomers.[6,33,34,67] In the last decade, several controlled NCA ROPs have been reported to prepare well-defined block copolypeptides by reducing side reactions that decrease the activity of the terminal amine during polymerizations.[46,50,54] However, it is still challenging to develop well-defined block copolypeptides with side-chain functionalities *via* a facile and easily operational strategy.[35] Due to the nucleophile- and base-sensitive nature of NCA ROP, the monomers used in the polymerizations are limited to NCAs with inert side-chain groups or NCAs with modified side-chains by suitable protecting groups. The selective protection and deprotection operations in both monomer synthesis and post-polymerization modification processes increase the difficulty to efficiently prepare well-defined functional block copolypeptides.[114] Recently, Hammond *et al.* reported an alkyne-containing NCA monomer, γ-propargyl-L-glutamate (PLG) NCA, by incorporation of an alkynyl functional group onto the side-chain of L-glutamic acid, and performed NCA ROPs to obtain functional homopolypeptides.[115] The efficient chemical modifications of alkyne-functionalized polypeptides *via* either copper-catalyzed azide-alkyne Huisgen 1,3-dipolar cycloaddition or radical-mediated thiol-yne click-type chemistry have advantages including rapid reaction, quantitative conversion and high

functional group tolerance with minimal by-products and side reactions.[115,116] Until now, well-defined diblock copolypeptides containing a polyPLG segment and other polypeptide blocks have not been reported. It was hypothesized that difficulties with the synthesis and purification of the PLG NCA monomer as well as the long polymerization time during NCA ROP (generally 3 days) may have hampered the efficient preparation of well-defined block copolypeptides, and further prevented the construction of functional polypeptide-based nanomaterials.

We had anticipated that our facile and easily operational synthetic strategy to construct well-defined polypeptides by conducting NCA ROP under normal Schlenk techniques, with the rate of polymerization being controlled by a straightforward N_2 flow method, could be utilized to prepare functional multi-block polypeptides. Diblock copolymers with incorporation of a copolypeptide segment as one block and the other block being poly(ethylene glycol) (PEG) by statistical ring-opening copolymerization of different NCA monomers from a PEG macroinitiator had been prepared *via* this strategy, and recently, the approach was shown to allow for the preparation of a series of di- and triblock polymers comprised of PEG and peptide segments, designed as multi-anchor systems for the functionalization of gold with PEG.[117] Herein, a functional and helical diblock copolypeptide, poly(γ-benzyl-L-glutamate)-*block*-poly(γ-propargyl-L-glutamate) (PBLG-*b*-PPLG **3**), was prepared by this N_2 flow method within 16 h by one-pot sequential ROPs of two NCA monomers, BLG **1** and PLG **2** NCAs. Subsequent modification of the diblock copolypeptide was conducted by a thiol-yne click-type reaction to attach charged and functional side-chain moieties onto the PPLG segment.

The obtained functionalized diblock copolypeptides were observed to assemble into micellar nanoparticles in aqueous solution with corresponding surface charges and expected helical conformations derived from the secondary sub-structure of the polypeptides. The cationic polypeptide nanoparticle was further investigated as a siRNA carrier *via* the electrostatic complexation between the positively-charged sites on the polypeptide side chains and negatively-charged phosphate groups of siRNA to construct gene delivery complex.

3.2 Experimental section

3.2.1 Materials

Ethyl acetate, *n*-hexane, isopropyl alcohol, diethyl ether, acetone, sodium hydroxide (NaOH, ≥ 97%), sodium chloride (NaCl, ≥ 99%), sodium bicarbonate ($NaHCO_3$, ≥ 99.7%), trifluoroacetic acid (TFA, ≥ 99%), magnesium sulfate ($MgSO_4$, anhydrous, ≥ 99.5%), *N,N*-dimethylformamide (DMF, anhydrous, ≥ 99.8%), γ-benzyl-L-glutamate (≥ 99%), L-glutamic acid (≥ 99%), propargyl alcohol (≥ 99%), chlorotrimethylsilane (≥ 99%), bis(trichloromethyl) carbonate (≥ 98%), *n*-hexylamine (≥ 99%), 2,2-dimethoxy-2-phenylacetophenone (DMPA, ≥ 99%), cysteamine hydrochloride (≥ 98%), 3-mercaptopropionic acid (≥ 99%), pyrene (≥ 99%) were purchased from Sigma-Aldrich company (USA). All chemicals were used without further purification, unless otherwise noted. Nanopure water (18.2 MΩ·cm) was acquired by means of a Milli-Q water filtration system, Millipore Corp. (St. Charles, MO). Dialysis membrane tubing with a molecular weight cut off (MWCO) of 6 - 8 kDa

was purchased from Spectrum Laboratories, Inc. (Rancho Dominguez, CA) and soaked for 5 min in nanopure water at room temperature before usage.

3.2.2 Instrumentation

^{1}H and ^{13}C NMR spectra were recorded on a Varian Inova 300 spectrometer interfaced to a UNIX computer using VnmrJ software. Chemical shifts were referenced to the solvent resonance signals. Attenuated total reflectance-Fourier transform infrared spectroscopy (ATR-FTIR) spectra were recorded on an IR Prestige 21 system (Shimadzu Corp., Kyoto, Japan) and analyzed using IRsolution v. 1.40 software. Circular dichroism (CD) spectra were recorded on a Chirascan CD spectrometer from Applied Photophysics, Ltd. (Leatherhead, UK) equipped with a 150 watt xenon arc lamp. The polymer solution samples for CD measurements were prepared at a concentration of 0.1 mg/mL in nanopure water. The samples were placed in a quartz cell with a path length of 1.0 mm and analyzed between 180 and 280 nm with a wavelength step of 1.0 nm. Measurements were analyzed using Pro-Data Version 5 software. Critical micelle concentration (CMC) determinations were made by pyrene fluorescence measurements that were conducted on a RF-5301PC spectrofluorophotometer system (Shimadzu Corp., Kyoto, Japan) and analyzed using Panorama Fluorescence v. 2.1 software. Fluorescence emission spectra ranging from 360 to 450 nm of the sample solutions were recorded using an excitation wavelength of 334 nm at room temperature. All the measurements were repeated three times.

N,N-Dimethylformamide-based gel permeation chromatography (DMF GPC) was conducted on a Waters Chromatography, Inc. (Milford, MA) system equipped with

an isocratic pump model 1515, a differential refractometer model 2414 and a four-column set of 5 μm Guard (50 × 7.8 mm), Styragel HR 4 5 μm DMF (300 × 7.8 mm), Styragel HR 4E 5 μm DMF (300 × 7.8 mm), and Styragel HR 2 5 μm DMF (300 × 7.8 mm). The system was equilibrated at 70 °C in pre-filtered DMF (containing 0.05 mol/L LiBr), which served as the polymer solvent and eluent (flow rate set to 1.00 mL/min). Polymer solutions were prepared at concentrations of *ca.* 3.0 mg/mL and an injection volume of 0.2 mL was used. Data collection and analysis was performed with Empower Pro software. The system was calibrated with polystyrene (PS) standards (Polymer Laboratories, Amherst, MA) ranging from 1480 to 1233000 Da.

Thermogravimetric analysis (TGA) was performed under argon atmosphere using a Mettler-Toledo model TGA/SDTA851^e (Mettler-Toledo, Inc., Columbus, OH), with a heating rate of 10 °C/min. Measurements were analyzed using Mettler-Toledo STAR^e v. 7.01 software. Glass transition temperatures (T_g) were measured by differential scanning calorimetry (DSC) on a Mettler-Toledo DSC822® (Mettler-Toledo, Inc., Columbus, OH), with a heating rate of 5 °C/min. Measurements were analyzed using Mettler-Toledo STAR^e v. 7.01 software. The T_g was taken as the midpoint of the inflection tangent, upon the second heating scan.

Transmission electron microscopy (TEM) images were collected on a JEOL 1200 EX (Tokyo, Japan) operating at 100 kV and micrographs were recorded at calibrated magnifications using a SLA-15C CCD camera. Samples for TEM measurements were prepared as follows: 10 μL of the dilute polymer solution was deposited onto a carbon-coated copper grid, and after 1 min, the excess of the solution

was quickly wicked away by a piece of filter paper. The samples were then negatively stained with 1 wt % phosphotungstic acid (PTA) aqueous solution. After 30 s, the excess staining solution was quickly wicked away by a piece of filter paper and the samples were left to dry in vacuum overnight.

Dynamic light scattering (DLS) measurements were conducted using a Delsa Nano C from Beckman Coulter, Inc. (Fullerton, CA) equipped with a laser diode operating at 658 nm. Scattered light was detected at 165° angle and analyzed using a log correlator over 70 accumulations for a 0.5 mL of sample in a glass size cell (0.9 mL capacity). The photomultiplier aperture and the attenuator were automatically adjusted to obtain a photon counting rate of *ca.* 10 kcps. The calculation of the particle size distribution and distribution averages was performed using CONTIN particle size distribution analysis routines using Delsa Nano 2.31 software. The peak averages of histograms from intensity, volume and number distributions out of 70 accumulations were reported as the average diameter of the particles. All determinations were repeated 10 times. The zeta potential values of the nanoparticles were determined by Delsa Nano C particle analyzer (Beckman Coulter, Fullerton, CA) equipped with a 30 mW dual laser diode (658 nm). The zeta potential of the particles in suspension was obtained by measuring the electrophoretic movement of charged particles under an applied electric field. Scattered light was detected at a 30° angle at 25 °C. The zeta potential was measured at five regions in the flow cell and a weighted mean was calculated. These five measurements were used to correct for electroosmotic flow that was induced in the cell due to the surface charge of the cell wall. All determinations were repeated 9 times.

3.2.3 Experimental procedures

Synthesis of γ-benzyl-L-glutamate *N*-carboxyanhydride (BLG NCA) monomer 1

In a 500 mL three-necked round bottom flask equipped with a magnetic stirrer, a septum and a pipet for N_2 inlet and a condenser with a tubing connector that allows outlet flow through a base solution (NaOH aqueous solution), BLG NCA monomer **1** was synthesized from γ-benzyl-L-glutamate (10.0 g, 42.1 mmol, 3 equiv) and bis(trichloromethyl) carbonate (4.2 g, 14 mmol, 1 equiv) in 300 mL ethyl acetate at 65 °C for 4 h.[81] After cooling to 5 °C, the crude product was extracted with 100 mL 5 °C nanopure water and 100 mL 5 °C 0.5 wt % sodium bicarbonate aqueous solution. The organic layer was then dried over $MgSO_4$, filtrated and concentrated. The resulting solid was purified by recrystallization three times with ethyl acetate/*n*-hexane 1:1 (v/v), and dried in vacuum to obtain a white crystal (2.6 g, yield: 71%). The product was stored in -20 °C freezer under N_2 atmosphere. ^{1}H NMR (300 MHz, $CDCl_3$, ppm): δ 2.21 (m, 2H, C*H*$_2$CH$_2$COOCH$_2$), 2.60 (t, *J* = 6.9 Hz, 2H, CH$_2$C*H*$_2$COOCH$_2$), 4.38 (dt, *J* = 1.0 Hz, *J* = 5.4 Hz, 1H, COC*H*NH), 5.14 (s, 2H, COOC*H*$_2$), 6.42-6.64 (br, 1H, COCHN*H*), 7.36 (m, 5H, Ar*H*). ^{13}C NMR (75 MHz, $CDCl_3$, ppm): δ 27.1, 30.1, 57.1, 67.3, 128.6, 128.8, 128.9, 135.3, 151.9, 169.5, 172.6. FTIR (cm^{-1}): 3449-2725, 3331, 3251, 2931, 1859, 1773, 1703, 1250, 1185, 1112, 930. HRMS: calculated [M-H]$^-$ for $C_{13}H_{13}NO_5$: 262.0715, found: 262.0710.

Synthesis of γ-propargyl-L-glutamate hydrochloride

In a 1 L round bottom flask, L-glutamic acid (12.0 g, 81.6 mmol) was suspended in propargyl alcohol (400 mL) under N_2 for 1 h at room temperature.[115]

Chlorotrimethylsilane (28.5 mL, 225 mmol) was added into the suspension dropwise over 1 h under N_2 atmosphere at room temperature. The resulting solution was stirred at room temperature over 36 h and then precipitated into diethyl ether (1.5 L) giving a white solid. The obtained solid was purified by dissolving into isopropyl alcohol (200 mL), heating to reflux, and precipitating into diethyl ether (1.5 L). The product was filtrated, washed with diethyl ether (200 mL × 3) and dried in vacuum (12.4 g, yield: 68 %). ^{1}H NMR (300 MHz, CD_3OD, ppm): δ 2.21 (m, 2H, CHC*H*$_2$CH$_2$), 2.65 (m, 2H, CH$_2$C*H*$_2$CO), 2.95 (t, *J* = 2.5 Hz, 1H, C≡C*H*), 4.06 (t, *J* = 6.7 Hz, 1H, NHC*H*CO), 4.74 (d, *J* = 2.5 Hz, 2H, COOC*H*$_2$). ^{13}C NMR (75 MHz, CD_3OD, ppm): δ 26.7, 30.5, 53.2, 53.3, 76.6, 78.8, 171.5, 173.0. FTIR (cm^{-1}): 3337-2154, 3292, 3142, 2906, 2124, 1963, 1737, 1720, 1502, 1489, 1220, 1172, 995, 837. HRMS: calculated $[M\text{-}Cl]^+$ for $C_8H_{12}NO_4Cl$: 186.0761, found: 186.0765.

Synthesis of γ-propargyl-L-glutamate (PLG) NCA monomer 2

In a 250 mL three-necked round bottom flask equipped with a magnetic stirrer, a septum and a pipet for N_2 inlet and a condenser with a tubing connector that allows outlet flow through a base solution (NaOH aqueous solution), PLG NCA monomer **2** was synthesized from γ-propargyl-L-glutamate hydrochloride (4.0 g, 18 mmol, 3 equiv) and bis(trichloromethyl) carbonate (1.8 g, 6.0 mmol, 1 equiv) in 100 mL ethyl acetate at 65 °C for 6 h.[70] After cooling to 5 °C, the crude product was extracted with 100 mL 5 °C nanopure water, 100 mL 5 °C saturated sodium bicarbonate aqueous solution, and 100 mL 5 °C saturated sodium chloride aqueous solution. The organic layer was dried over $MgSO_4$, filtrated and concentrated. The resulting yellow viscous oil was purified

by three times precipitation with ethyl acetate/*n*-hexane 1:5 (v/v), and dried in vacuum to obtain viscous oil (0.9 g, yield: 71%). The product was stored in -20 °C freezer under N_2 atmosphere. ^{1}H NMR (300 MHz, $CDCl_3$, ppm): δ 2.21 (m, 2H, C*H*$_2$CH$_2$COOCH$_2$), 2.52 (t, *J* = 2.5 Hz, 1H, C≡C*H*), 2.60 (t, *J* = 7.1 Hz, 2H, CH$_2$C*H*$_2$COOCH$_2$), 4.45 (dt, *J* = 5.8 Hz, *J* = 1.0 Hz, 1H, COC*H*NH), 4.70 (d, *J* = 2.5 Hz, 2H, COOC*H*$_2$), 7.00-7.06 (br, 1H, COCHN*H*). ^{13}C NMR (75 MHz, $CDCl_3$, ppm): δ 26.7, 29.4, 52.6, 56.8, 75.5, 77.2, 152.3, 169.5, 171.8. FTIR (cm^{-1}): 3487-3030, 3284, 2945, 2131, 1854, 1776, 1732, 1163, 1103, 918, 756. HRMS: calculated [M-H]$^-$ for $C_9H_9NO_5$: 210.0402, found: 210.0406.

Synthesis of diblock copolypeptide, poly(γ-benzyl-L-glutamate)-*block*-poly(γ-propargyl-L-glutamate) (PBLG-*b*-PPLG) 3, initiated by *n*-hexylamine

Diblock copolypeptide PBLG-*b*-PPLG **3** was obtained by sequential addition of BLG NCA **1** and PLG NCA **2** monomers into the reaction solution with the method of N_2 flow accelerated ring-opening polymerization (ROP). Into a 25 mL flame-dried Schlenk flask equipped with a magnetic stirrer, *n*-hexylamine (10.2 mg, 0.101 mmol, 1 equiv) was added into a solution of BLG NCA **1** (797.6 mg, 3.030 mmol, 30 equiv) in 14.0 mL anhydrous DMF solution. The reaction mixture was stirred at a stir rate of 400 rpm under continuous N_2 flow (100 mL/min) at room temperature. The Schlenk flask was capped with a rubber stopper with a needle outlet connected with a drying tube. FTIR was used to monitor the polymerization and more than 99% of BLG NCA **1** monomer was consumed in 3.5 h. PLG NCA **2** monomer (639.8 mg, 3.030 mmol, 30 equiv) in 4.0 mL anhydrous DMF was transferred into the reaction solution by syringe

and was consumed greater than 99% over another 12 h. The resulting reaction solution was precipitated into diethyl ether under vigorous stirring and a white powder was obtained after centrifuging and drying in vacuum at room temperature (1003.8 mg, yield: 85%). ^{1}H NMR (300 MHz, TFA-D, ppm): δ 0.71-0.82 (br, 3H, C*H*$_3$), 1.75-2.31 (br, 120H, C*H*$_2$CH$_2$COOCH$_2$), 2.32-2.68 (br, 30H, C≡C*H*, br, 120H, CH$_2$C*H*$_2$COOCH$_2$), 4.50-4.77 (br, 60H, COC*H*NH; br, 60H, COOC*H*$_2$), 4.93-5.15 (br, 60H, COOC*H*$_2$), 7.06-7.30 (br, 150H, Ar*H*). ^{13}C NMR (75 MHz, TFA-D, ppm): δ 26.5, 29.6, 29.7, 53.2, 53.3, 68.3, 75.0, 75.2, 127.8, 128.2, 128.4, 134.0, 173.3, 175.1, 175.7. FTIR (cm^{-1}): 3418-3127, 3065, 3034, 2941, 2126, 1730, 1649, 1545, 1159, 1121, 991, 696. GPC: M_n = 38.5 kDa, PDI = 1.08. DSC: T_g = 22 °C, T_g = 79 °C. TGA in N$_2$: 25-240 °C, 3% mass loss; 240-447 °C, 61% mass loss; 447-500 °C, 2% mass loss; 34% mass remaining above 500 °C.

Synthesis of positively-charged diblock copolypeptide 4 *via* thiol-yne click chemistry between PBLG$_{30}$-*b*-PPLG$_{30}$ with cysteamine hydrochloride

Diblock copolypeptide PBLG$_{30}$-*b*-PPLG$_{30}$ **3** (200.0 mg, 0.01709 mmol, 1 equiv) and cysteamine hydrochloride (1165.0 mg, 10.254 mmol, 600 equiv) were added into 6.0 mL anhydrous DMF in a 20 mL vial. DMPA (264.0 mg, 1.025 mmol, 60 equiv) was added into the reaction solution after both the solids were dissolved. The reaction solution was then bubbled by N$_2$ flow for half an hour, and placed under UV light with a wavelength of 365 nm for 2 h. The crude product was precipitated into acetone and centrifuged to get a white solid. The white solid was then dissolved into 5.0 mL TFA and the resulting solution was added into 20 mL nanopure water. The mixture was

transferred into a presoaked dialysis membrane tubing (MWCO 6 - 8 kDa), dialyzed against nanopure water for another 3 days, and later lyophilized to get the final product (256.4 mg, yield: 81%). ^{1}H NMR (300 MHz, TFA-D, ppm): δ 0.74-0.85 (br, 3H, C*H*$_3$), 1.80-2.35 (br, 120H, C*H*$_2$CH$_2$COOCH$_2$), 2.35-2.73 (br, 120H, CH$_2$C*H*$_2$COOCH$_2$), 2.73-2.86 (br, 30H, SC*H*CH$_2$S), 2.86-3.20 (br, 60H, SCHC*H*$_2$S; br, 120H, SC*H*$_2$CH$_2$NH$_3$), 3.30-3.54 (br, 120H, SCH$_2$C*H*$_2$NH$_3$), 4.10-4.53 (br, 30H, COC*H*NH; br, 30H, COOC*H*$_2$CH), 4.55-4.78 (br, 30H, COC*H*NH; br, 30H, COOC*H*$_2$CH), 4.95-5.25 (br, 60H, COOC*H*$_2$Ar), 6.86-7.11 (br, 180H, CH$_2$CH$_2$N*H*$_3$), 7.11-7.34 (br, 150H, Ar*H*). ^{13}C NMR (75 MHz, TFA-D, ppm): δ 26.6, 28.2, 29.7, 29.8, 33.8, 39.4, 39.8, 44.9, 53.2, 66.6, 68.4, 127.9, 128.3, 128.5, 134.1, 173.3, 175.5, 175.8. FTIR (cm^{-1}): 3720-2181, 3288, 3034, 2936, 2129, 1730, 1672, 1651, 1547, 1171, 1126, 835, 799, 721. DSC: T_g = 29 °C, T_g = 70 °C. TGA in N$_2$: 25-155 °C, 2% mass loss; 155-242 °C, 20% mass loss; 242-424 °C, 52% mass loss; 424-500 °C, 2% mass loss; 24% mass remaining above 500 °C.

Synthesis of negatively-charged diblock copolypeptide 5 *via* thiol-yne click chemistry between PBLG$_{30}$-*b*-PPLG$_{30}$ with 3-mercaptopropionic acid

Diblock copolypeptide PBLG$_{30}$-*b*-PPLG$_{30}$ **3** (200.0 mg, 0.01709 mmol, 1 equiv) and 3-mercaptopropionic acid (1088.3 mg, 10.254 mmol, 600 equiv) into 6.0 ml anhydrous DMF in a 20 ml vial. DMPA (264.0 mg, 1.025 mmol, 60 equiv) was added into the reaction solution after both the solids were dissolved. The reaction solution was then bubbled by N$_2$ flow for half an hour, and placed under UV light (365 nm) for 2 h. The crude product was precipitated into diethyl ether three times, centrifuged and dried in vacuum to get the final product (219.3 mg, yield: 71%). ^{1}H NMR (300 MHz, TFA-D,

ppm): δ 0.72-0.82 (br, 3H, C*H*$_3$), 1.65-2.32 (br, 120H, C*H*$_2$CH$_2$COOCH$_2$), 2.33-2.66 (br, 120H, CH$_2$C*H*$_2$COOCH$_2$), 2.67-2.80 (br, 120H, SCH$_2$C*H*$_2$COOH), 2.80-2.99 (br, 60H, SCHC*H*$_2$S; br, 120H, SC*H*$_2$CH$_2$COOH), 3.08-3.30 (br, 30H, SC*H*CH$_2$S), 4.16-4.52 (br, 30H, COC*H*NH; br, 30H, COOC*H*$_2$CH), 4.55-4.85 (br, 30H, COC*H*NH; br, 30H, COOC*H*$_2$CH), 4.92-5.22 (br, 60H, COOC*H*$_2$Ar), 7.03-7.35 (br, 150H, Ar*H*). ^{13}C NMR (75 MHz, TFA-D, ppm): δ 25.6, 26.5, 26.9, 29.1, 29.7, 31.3, 33.0, 44.5, 53.1, 65.9, 68.3, 127.8, 128.3, 128.4, 134.0, 173.3, 175.7, 179.4. FTIR (cm^{-1}): 3696-2155, 3285, 3034, 2928, 1728, 1649, 1547, 1242, 1163, 1123, 968, 799, 696. DSC: T_g = 7 °C, T_g = 63 °C. TGA in N$_2$: 25-207 °C, 1% mass loss; 207-340 °C, 69% mass loss; 340-500 °C, 6% mass loss; 24% mass remaining above 500 °C.

Preparation of cationic nanoparticle 6 from self-assembly of positively-charged diblock copolypeptide 4 by direct re-suspension into nanopure water

The positively-charged diblock copolypeptide **4** (1.0 mg) was suspended into nanopure water (1.0 mL), followed by sonication for 10 min at room temperature to obtain a clear aqueous solution of **4** at a concentration of 1.0 mg/mL.

Preparation of anionic nanoparticle 7 from self-assembly of negatively-charged diblock copolypeptide 5 by nanoprecipitation method

The negatively-charged diblock copolypeptide **5** was dissolved into anhydrous DMF to obtain a polymer solution with a concentration of 3.0 mg/mL. The polymer solution (1.0 mL) was then added into nanopure water (4.0 mL) *via* a syringe pump at an addition rate of 0.2 mL/min. The mixture was then transferred into a presoaked dialysis membrane tubing (MWCO 6 - 8 kDa), and dialyzed against nanopure water for 24 h to

remove DMF at room temperature. The final concentration of **5** was adjusted to 0.5 mg/mL by addition of nanopure water.

Determination of critical micelle concentrations (CMCs) for positively-charged 4 and negatively-charged 5 diblock copolypeptides in nanopure water

The CMCs for positively-charged **4** and negatively-charged **5** diblock copolypeptides in nanopure water were determined by using pyrene as the fluorescent probe following the protocol in literature.[118] The sample solution was prepared by mixing 1.0 mL of a polypeptide aqueous solution with 1.0 mL of a pyrene aqueous stock solution (6.0×10^{-7} mol/L). Samples with polymer concentrations ranging from 0.01 – 1.0 g/L for **4** and 0.01 – 0.25 g/L for **5** were prepared. All the sample solutions were then stored at room temperature overnight to equilibrate the pyrene and the micelles. The fluorescence measurement was conducted at room temperature, in which the pyrene was excited at 334 nm and its emission spectrum was recorded at 373 and 384 nm, corresponding to the first and third vibrational peaks, respectively. All the measurements were repeated three times and the ratios of intensities of the first (I_{I}) and third (I_{III}) peaks were plotted against the concentrations of polypeptides in the sample solutions. The CMC was taken as the intersection of the tangent to the curve at the inflection with tangent through the points at high polymer concentration.

Gel retardation assays to determine the binding affinity of cationic nanoparticle 6 with small interfering ribonucleic acid (siRNA)

The siRNA binding affinity with the cationic nanoparticle **6** was investigated by gel retardation assay. Agarose gels (1 wt %) were prepared in Tris-acetate-EDTA buffer

(Bio-Rad Laboratories, Inc., Hercules, CA). The siRNA (5'-Cy3-(sense strand)-GGCCACAUCGGAUUUCACU, M_w = 13814 g/mol, Dharmacon, Chicago, IL), either free, or complexed to ammonium-functionalized amphiphilic diblock copolypeptide (total molar concentration of the ammonium in the polymers to phosphate groups in the siRNA (N^+/P^-) ratios ranging from 0.5-20 (1.3 μg siRNA/25 μL/well)), were mixed with glycerol (20% v/v) prior to the electrophoresis. Gel electrophoresis was carried out using a horizontal apparatus at 100 V for 20 min and fluorescence imaging of the separated siRNA bands was performed using a ChemiDoc XRS imager and the data were analyzed by using Image Lab software (Bio-Rad Laboratories, Inc., Hercules, CA).

Cytotoxicity assays

RAW 264.7 mouse macrophages (2×10^4 cells/well) and Human ovarian adenocarcinoma (OVCAR-3) cells (5×10^3 cells/well) were plated in 96-well plate in Dulbecco's Modified Eagle Medium (DMEM) and RPMI-1640 medium (10% and 20% fetal bovine serum, for the RAW 264.7 and OVCAR-3, respectively and 1% penicillin/streptomycin). Cells were incubated at 37 °C in a humidified atmosphere containing 5% CO_2 for 24 h to adhere. Then, the medium was replaced with a fresh medium 1 h prior to the addition of 20 μL of cationic nanoparticle **6** stock solution to 100 μL of the medium (final concentrations ranged from 0.2 - 500 μg/mL). The cells were incubated with the formulations for 72 h, and then the medium was replaced with 100 μL of the fresh complete media. MTS combined reagent (20 μL) was added to each well (Cell Titer 96® Aqueous Non-Radioactive Cell Proliferation Assay, Promega Co., Madison, WI). The cells were incubated with the reagent for 2 h at 37 °C in a

humidified atmosphere containing 5% CO_2 protected from light. Absorbance was measured at 490 nm using SpectraMax M5 (Molecular Devices Co., Sunnyvale, CA). The cell viability was calculated based on the relative absorbance to the control-untreated cells.

Laser scanning confocal microscopy (LSCM)

RAW 264.7 mouse macrophages and OVCAR-3 cells (5×10^5 cells/well) were plated in glass-bottom six-well plate (MatTek Co., Ashland, MA) in RPMI-1640 medium and DMEM (10% and 20% fetal bovine serum, for the RAW 264.7 and OVCAR-3, respectively, and 1% penicillin/streptomycin) and incubated at 37 °C in a humidified atmosphere containing 5% CO_2 for 24 h to adhere. Then, the medium was replaced with a fresh media 1 h prior to the addition of Cy3-labeled siRNA complexed with cationic nanoparticle **6** at a N^+/P^- ratio of 10 or Lipofectamine (200 nM final concentration of the Cy3-siRNA). The cells were incubated with the formulations for 3 h and washed extensively with phosphate buffered saline (PBS). Then, DRAQ5 (Biostatus Ltd., Shepshed, Leicestershire, UK) was utilized to stain the nucleus (30 min incubation, followed by extensive washing with PBS). Cells were then fixed with 1% formaldehyde for 20 min and washed once with PBS. The cells were then stored in 1 mL PBS in the refrigerator and analyzed by laser scanning confocal microscopy (LSM 510, Zeiss, Jena, Germany). The images were collected under the same conditions (laser power, detector gain, *etc.*) for consistency, and $\lambda_{excitation}$ of 543 and 635 nm were utilized for Cy3 and DRAQ5, respectively.

Death-siRNA transfection assays

OVCAR-3 cells (5×10^3 cells/well) were plated in 96-well plate in RPMI-1640 medium (20% fetal bovine serum, and 1% penicillin/streptomycin). Cells were incubated at 37 °C in a humidified atmosphere containing 5% CO_2 for 24 h to adhere. Then, the medium was replaced with a fresh medium 1 h prior to the addition of the siRNA mixed with cationic nanoparticle **6**, Lipofectamine (100 nM final concentrations of AllStars death- or negative control-siRNA (Qiagen, Valencia, CA)) at N^+/P^- ratios of 5, 10 and 20. The cells were incubated with the various formulations for 48 h and then the medium was replaced with 100 μL of fresh medium prior to the addition of 20 μL MTS combined reagent to each well (Cell Titer 96® Aqueous Non-Radioactive Cell Proliferation Assay, Promega Co., Madison, WI). The cells were incubated with the reagent for 2 h at 37 °C in a humidified atmosphere containing 5% CO_2 protected from light. Absorbance was measured at 490 nm using SpectraMax M5 (Molecular Devices Co., Sunnyvale, CA). The cell viability was calculated by estimating the relative cell viability of the cells treated with death-siRNA to the negative control siRNA-loaded formulations. The Lipofectamine-siRNA complexes were prepared according to the manufacturer instructions and the transfection efficiency was measured following the same procedures of the siRNA-complexes.

3.3 Results and discussions

The diblock copolypeptide, poly(γ-benzyl-L-glutamate)-*block*-poly(γ-propargyl-L-glutamate) (PBLG-*b*-PPLG) **3**, was prepared by sequentially adding **1** and **2** into a

solution of *n*-hexylamine in anhydrous *N,N*-dimethylformamide (DMF) (Figure 3.1), which provided a facile and straightforward approach to construct well-defined diblock copolypeptides. This strategy extends from our previous study, in which the propagating chain-ends of the polypeptides in the N_2 flow method had the capability to undergo chain extension by sequentially introducing additional aliquots of *N*-carboxyanhydride (NCA) monomers into the reaction mixture. The required amount of **1** in anhydrous DMF was added into *n*-hexylamine, the initiator, with the monomer : initiator = 30 : 1 and allowed to proceed at room temperature, using standard Schlenk techniques. An aliquot of **2** in anhydrous DMF with the monomer : initiator = 30 : 1 was introduced into the reaction mixture *via* syringe after 3.5 h, when the monomer conversion of **1** had reached 99%, as determined by attenuated total reflectance-Fourier transform infrared spectroscopy (ATR-FTIR) using the intensity of NCA anhydride absorption at 1788 cm^{-1}. The conversion of **2** was greater than 99% after another 12 h, and the reaction mixture was then precipitated into diethyl ether to isolate $PBLG_{30}$-*b*-$PPLG_{30}$ **3** as a white solid product. Due to the accelerated polymerization rate of the N_2 flow method, **3** was prepared in a rapid (16 h) and atom-efficient manner (each monomer conversion > 99%, yield > 85%) with a well-defined structure, as confirmed by the observed gel permeation chromatography (GPC) analyses of a peak shift from 24.9 to 22.8 min elution time from the first to second block growth profiles and a narrow molecular weight distribution (PDI = 1.08) for **3** (Figure 3.2). It is worth mentioning that the polymerizations under continuous N_2 flow did not require solvent purification and the PLG NCA monomer

could be purified simply by repeated precipitations, which reduced the time and effort required for scale-up to gram-scale polymerizations.

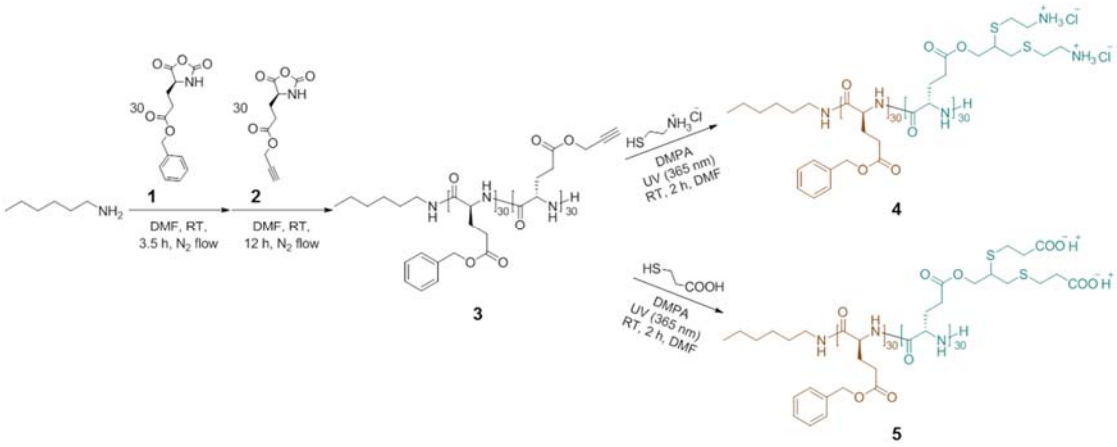

Figure 3.1. Synthetic route of diblock copolypeptide PBLG$_{30}$-*b*-PPLG$_{30}$ **3** *via* one-pot sequential polymerizations of BLG **1** and PLG **2** NCA monomers, followed by post-polymerization modifications to prepare positively-charged diblock copolypeptide **4** or negatively-charged diblock copolypeptide **5** *via* radical-mediated thiol-yne click-type chemistry with corresponding 2-aminoethanethiol hydrochloride or 3-mercaptopropionic acid, respectively.

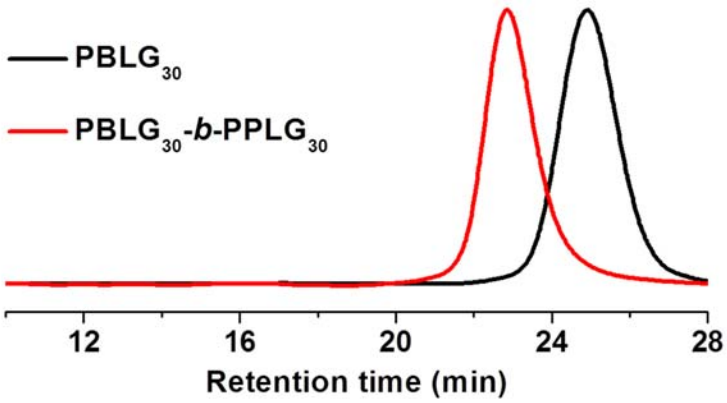

Figure 3.2. GPC traces of homopolypeptide PBLG$_{30}$ at M_n = 6.7 kDa (from ^{1}H NMR) and PDI = 1.10 (from GPC, black line) and diblock copolypeptide PBLG$_{30}$-*b*-PPLG$_{30}$ 3 at M_n = 11.7 kDa (from ^{1}H NMR) and PDI = 1.08 (from GPC, red line) *via* one-pot sequential polymerizations with the N_2 flow method.

The radical-mediated thiol-yne click-type reaction is a robust and versatile approach that tolerates a variety of functional groups, such as carboxylic acid or amino groups, to rapidly and efficiently functionalize the alkynyl groups without the use of a metal catalyst.[119] In order to graft charged side-chain moieties onto the backbones of copolypeptides in the construction of amphiphilic block copolypeptides, the thiol-yne click chemistry was applied by coupling two thiol reagents with one alkynyl group of each repeat unit within the PPLG block to achieve a double addition product with 1,2-regioselectivity. With the aim of avoiding chain-chain coupling or crosslinking, as well as ensuring high efficiency, a total amount of 20 equivalents of thiol reagents relative to the alkynyl groups were used in the thiol-yne click reaction under UV irradiation with 2,2-dimethoxy-2-phenylacetophenone (DMPA) as the photoinitiator. The commercially-available 2-aminoethanethiol hydrochloride and 3-mercaptopropionic acid were utilized to synthesize the corresponding positively-charged **4** and negatively-charged **5** diblock copolypeptides, followed by their self-assembly into cationic **6** and anionic **7** micellar nanoparticles, respectively (Figure 3.3). In addition, the linkers between the side-chain charged groups along the polypeptide backbones (10 and 11 σ-bonds) were expected to minimize the effect of side-chain repulsion and maintain the helical conformation of **4** and **5**.[30] The obtained 1,2-dithioester products were characterized by ^{1}H NMR spectroscopy by using deuterated trifluoroacetic acid (TFA-D) as the solvent, which was capable of breaking the strong hydrogen-bonding between the polypeptide segments and maintaining the diblock copolypeptides in the solution state (Figure 3.4). The diastereotopic splitting of the methylene protons (j in

both Figure 3.4b and 3.4c), corresponding to the 1,2-regioselectivity from the thiol-yne reaction, together with the observation of other functional groups demonstrated the successful installation of the charged and functionalized thiol reagents onto the backbone of **3**.

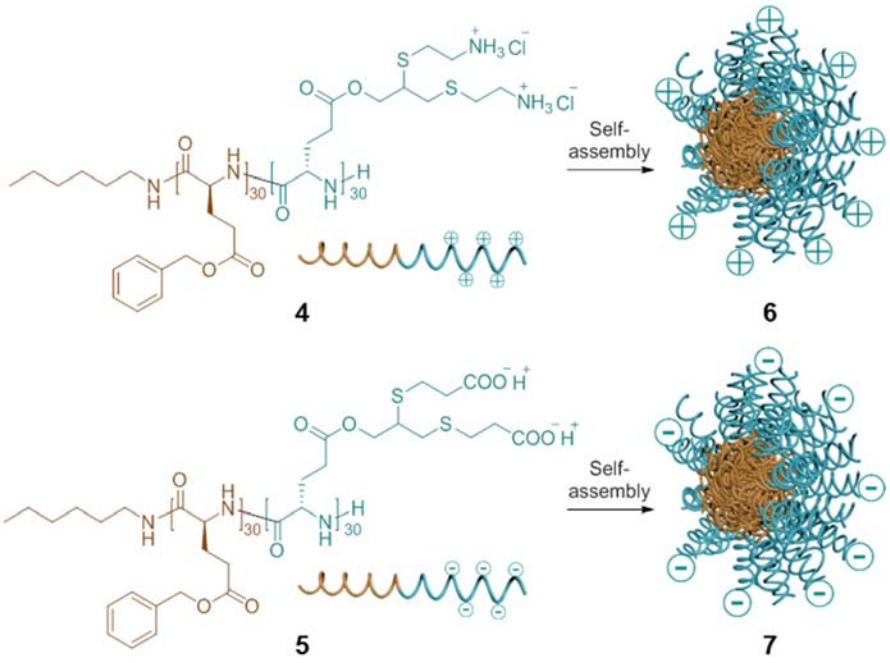

Figure 3.3. Schematic representation of the self-assembly of **4** and **5** into micellar cationic **6** and anionic **7** nanoparticles, respectively.

The self-assembly behaviors of the two amphiphilic diblock copolypeptides were evaluated by either direct re-suspension of lyophilized polymer **4** into nanopure water or a nanoprecipitation method by adding the organic solution of polymer **5** into nanopure water. The positively-charged diblock copolypeptide **4** was directly suspended into nanopure water at a concentration of 1 mg/mL, followed by sonication for 10 min at

room temperature, resulting in spontaneous formation of cationic nanoparticles **6**. However, the negatively-charged diblock copolypeptide **5** was unable to be directly suspended into water, rather, the corresponding anionic nanoparticles **7** were prepared by adding a DMF solution of the polymer into nanopure water, followed by further dialysis against nanopure water. The morphologies of the resulting nanoparticles were characterized by transmission electron microscopy (TEM) and dynamic light scattering

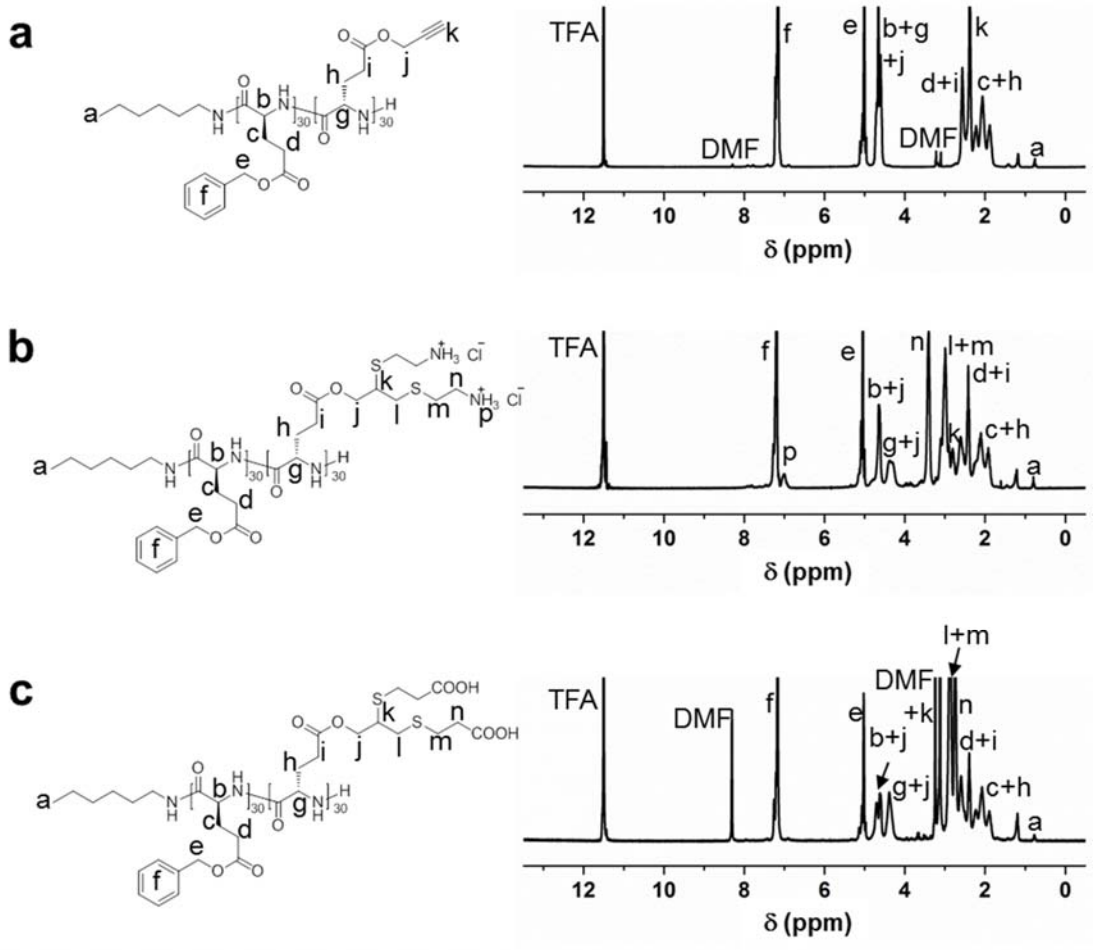

Figure 3.4. ^{1}H NMR spectra of diblock copolypeptide **3** (a), charged diblock copolypeptides **4** (b) and **5** (c) after thiol-yne modifications.

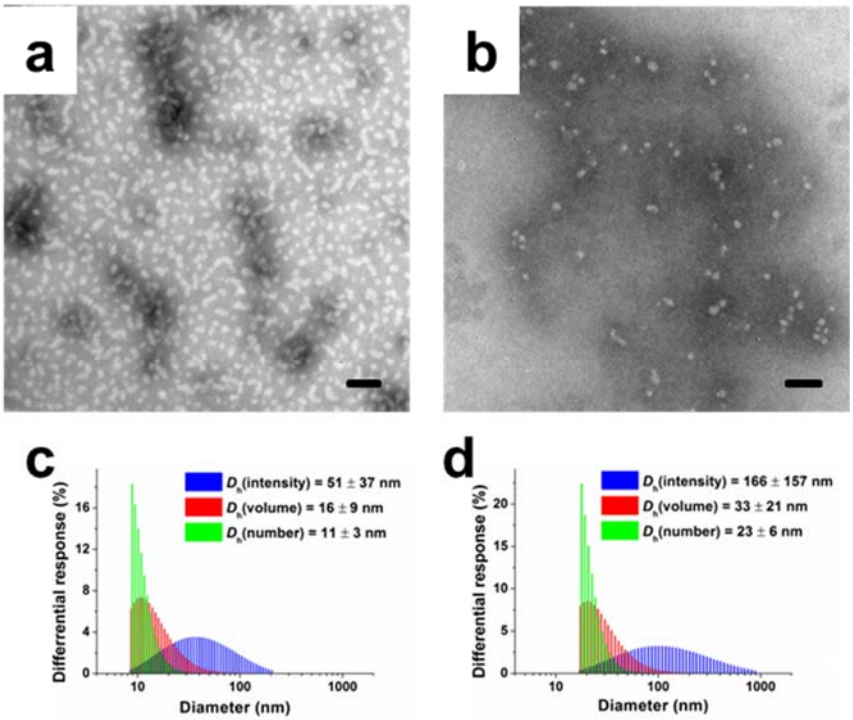

Figure 3.5. TEM images for cationic **6** (a) and anionic **7** (b) nanoparticles. The scale bars in both TEM images are 50 nm. (c) DLS results of cationic nanoparticles **6**: D_h (intensity) = 51 ± 37 nm, D_h (volume) = 16 ± 9 nm and D_h (number) = 11 ± 3 nm. (d) DLS results of anionic nanoparticles **7**: D_h (intensity) = 166 ± 157 nm, D_h (volume) = 33 ± 21 nm and D_h (number) = 23 ± 6 nm.

(DLS). DLS analyses revealed that **4** underwent assembly with high uniformity of the resulting nanoparticles, giving a number-averaged hydrodynamic diameter of 11 ± 3 nm for **6** (Figure 3.5c), whereas the assemblies from **5** were larger and of broader size distribution, 23 ± 6 nm for **7** (Figure 3.5d). The monomodal distributions in DLS for both **6** and **7** suggested that the nanoparticle assemblies were well-defined, which were also observed in TEM images (Figure 3.5a and 3.5b, respectively). However, TEM imaging reveals that the morphologies are not spherical, but more likely of a globular

nature. Moreover, upon storage, elongation of the nanoassembly morphologies occurred to produce rod-like or cylindrically-shaped nanostructures. These unique long-term assembly processes are under further evaluation. The surface charge densities were characterized *via* zeta potential analyses in nanopure water at pH 5.6. Zeta potential values of 28 ± 2 mV (**6**) and -62 ± 1 mV (**7**) indicated the cationic and anionic surface characteristics of the self-assembled nanoparticles.

Due to the distances between the charged side-chain groups and the polypeptide backbones, helical conformations were expected for the charged block polypeptides **4** and **5**. FTIR and circular dichroism (CD) studies were employed to confirm the α-helical conformations of the polypeptide backbones. For both charged block copolypeptides, the absorbances in the FTIR spectra (Figure 3.6a and 3.6b, respectively) at ~1650 cm^{-1} (amide I region) and 1547 cm^{-1} (amide II region) were attributed to α-helical conformations.[120] In the CD measurement, the polymer concentration of the nanoparticle solution in nanopure water was diluted to 0.1 mg/mL. The one positive band at 196 nm as well as two negative bands at 208 and 222 nm in the CD spectra indicated α-helical structures for both **4** and **5** (Figure 3.6c and 3.6d, respectively). The critical micelle concentration (CMC) of **4** and **5** were measured to be 0.19 mg/mL and 0.10 mg/mL, which means that the CD measurements conducted at 0.1 mg/mL observed α-helical conformations primarily for free polymer chains. However, the negative bands were maintained (while the intensity of the positive band was off-scale) when the solution concentrations were increased to above the CMC values, suggesting that the α-helical conformations were largely maintained for the polypeptide backbones in the

self-assembled cationic **6** and anionic **7** micellar nanoparticles.[121] Due to the significant role of α-helical conformation in the regulation of protein folding and biological activity, its presence in these polypeptide nanoassemblies is an attractive property to impart biological activity, such as cell penetration efficiency, for the polypeptide-based nanoparticles for biomedical applications.

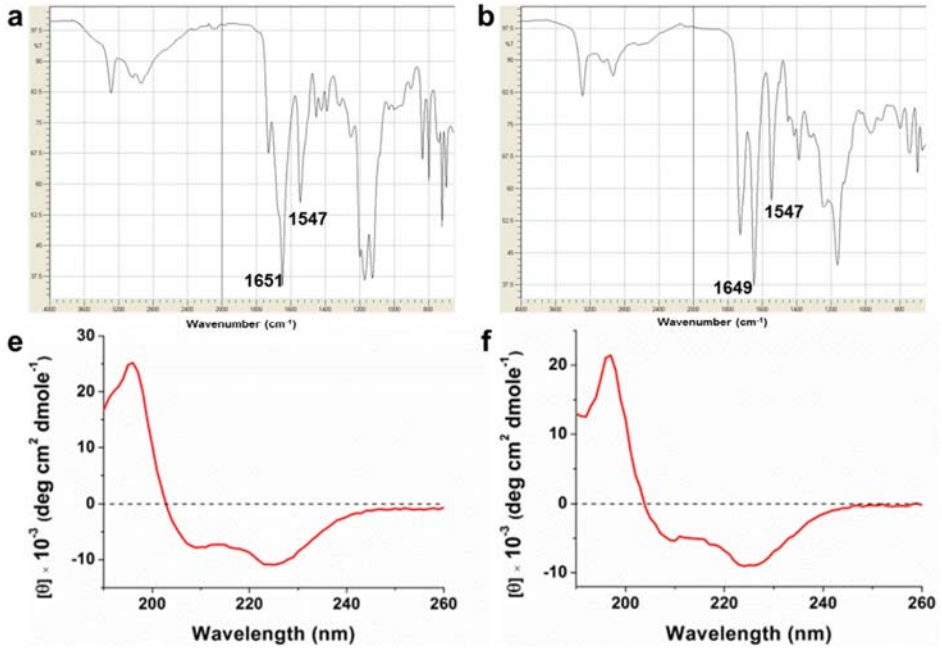

Figure 3.6. FTIR spectra of charged diblock copolypeptides **4** (a) and **5** (b) in the solid state. CD spectra of **4** (e) and **5** (f) in nanopure water at a polymer concentration of 0.1 mg/mL.

With the development of cationic nanoparticle **6** from the positively-charged diblock copolypeptide **4**, the ability of cationic nanoparticle **6** to efficiently complex Cy3-labeled small interfering ribonucleic acid (siRNA, molecular weight *ca.* 13814.3 g/mol) *via* electrostatic interaction, was investigated at a wide range of ammonium to

phosphorous (N^+/P^-) ratios. At an N^+/P^- ratio of 4, the cationic nanoparticle **6** was able to completely bind siRNA, as confirmed by the gel retardation assay (Figure 3.7), in which the dye-labeled siRNA was maintained in the loading well during the gel electrophoresis experiment.

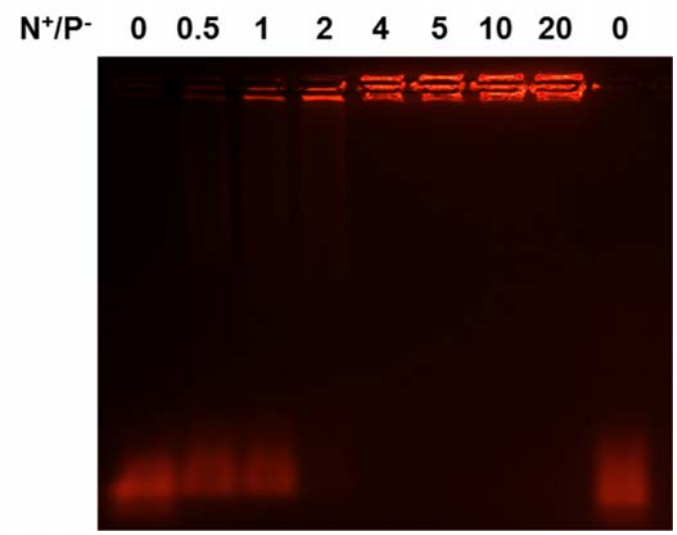

Figure 3.7. Gel retardation assay of siRNA binding to cationic nanoparticle **6** at various N^+/P^- ratios by mixing the nanoparticle solutions at different concentrations with Cy3-labeled siRNA. Agarose gel electrophoresis was run at 100 V for 20 min.

The cytotoxicity of the cationic nanoparticle **6** was evaluated in RAW 264.7 mouse macrophages and human ovarian adenocarcinoma (OVCAR-3) cells. In the concentration range of 0.2 - 100 μg/mL, the cationic nanoparticle **6** exhibited minimum cytotoxicity to both cells (Figure 3.8). Actually in OVCAR-3 cells, a largely higher cell viability compared with the control group was observed, indicating interesting positive effect of the nanoparticle on the cell growth at the low concentration. With the concentration of the nanoparticle higher than 100 μg/mL, cytotoxicity was observed in

both RAW 264.7 and OVCAR-3 cells, which might result from the attachment of the extra ammonium sites onto cell membrane to affect cell growth.

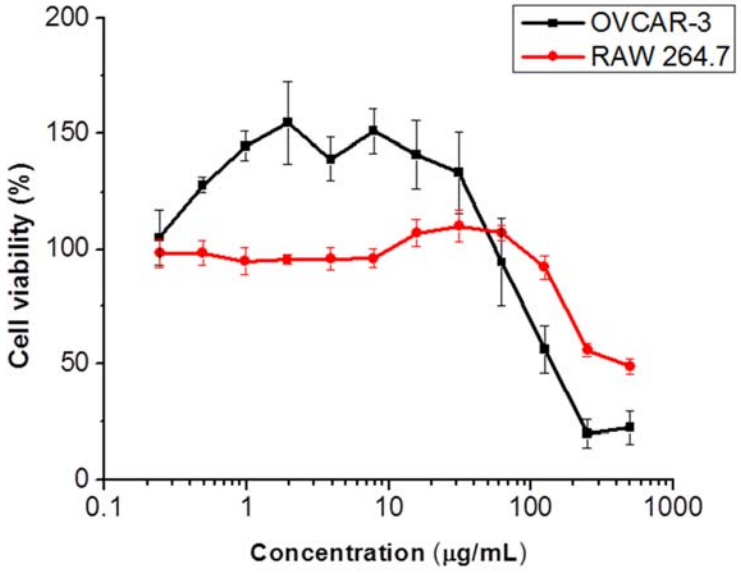

Figure 3.8. Viability of RAW 264.7 mouse macrophages and OVCAR-3 cells of cationic nanoparticle **6** with final concentrations ranging from 0.2 – 500 μg/mL and incubation time of 72 h.

The cellular uptake of Cy3-labeled siRNA complexed with cationic nanoparticle **6** at N^+/P^- ratio of 10 was studied by laser scanning confocal microscopy and compared to Lipofectamine (Figure 3.9). The complex of siRNA and cationic nanoparticle **6** was efficiently taken up by OVCAR-3 cells and RAW 264.7 mouse macrophages, as indicated by the distribution of the red color (Cy3-siRNA) in the two-dimensional images collected by the confocal microscopy. Lower uptake was observed for siRNA complex with Lipofectamine.

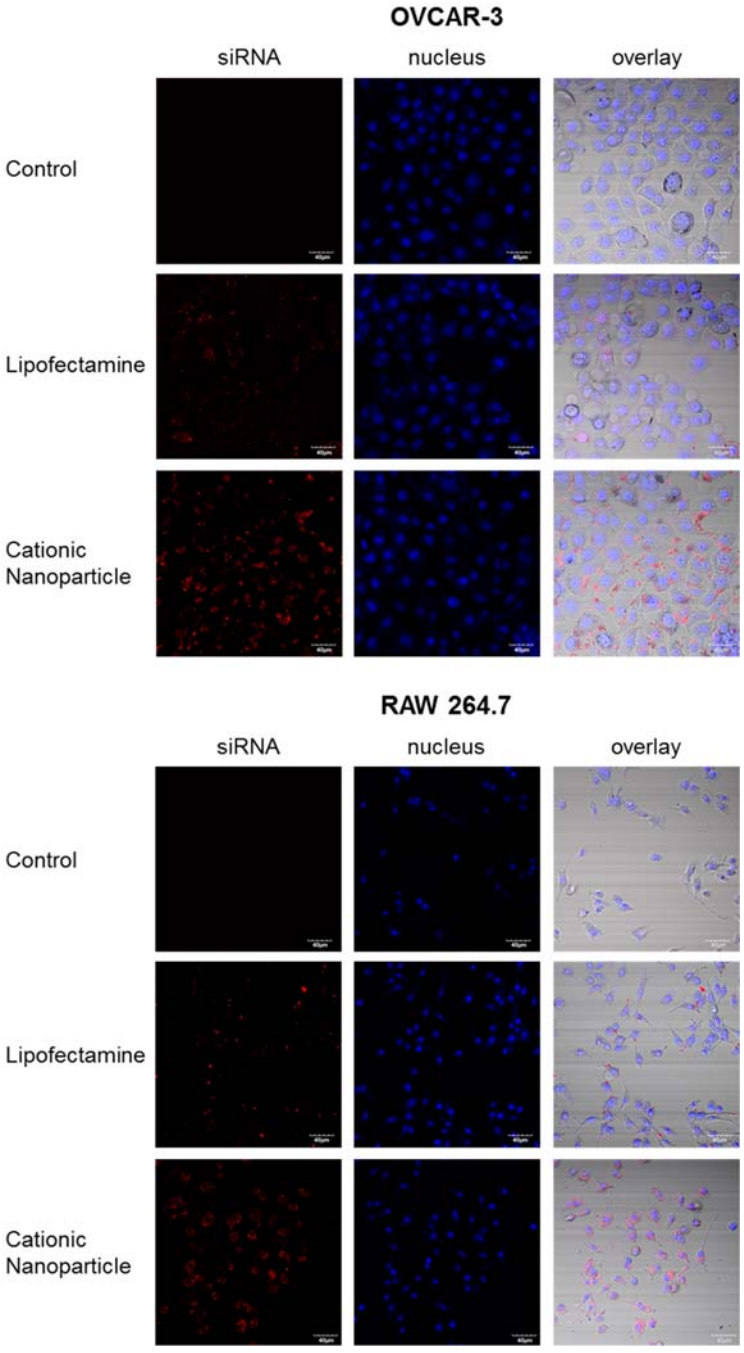

Figure 3.9. Fluorescence confocal images of siRNA delivery by cationic nanoparticle **6** with control group (siRNA only) and Lipofectamine at N^+/P^- ratio of 10 in OVCAR-3 cells and RAW 264.7 mouse macrophages.

The abilities of the cationic nanoparticle **6** loaded with AllStars cell-death siRNA to affect cell viability were determined, with comparisons made against the nanoparticle complexed with negative-control siRNA and Lipofectamine control (Figure 3.10). The effect of N^+/P^- ratio on the transfection efficiency of cell-death siRNA complexed to cationic nanoparticle **6** was studied in OVCAR-3 cells. As indicated from the high cell viability in Figure 3.10, very low transfection efficiency of siRNA complex with cationic nanoparticle **6** at various N^+/P^- ratios was observed, which might result from the strong complexation between siRNA and cationic nanoparticle **6**.

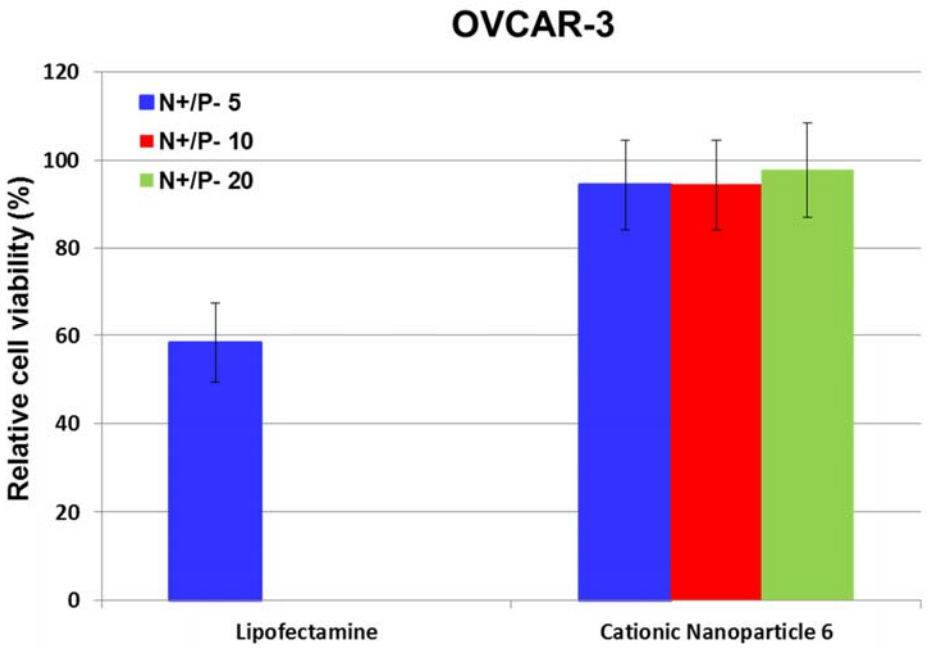

Figure 3.10. Transfection efficiency of cell-death siRNA complexed with Lipofectamine, cationic nanoparticle **6** into OVCAR-3 cells at N^+/P^- ratios of 5, 10, and 20. The transfection efficiency was determined by comparing the viabilities of cells treated with cell-death siRNA complexes *vs.* negative control-siRNA complexes.

3.4 Conclusions

In summary, a polypeptide-based versatile and functional nanoparticle platform with reactive, positively- or negatively-charged functionalities was developed from a sequential ring-opening polymerization (ROP) and chemical transformation strategy. Well-defined diblock copolypeptide, PBLG-*b*-PPLG, with the incorporation of the alkynyl functional groups was prepared by performing facile and straightforward one-pot sequential ROPs of BLG and PLG NCA monomers with accelerated polymerization rates by N_2 flow. The clickable alkynyl groups were then modified to install different charges and side-chain functionalities onto the polypeptide backbones with diverse thiol reagents by photoinitiated, radical-medicated thiol-yne click-type chemistry. The resulting amphiphilic block copolypeptides were self-assembled by either direct re-suspension or a nanoprecipitation method into nanopure water to form globular nanoparticles with distinct surface charges, as shown from DLS, TEM and zeta potential analyses. The distances between charged side-chain groups and polypeptide backbones rendered the charged block copolypeptides to maintain the helical conformations in aqueous solution, which was demonstrated by a combination of FTIR and CD characterizations.

The polypeptide-based cationic nanoparticle was further investigated as a potential siRNA carrier by the formation of delivery complex with siRNA *via* the electrostatic interaction. At the N^+/P^- ratio of 4, the cationic nanoparticle was demonstrated to be able to completely bind siRNA, which was indicated in the gel retardation assay. Minimum cytotoxicity of the cationic nanoparticle was achieved at

the concentration lower than 100 μg/mL and highly efficient cellular uptake of the delivery complex was shown in the confocal images for both RAW 264.7 mouse macrophages and OVCAR-3 cells. However, quite low transfection efficiency was observed for this delivery complex and current research effort is focused on reconfiguring the linear polypeptide into molecular brush structures to explore the effect of molecular architecture to improve gene delivery efficiency.

CHAPTER IV

FACILE SYNTHESES OF POLYPEPTIDE MOLECULAR BRUSHES WITH TWO-DIMENSIONAL CONTROL: *N*-CARBOXYANHYDRIDE RING-OPENING POLYMERIZATION AND RING-OPENING METATHESIS POLYMERIZATION[*]

4.1 Introduction

Molecular brushes are a novel class of cylindrical polymer materials, in which the linear flexible or rigid side chains are densely attached and packed along a linear polymer main chain.[122] With the high rigidity and large persistent length, versatile chemical structure variability, and the nanosized dimension of individual molecule, molecular brushes have gathered intense research attention with broad applications, including in the biomedical and microelectronic fields.[123-125] With the densely-packed brush side chains, molecular brush architecture can improve the efficiency of the delivery system and enhance the protection of therapeutic agents when acting as a therapeutic career.[125-128] Most recently, Zhang and coworkers reported a novel brush-polymer/DNA conjugation system that provided DNA with nanoscale steric selectivity when DNA was attached onto one end of brush backbone.[125] The hybridization with complementary DNA remained unaffected due to the small size while the interactions with protein were limited due to the steric hindrance from the

[*] In collaboration with Yannick P. Borguet, Lu Su, Xun He, Tan Nguyen, Karen L. Wooley, Departments of Chemistry, Chemical Engineering, Materials Science and Engineering, and Laboratory for Synthetic-Biologic Interactions, Texas A&M University.

densely-packed side chains, resulting in the enhanced resistance of the DNA against proteinases. The retarded protein adhesion also improved *in vivo* biodistribution with longer blood circulation, which enabled this conjugation system for oligonucleotide-based therapies. Most molecular brushes developed so far contain flexible side chains made from polyolefins, polyesters and polyethers.[129,130] Molecular brushes containing rigid side chains would render brushes with unique properties, while synthetic challenges for such materials with controlled molecular weights (MWs) and narrow molecular weight distributions (MWDs) are remained.[131-133]

Polypeptides consisting of α-amino acids with covalent linkages share significant similarities to natural proteins, and recent synthetic methodology developments have facilitated their extensive utilization in biomedical areas, such as serving as scaffolds for tissue engineering, matrices for drug and gene delivery, and responsive materials for biosensors.[59,75,76] Polypeptides have been recently utilized as rigid polymers due to their capability to form well-defined secondary structures, including α-helix and β-sheet.[123,131,132] Thus, incorporating polypeptides with well-defined structures into the molecular brush architecture can provide brush-like materials with novel and unique properties.[134,135] The most common approach to synthesize polypeptide materials involves ring-opening polymerizations (ROPs) of amino acid *N*-carboxyanhydride (NCA) monomers. In the last decade, several controlled NCA ROPs have been reported to prepare well-defined polypeptides by reducing side reactions that decrease the activity of the terminal amine during polymerizations.[46,50,52,53] Our group had previously reported a straightforward method to enhance the polymerization rate while maintain the controlled

features of NCA polymerization by applying continuous N_2 flow to remove the CO_2 from the polymerization, which offered a easily operational method for the syntheses of polypeptides with controllable polymerization rates, predictable MWs, and narrow MWDs.

Molecular brushes are commonly prepared *via* three synthetic strategies: "grafting onto", "grafting from" and "grafting through", with unique advantages and challenges for each method. "Grafting onto" and "grafting from" strategies had been widely used to construct polypeptide-based molecular brushes.[115,123,131-133,136-139] In 2009, Dr. Hammond's group reported an alkyne-functionalized polypeptide and the molecular brushes were synthesized by grafting azido-terminated poly(ethylene glycol) (PEG) onto the polypeptide backbones.[115] With the efficient azide-alkyne cycloaddition click chemistry, the grafting efficiency was achieved higher than 95%. Cheng and coworkers reported a one-pot synthesis of polypeptide molecular brush by firstly polymerizing norbornene monomer containing *N*-trimethylsilyl (N-TMS) group using ring-opening metathesis polymerization (ROMP).[132] The N-TMS not only served as a protection group for amino groups during the ROMP for the brush backbones, but also could initiate the polymerization of NCA monomers in a controlled manner. However, polypeptide-based molecular brushes were rarely reported by using "grafting through" synthetic strategy. Herein, we reported a "grafting through" synthetic approach for the preparation of well-defined molecular brushes bearing polypeptide side chains by integrating NCA ROPs with ROMPs. A two-dimensional control over the molecular architectures of brushes was realized by building the desirable segment lengths of

polypeptide side chains and brush backbones, independently, in controlled manners. A new type of brush-like polymer, poly(norbornene-*graft*-poly(β-benzyl-L-aspartate)) (P(NB-*g*-PBLA)), was synthesized *via* the ROMP of NB-terminated polypeptide macromonomers in a mixture of ionic liquid and dichloromethane (DCM). The N_2 flow accelerated NCA ROP was utilized to prepare polypeptide macromonomers with different lengths by using NB-based primary amine as the initiator.

4.2 Experimental section

4.2.1 Materials

Ethyl acetate, *n*-hexane, diethyl ether, methanol, dichloromethane (DCM, anhydrous, ≥ 99.8%), *N,N*-dimethylformamide (DMF, anhydrous, ≥ 99.8%), *N,N*-dimethylacetamide (DMAc, anhydrous, ≥ 99.8%), potassium hydroxide (KOH, ≥ 97%), sodium chloride (NaCl, ≥ 99%), potassium carbonate (K_2CO_3, ≥ 99%), β-benzyl-L-aspartate (≥ 99%), bis(trichloromethyl) carbonate (≥ 98%), 1,8-diaminooctane, acetyl anhydride, *exo*-5-norbornenecarboxylic acid, *N*-hydroxysuccinimide, 1-ethyl-3-(3-dimethylaminopropyl) carbodiimide (EDC) hydrochloride, *N*-Boc-ethylenediamine, 1-butyl-3-methylimidazolium tetrafluoroborate ([bmim][BF_4]), 1-butyl-2,3-dimethylimidazolium tetrafluoroborate ([bdmim][BF_4]) were purchased from Sigma-Aldrich company (USA). All chemicals were used without further purification, unless otherwise noted. The modified Grubbs' catalyst was synthesized according to the literature report.[140]

4.2.2 Instrumentation

^{1}H and ^{13}C NMR spectra were recorded on a Varian Inova 500 spectrometer interfaced to a UNIX computer using VnmrJ software. Chemical shifts were referenced to the solvent resonance signals. Attenuated total reflectance-Fourier transform infrared spectroscopy (ATR-FTIR) spectra were recorded on an IR Prestige 21 system (Shimadzu Corp., Kyoto, Japan) and analyzed using IRsolution v. 1.40 software.

N,N-Dimethylformamide-based gel permeation chromatography (DMF GPC) was conducted on a Waters (Waters Chromatography, Inc., Milford, MA) system equipped with an isocratic pump model 1515, a differential refractometer model 2414, a PD2020 dual-angle (15° and 90°) light scattering detector (Precision Detectors, Inc.), and a four-column set of 5 μm Guard (50 × 7.8 mm), Styragel HR 4 5 μm DMF (300 × 7.8 mm), Styragel HR 4E 5 μm DMF (300 × 7.8 mm), and Styragel HR 2 5 μm DMF (300 × 7.8 mm). The system was equilibrated at 70 °C in pre-filtered DMF (containing 0.05 mol/L LiBr), which served as the polymer solvent and eluent (flow rate set to 1.00 mL/min). Polymer solutions were prepared at a known concentration (3.0 – 5.0 mg/mL) and an injection volume of 200 μL was used. Data collection and analysis were performed with Precision Acquire software and Discovery 32 software (Precision Detectors, Inc.), respectively. Inter-detector delay volume and the light scattering detector calibration constant were determined by calibration using a nearly monodispersed polystyrene (PS) standard (Polymer Laboratories, M_p = 90 kDa, M_w/M_n < 1.04). The differential refractometer was calibrated with stand PS material (SRM 706 NIST), of known specific refractive index increment dn/dc (0.184 mL/g). The dn/dc

values of the analyzed polymers were then determined from the differential refractometer response. The system was calibrated with PS standards (Polymer Laboratories, Amherst, MA) ranging from 1480 to 1233000 Da and poly(ethylene oxide) (PEO) standards (Polymer Laboratories, Amherst, MA) ranging from 1010 to 723500 Da.

Thermogravimetric analysis (TGA) was performed under argon atmosphere using a Mettler-Toledo model TGA/SDTA851^e (Mettler-Toledo, Inc., Columbus, OH), with a heating rate of 10 °C/min. Measurements were analyzed using Mettler-Toledo STAR^e v. 7.01 software. Glass transition temperatures (T_g) were measured by differential scanning calorimetry (DSC) on a Mettler-Toledo DSC822® (Mettler-Toledo, Inc., Columbus, OH), with a heating rate of 5 °C/min. Measurements were analyzed using Mettler-Toledo STAR^e v. 7.01 software. The T_g was taken as the midpoint of the inflection tangent, upon the second heating scan.

4.2.3 Experimental procedures

Synthesis of *exo*-*N*-(8-aminooctyl)bicyclo[2.2.1]hept-5-ene-2-carboxamide (NB-amine initiator, 1)

A mixture of *exo*-5-norbornenecarboxylic acid (1.50 g, 10.8 mmol), *N*-hydroxysuccinimide (1.58 g, 14.7 mmol) and 1-ethyl-3-(3-dimethylaminopropyl) carbodiimide (EDC) hydrochlorid (2.68 g, 14.1 mmol) was stirred in dry dichloromethane (DCM) (30 mL) for 8 hours at room temperature. The solvent was evaporated in vacuum (rotovap) and the crude reaction mixture was purified by flash chromatography (ethyl acetate : *n*-hexane = 1 : 2). The solution of the activated ester in dry DCM (60 mL) was added dropwise over 1 h period to a vigorously stirred solution

of 1,8-diaminooctane (7.8 g, 54 mmol) in dry DCM (30 mL). The solution was stirred overnight at room temperature and quenched with concentrated potassium hydroxide (20 mL). The product was extracted with ethyl acetate (3 × 150 mL), the organic fraction were collected and washed with basic water (pH ~ 14, 20 mL) and finally basic brine (20 mL). The organic phase was dried over potassium carbonate and the product purified by flash chromatography (silica, eluent: methanol/chloroform/$NH_4OH_{aq,\ conc.}$ = 100/800/10) upon removal of the volatiles under reduced pressure, and the residual methanol was removed by azeotropic distillation with DCM (3 × 30 mL). The targeted compound appeared as light yellow oil (2.45 g, 86 %). ^{1}H NMR (500 MHz, $CDCl_3$, ppm): δ 1.20-1.33 (m, 12H), 1.35-1.42 (m, 2H), 1.42-1.51 (m, 2H), 1.69 (d, *J* = 8.3 Hz, 1H), 1.87 (dt, *J* = 8.1, 3.8 Hz, 1H), 1.91-1.96 (m, 1H), 2.60-2.67 (m, 2H), 2.84-2.89 (m, 2H), 3.18-3.24 (m, 2H), 5.51 (s, 1H), 6.06 (dd, *J* = 5.6, 3.2 Hz, 1H), 6.10 (dd, *J* = 5.6, 3.1 Hz, 1H). ^{13}C NMR (125 MHz, $CDCl_3$, ppm): δ 27.0, 27.1, 29.4, 29.6, 29.9, 30.7, 34.0, 39.8, 41.7, 42.4, 45.0, 46.5, 47.4, 136.2, 138.4, 175.7. FTIR (cm^{-1}): 3294, 2924, 2852, 1643, 1537, 1454, 1440, 1244. HRMS: calculated $[M+H]^+$ for $C_{15}H_{24}N_2O_3$: 265.2280, found: 265.2270.

Synthesis of β-benzyl-L-aspartate *N*-carboxyanhydride (BLA NCA) monomer

In a 250 mL three-necked round bottom flask equipped with a magnetic stirrer, condenser and N_2 inlet, BLA NCA monomer was synthesized from β-benzyl-L-aspatate (5.0 g, 22 mmol, 2 equiv) and bis(trichloromethyl) carbonate (3.3 g, 11 mmol, 1 equiv) in 100 mL dry ethyl acetate at 80 °C under N_2 flow for 3 hours.[141] The reaction solution became clear around 1 h after the addition of bis(trichloromethyl) carbonate. After cooling to room temperature, the reaction mixture was concentrated into white solid,

which was further purified by three times recrystallization with ethyl acetate/*n*-hexane 1:1 (v/v), and dried in vacuum to obtain a white needle-like crystal (3.5 g, yield: 63%). The product was stored in -20 °C freezer under N_2 atmosphere. ^{1}H NMR (500 MHz, DCM-D_2, ppm): δ 2.91 (dd, *J* = 8.4 Hz, *J* = 17.8 Hz, 1H, CHC*H*$_2$COO), 3.07 (dd, *J* = 3.4 Hz, *J* = 17.8 Hz, 1H, CHC*H*$_2$COO), 4.60 (ddd, *J* = 3.4 Hz, *J* = 8.4 Hz, *J* = 1.2 Hz, 1H, C*H*CH$_2$COO), 5.18 (s, 2H, COOC*H*$_2$), 6.32 (br, 1H, CON*H*CH), 7.37 (m, 5H, Ar*H*). ^{13}C NMR (125 MHz, DCM-D_2, ppm): δ 34.9, 53.6, 66.3, 128.2, 128.2, 128.5, 135.5, 152.2, 169.3, 171.0. FTIR (cm^{-1}): 3450-3100, 3030, 2971, 2941, 2900, 1833, 1782, 1725, 1258, 1173, 1110, 923, 747. HRMS: calculated [M-H]$^-$ for $C_{12}H_{11}NO_5$: 248.0559, found: 248.0561.

Synthesis of poly(β-benzyl-L-aspartate) (PBLA) initiated by NB-amine initiator, 1

In a 25 mL flame dried Schlenk flask equipped with a magnetic stirrer, *exo*-*N*-(8-aminooctyl)bicyclo[2.2.1]hept-5-ene-2-carboxamide (NB-amine, **1**, 106.1 mg, 0.401 mmol, 1 equiv) was added into a solution of BLA NCA (1.0 g, 4.0 mmol, 10 equiv) in 15 mL anhydrous DMF solution. The reaction mixture was stirred with a stir rate of 400 rpm under continuous N_2 flow (100 mL/min) at room temperature. The Schlenk flask was capped with a rubber stopper with a needle outlet connected with a drying tube. FTIR was used to monitor the process of reaction and over 99% of BLA NCA monomer was consumed in 12 h. After evaporation of DMF, the crude product was re-dissolved into 30 mL DCM and precipitated into 300 mL diethyl ether at 0 °C under vigorous stirring three times. A white powder was obtained after centrifuging and drying in vacuum at room temperature (0.53 g, yield: 57 %). ^{1}H NMR (500 MHz, DMSO-D_6,

ppm): δ 1.17 (br, 12H, $CH_2CH_2CH_2$), 1.33 (br, 4H, $CONHCH_2$), 1.63 (d, 1H), 1.75 (dt, 1H), 2.00 (dd, 1H), 2.61 (br, 10H, $CHCH_2CO$), 2.81 (br, 10H, $CHCH_2CO$; br, 4H), 4.11 (br, 1H, chain-end $COCHNH_2$), 4.63 (br, 9H, COCHNH), 5.03 (br, 20H, $COOCH_2Ar$), 6.11 (s, 2H, NB alkenyl protons), 7.31 (br, 50H, ArH), 8.21 (br, 13H, NH). ^{13}C NMR (125 MHz, DMSO-D_6, ppm): δ 26.2, 26.4, 28.7, 28.8, 29.2, 29.8, 35.9, 38.6, 41.0, 43.0, 45.6, 46.9, 49.5, 64.9, 65.8, 127.9, 128.1, 128.3, 136.0, 136.3, 137.6, 170.0, 174.3. FTIR (cm^{-1}): 3277, 3065, 3034, 2934, 1730, 1634, 1530, 1454, 1385, 1165, 970, 735, 694. GPC: PEO standard: M_n = 1.1 kDa, M_w = 1.2 kDa, PDI = 1.17, PS standard: M_n = 6.0 kDa, M_w = 6.4 kDa, PDI = 1.07.

Synthesis of PBLA macromonomer initiated by NB-amine initiator, 1, with direct chain-end modification after polymerization

Norbornene(NB)-PBLA macromonomers with different chain length were synthesized in a similar approach and the detailed synthesis of NB-$PBLA_{10}$ was described here. In a 25 mL flame dried Schlenk flask equipped with a magnetic stirrer, NB-amine, **1**, (106.1 mg, 0.401 mmol, 1 equiv) was added into a solution of BLA NCA (1.0 g, 4.0 mmol, 10 equiv) in 10 mL anhydrous DMF solution. The reaction mixture was stirred with a stir rate of 400 rpm under continuous N_2 flow (100 mL/min) at room temperature. The Schlenk flask was capped with a rubber stopper with a needle outlet connected with a drying tube. FTIR was used to monitor the process of reaction and over 99% of BLA NCA monomer was consumed in 12 h. Then acetyl anhydride (204.8 mg, 2.0 mmol, 5 equiv) was added into the reaction mixture by syringe in a dropwise manner and the reaction mixture was allowed to proceed at room temperature for 3 h.

After evaporation of DMF, the crude product was re-dissolved into 30 mL DCM and precipitated into 300 mL diethyl ether at 0 °C under vigorous stirring three times. A white powder was obtained after centrifuging and drying in vacuum at room temperature (612.8 mg, yield: 75 %). ^{1}H NMR (500 MHz, DMSO-D_6, ppm): δ 1.18 (br, 12H, $CH_2CH_2CH_2$), 1.33 (br, 4H, CONHCH_2), 1.64 (d, 1H), 1.75 (dt, 1H), 1.79 (s, 3H, COCH_3), 2.00 (dd, 1H), 2.61 (br, 10H, CHCH_2CO), 2.81 (br, 10H, CHCH_2CO; br, 4H), 4.62 (br, 10H, COC*H*NH), 5.03 (br, 20H, COOCH_2Ar), 6.10 (s, 2H, NB alkenyl protons), 7.31 (br, 50H, Ar*H*), 8.16 (br, 12H, N*H*). ^{13}C NMR (125 MHz, DMSO-D_6, ppm) δ 22.5, 26.2, 26.4, 28.7, 28.9, 29.2, 29.8, 35.8, 38.6, 41.0, 43.0, 45.6, 46.9, 49.6, 65.8, 127.9, 128.0, 128.4, 136.0, 136.3, 137.7, 169.4, 169.7, 169.8, 170.1, 170.3, 170.7, 174.3. FTIR (cm^{-1}): 3277, 3065, 2932, 2857, 1732, 1634, 1526, 1454, 1383, 1356, 1215, 1163, 970, 908, 735, 694. GPC: PEO standard: M_n = 1.2 kDa, M_w = 1.4 kDa, PDI = 1.13, PS standard: M_n = 6.5 kDa, M_w = 6.8 kDa, PDI = 1.05. DSC: T_g = 76 °C. TGA in N_2: 20-218 °C, 1% mass loss; 218-269 °C, 38% mass loss; 269-380 °C, 26% mass loss; 380-500 °C, 13% mass loss; 22% mass remaining above 500 °C.

NB-PBLA$_{20}$ was synthesized in the same approach with the reaction concentration diluted to 50 mg/mL for BLA NCA monomer and the recovery yield of the target polypeptide macromonomer was 68%. ^{1}H NMR (500 MHz, DMSO-D_6, ppm): δ 1.17 (br, 12H, $CH_2CH_2CH_2$), 1.32 (br, 4H, CONHCH_2), 1.63 (d, 1H), 1.75 (dt, 1H), 1.79 (s, 3H, COCH_3), 2.00 (dd, 1H), 2.61 (br, 20H, CHCH_2CO), 2.80 (br, 20H, CHCH_2CO; br, 4H), 4.61 (br, 20H, COC*H*NH), 5.03 (br, 40H, COOCH_2Ar), 6.10 (s, 2H, NB alkenyl protons), 7.28 (br, 100H, Ar*H*), 8.16 (br, 22H, N*H*). FTIR (cm^{-1}): 3292,

3034, 2936, 2857, 1732, 1659, 1537, 1454, 1385, 1358, 1215, 1165, 988, 908, 735, 696. GPC: PEO standard: M_n = 1.6 kDa, M_w = 1.9 kDa, PDI = 1.13, PS standard: M_n = 8.1 kDa, M_w = 8.8 kDa, PDI = 1.10. DSC: T_g = 46 °C. TGA in N_2: 20-203 °C, 1% mass loss; 203-254 °C, 36% mass loss; 254-390 °C, 24% mass loss; 390-500 °C, 9% mass loss; 30% mass remaining above 500 °C.

NB-PBLA$_{50}$ was synthesized by changing the reaction solvent from neat DMF to the mixture of DMF : DCM = 1 : 9 (v/v) and the reaction concentration of BLA NCA monomer was diluted to 50 mg/mL. Without the utilization of N_2 flow method during the reaction, the polymerization time extended to 48 h and the recovery yield of the target polypeptide macromonomer was 67%. ^{1}H NMR (500 MHz, DMSO-D_6, ppm): δ 1.17 (br, 12H, $CH_2CH_2CH_2$), 1.33 (br, 4H, CONHCH_2), 1.64 (d, 1H), 1.75 (dt, 1H), 1.79 (s, 3H, COCH_3), 2.00 (dd, 1H), 2.60 (br, 50H, CHCH_2CO), 2.82 (br, 50H, CHCH_2CO; br, 4H), 4.62 (br, 50H, COC*H*NH), 5.01 (br, 100H, COOCH_2Ar), 6.10 (s, 2H, NB alkenyl protons), 7.27 (br, 250H, Ar*H*), 8.18 (br, 52H, N*H*). FTIR (cm^{-1}): 3292, 3034, 2934, 2859, 1732, 1657, 1547, 1454, 1387, 1358, 1256, 1165, 988, 908, 737, 696. GPC: PEO standard: M_n = 3.4 kDa, M_w = 3.9 kDa, PDI = 1.15, PS standard: M_n = 15.7 kDa, M_w = 17.3 kDa, PDI = 1.11. DSC: T_g = 45 °C. TGA in N_2: 20-232 °C, 4% mass loss; 232-313 °C, 41% mass loss; 313-411 °C, 24% mass loss; 411-500 °C, 5% mass loss; 26% mass remaining above 500 °C.

Syntheses of poly-(norbornene-*graft*-poly(β-benzyl-L-aspartate) (P(NB-*g*-PBLA)) brushes *via* ring-opening metathesis polymerizations (ROMPs) with the use of 1-butyl-3-methylimidazolium tetrafluoroborate ([bmim][BF_4])

The polypeptide molecular brush, P(NB-*g*-PBLA) was synthesized by using the ROMP of NB-PBLA macromonomers *via* "grafting through" strategy. As a representative reaction, to a 10 mL Schelenk flask equipped with a magnetic stirring bar dried with flame under N_2 atmosphere, was added the macromonomer NB-$PBLA_{10}$ (300 mg, 125 μmol, 50 equiv) and 3 mL of solvent mixture with DCM : [bmim][BF_4] = 9 : 1 (v/v). The mixture was stirred until the dissolve of macromonomer at room temperature, deoxygenated through three cycles of freeze-pump-thaw and back-filled with N_2. After the last cycle, the stock solution of the modified Grubbs catalyst (1.82 mg, 2.5 μmol, 1 equiv) in 0.05 mL anhydrous DCM (deoxygenated through three cycles of freeze-pump-thaw) was quickly added with an airtight syringe. The reaction mixture was allowed to stir for 3 h at room temperature before quenching the polymerization by adding 20 μL of ethyl vinyl ether (EVE) in 80 μL DCM, and was further allowed to stir for 30 min at room temperature. The solution was precipitated into 40 mL methanol twice and the precipitate was collected through centrifugation, and re-dissolved into 10 mL of DMF. The solution was then precipitated into 40 mL of diethyl ether. The precipitate was collected through centrifugation and kept under vacuum overnight to obtain the target product (225.2 mg, yield: 75% based upon 95% conversion of NB-$PBLA_{10}$). ^{1}H NMR (500 MHz, DMSO-D_6, ppm): δ 1.11 (br, 600H, $CH_2CH_2CH_2$), 1.28 (br, 200H, CONHCH_2), 1.79 (s, 150H, COCH_3), 1.79 (br, 100H), 2.27 (br, 50H),

2.61 (br, 500H, CHC*H*$_2$CO), 2.81 (br, 500H, CHC*H*$_2$CO; br, 200H), 4.62 (br, 500H, COC*H*NH), 5.03 (br, 1000H, COOC*H*$_2$Ar, br, 100H, NB alkenyl protons), 7.27 (br, 2500H, Ar*H*), 8.16 (br, 600H, N*H*). ^{13}C NMR (125 MHz, DMSO-D$_6$, ppm): δ 22.6, 26.4, 26.5, 28.8, 28.9, 29.4, 35.8, 42.6, 49.7, 65.8, 66.0, 127.9, 128.0, 128.5, 135.9, 136.0, 169.6, 169.9, 170.0, 170.2, 170.3, 170.8, 170.9. FTIR (cm^{-1}): 3279, 3030, 2970, 2936, 1738, 1634, 1526, 1454, 1379, 1217, 1163, 1094, 970, 908, 737, 696. GPC: M_n = 144.3 kDa, M_w = 166.0 kDa, PDI = 1.15 (laser detector, dn/dc = 0.0790 mL/g), PEO standard: M_n = 29.2 kDa, M_w = 38.1 kDa, PDI = 1.31, PS standard: M_n = 97.2 kDa, M_w = 122.8 kDa, PDI = 1.26. DSC: T_g = 75 °C, T_g = 122 °C. TGA in N$_2$: 20-200 °C, 2% mass loss; 200-266 °C, 28% mass loss; 266-384 °C, 26% mass loss; 384-500 °C, 10% mass loss; 34% mass remaining above 500 °C.

Syntheses of P(NB-*g*-PBLA) brushes *via* ROMPs with the use of 1-butyl-2,3-dimethylimidazolium tetrafluoroborate ([bdmim][BF$_4$])

The polypeptide molecular brush, P(NB-*g*-PBLA) was synthesized by using the ROMP of NB-PBLA macromonomers *via* "grafting through" strategy. As a representative reaction, to a 10 mL Schelenk flask equipped with a magnetic stirring bar dried with flame under N$_2$ atmosphere, was added the macromonomer NB-PBLA$_{10}$ (300 mg, 125 μmol, 50 equiv) and 3 mL of solvent mixture with DCM : [bdmim][BF$_4$] = 9 : 1 (v/v). The mixture was stirred at 40 °C until the dissolve of macromonomer, deoxygenated through three cycles of freeze-pump-thaw and back-filled with N$_2$. After the last cycle, the reaction mixture was heated up to 40 °C and the stock solution of the modified Grubbs catalyst (1.82 mg, 2.5 μmol, 1 equiv) in 0.05 mL anhydrous DCM

(deoxygenated through three cycles of freeze-pump-thaw) was quickly added with an airtight syringe. The reaction mixture was allowed to stir for 3 h at 40°C before quenching the polymerization by adding 20 μL of EVE in 80 μL DCM, and was further allowed to stir for 30 min at 40 °C. The solution was precipitated into 40 mL methanol twice and the precipitate was collected through centrifugation, and redissolved into 10 mL of DMF. The solution was then precipitated into 40 mL of diethyl ether. The precipitate was collected through centrifugation and kept under vacuum overnight to obtain the target product (200.5 mg, yield: 70% based upon 95% conversion of NB-PBLA$_{10}$). GPC: M_n = 138.7 kDa, M_w = 163.9 kDa, PDI = 1.18 (laser detector, dn/dc = 0.0790 mL/g), PEO standard: M_n = 51.6 kDa, M_w = 62.2 kDa, PDI = 1.21, PS standard: M_n = 94.7 kDa, M_w = 116.4 kDa, PDI = 1.23. The ^{1}H NMR, ^{13}C NMR, FTIR spectra and thermal analyses results were similar to the polypeptide molecular brush described above.

Post-polymerization modification of P(NB-*g*-PBLA) *via* aminolysis of PBLA

Following the highly reactive aminolysis reaction of PBLA with primary amine under basic condition to produce the corresponding amide product, the post-polymerization modification was performed by using the polypeptide molecular brush with small primary amine-derived reagent. In a flame-dried 10 mL Schlenk flask, P(NB-*g*-PBLA$_{10}$)$_{50}$ (100 mg, 0.758 μmol, 1 equiv, 500 equiv for BLA repeat unit) was dissolved into 2 mL anhydrous *N,N*-dimethylacetamide (DMAc). *N*-Boc-ethylenediamine (3.34 g, 20.9 mmol, 25000 equiv, 50 equiv to BLA repeat unit) was dissolved into 3 mL anhydrous DMAc and added into the reaction flask *via* syringe. The

reaction was allowed to proceed at 50 °C overnight and the reaction solution was precipitated into diethyl ether three times. The precipitate was collected through centrifugation and kept under vacuum to obtain the target product as white powder (88.6 mg, yield: 73% based on upon 95% modification efficiency). ^{1}H NMR (500 MHz, DMSO-D_6, 70 °C, ppm): δ 1.23 (br, 600H, $CH_2CH_2CH_2$), 1.38 (br, 4500H, $NHC(CH_3)_3$, br, 200H, $CONHCH_2$), 1.87 (s, 150H, $COCH_3$), 1.96 (br, 100H), 2.09 (br, 50H), 2.61 (br, 1000H, $CHCH_2CO$), 3.02 (br, 1000H, $CH_2CONHCH_2$), 3.14 (br, 1000H, CH_2CH_2NHCO), 4.55 (br, 500H, $COCHNH$), 5.17 (br, 100H, NB alkenyl protons), 6.51 (br, 500H, $NHBoc$), 8.03 (br, 1110H, NH). FTIR (cm^{-1}): 3289, 3073, 2934, 1736, 1643, 1520, 1447, 1366, 1248, 1167, 1099, 974, 866, 660. GPC: M_n = 152.5 kDa, M_w = 180.1 kDa, PDI = 1.18 (laser detector, dn/dc = 0.0938 mL/g), PEO standard: M_n = 34.3 kDa, M_w = 43.1 kDa, PDI = 1.26, PS standard: M_n = 112.8 kDa, M_w = 139.1 kDa, PDI = 1.23. DSC: T_g = 129 °C. TGA in N_2: 20-202 °C, 1% mass loss; 202-264 °C, 37% mass loss; 264-389 °C, 12% mass loss; 389-500 °C, 10% mass loss; 40% mass remaining above 500 °C.

4.3 Results and discussions

In order to prepare well-defined brush-like polymers bearing polypeptides as the brush side chains with two-dimensional control over the brush molecular architectures, a "grafting-through" synthetic approach integrating ring-opening polymerizations (ROPs) of amino acid *N*-carboxyanhydrides (NCAs) and ring-opening metathesis polymerizations (ROMPs) of norbornene (NB) derivatives was designed and expected to

be capable of building desirable segment lengths of the polypeptide side chains and brush backbones, independently, in controlled manners (Figure 4.1). The bifunctional initiator (NB-amine, **1**) consisted of a primary amine and a NB group, in which the primary amine was first utilized as the initiator in the NCA ROP to build poly(β-benzyl-L-aspartate) (PBLA) side chain and then the NB group acted as the polymerizable unit in the Ruthenium-catalyzed ROMP to construct the brush backbone. Highly efficient post-polymerization modification was achieved *via* the aminolyses of PBLA side chains and could be used to conjugate functional moieties onto the polypeptide molecular brush.

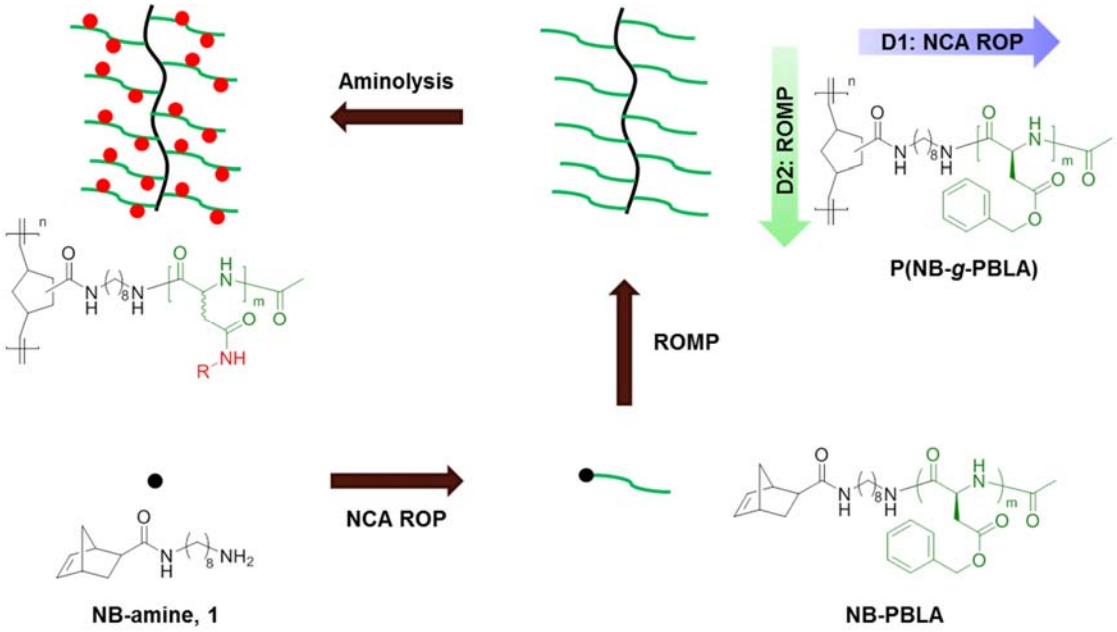

Figure 4.1. Synthetic design of polypeptide molecular brush *via* "grafting through" synthetic strategy with post-polymerization modification using aminolyses of PBLA side chains.

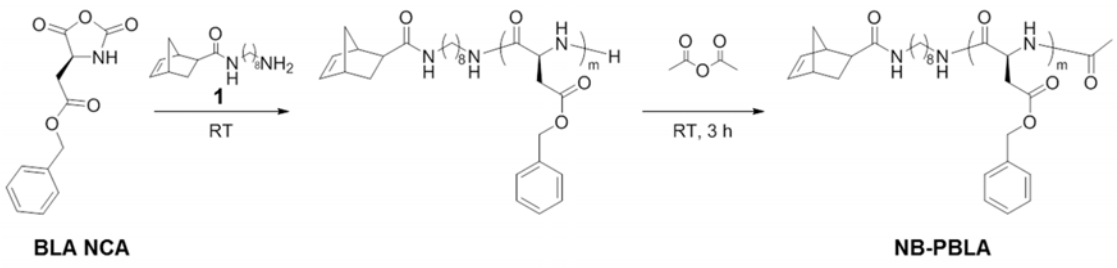

Figure 4.2. Synthetic route of NB-PBLA from ROP of BLA NCA using the N_2 flow method, followed by direct chain-end modification with acetyl anhydride without the need to isolate polypeptide after polymerization.

The polypeptide brush side chain, NB-PBLA, was synthesized by the controlled ROP of BLA NCA monomer with **1** as the initiator *via* our previously reported N_2 flow method (Figure 4.2), which provided a facile and straightforward approach to construct well-defined polypeptides. Due to the coordination effect of primary amine to the Ruthenium catalyst used in the next-step ROMP,[142] the chain-end amino group of NB-PBLA was directly modified with acetyl anhydride without isolation of polymer after NCA polymerization, resulting from the living property of the propagating chain end in the N_2 flow method.[64] The required amount of BLA NCA monomer in anhydrous *N,N*-dimethylformamide (DMF) was added into the DMF solution of **1** and allowed to proceed at room temperature, using standard Schlenk techniques. Acetyl anhydride was introduced into the reaction mixture *via* syringe after the conversion of BLA NCA reached at least 95%, which was determined by attenuated total reflectance-Fourier transform infrared spectroscopy (ATR-FTIR) using the intensity of NCA anhydride absorption at 1788 cm^{-1}. The reaction mixture was then precipitated into diethyl ether

after another 3 h to isolate NB-PBLA as a white solid product. NB-PBLAs with different chain lengths were synthesized in a similar manner by using monomer to initiator ratios of 10, 20 and 50, in which the solvent for NB-PBLA$_{50}$ changed to the mixture of DMF and DCM due to the low solubility of NB-PBLA$_{50}$ in neat DMF (Entry 3 in Table 4.1). The average degree of polymerization and number-averaged molecular weight of NB-PBLA were determined by comparison of the methylene proton intensities of the NB groups resonating at *ca.* 6.10 ppm (a in Figure 4.3a) with the intensities of the PBLA benzyl methylene protons resonating at *ca.* 5.03 ppm (c in Figure 4.3a), and the PBLA methine proton at *ca.* 4.61 ppm (e in Figure 4.3a), and the PBLA phenyl protons at *ca.* 7.28 ppm (b in Figure 4.3a). Due to the accelerated polymerization rates, NB-PBLAs were synthesized in a rapid manner with well-defined structures, as confirmed by the observed gel permeation chromatography (GPC) analyses of a peak shift from 26.2 to 25.6 to 23.6 min with the increase of BLA repeat unit numbers from

Table 4.1. BLA NCA ROP initiated by **1** with different monomer to initiator feed ratios.

Entry[a]	M/I[a]	Condition	Conc. (mg/mL)	Time (h)[a]	M_n (kDa)[b]	DP_n[b]	PDI[c]
1	10	DMF, N_2 (100 mL/min)	100	12	2.4	10	1.05
2	20	DMF, N_2 (100 mL/min)	50	25	3.8	18	1.10
3	50	DMF : DCM = 1 : 9	50	48	12.0	57	1.11

[a]All the polymerizations were performed with **1** as the initiator at room temperature and terminated after monomer conversion reached > 95%, M: monomer, I: initiator. [b]Determined by ^{1}H NMR spectroscopy. [c]Determined by DMF GPC characterization.

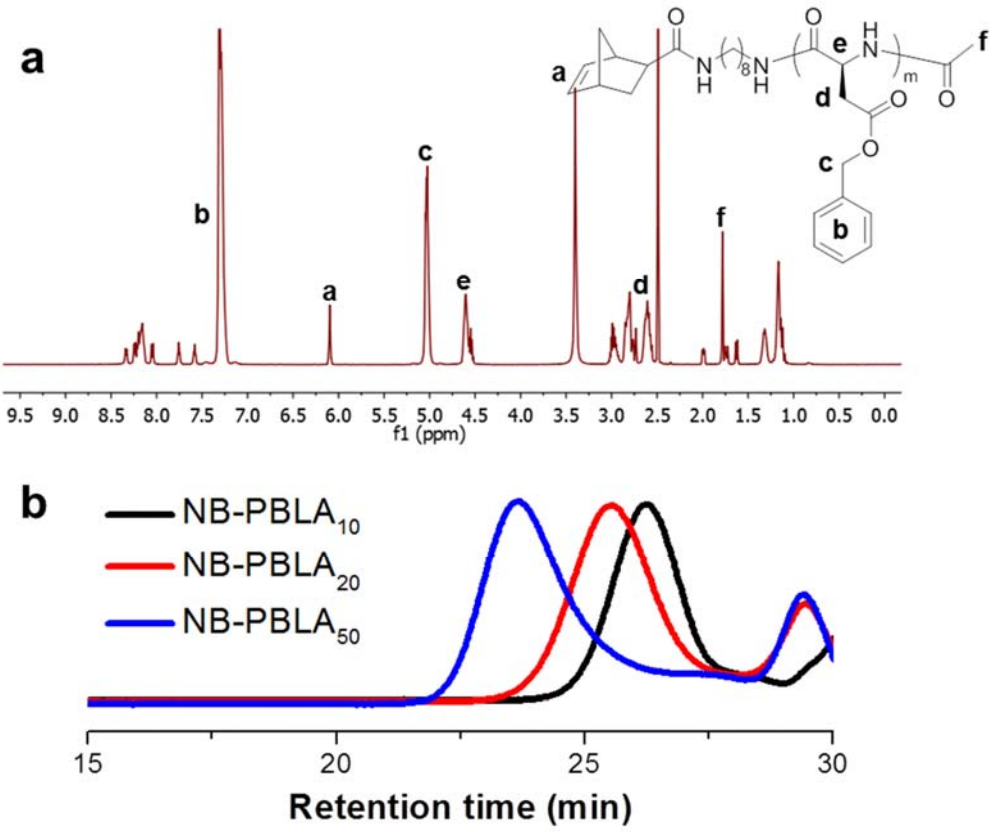

Figure 4.3. (a) ^{1}H NMR spectrum for NB-PBLA$_{10}$ and (b) GPC traces for NB-PBLA$_{10}$ (black line), NB-PBLA$_{20}$ (red line) and NB-PBLA$_{50}$ (blue line).

10 to 20 to 50, and the narrow molecular weight distributions (MWDs) for all three polypeptides (Figure 4.3b and Table 4.1). Therefore, the N_2 flow accelerated NCA ROP provided the first-dimensional control over the brush molecular architecture by building the polypeptide side chain with desirable segment length.

The Ruthenium-catalyzed ROMP is a robust and well-established polymerization technique to prepare polymeric materials in a living manner with high tolerance of functional groups, such as carboxylic acids and alcohols.[143] In order to synthesize

polypeptide molecular brush, poly(norbornene-*graft*-poly(β-benzyl-L-aspartate)) (P(NB-*g*-PBLA)), *via* the "grafting-through" approach with the expectation to control the brush backbone, the ROMP was utilized to polymerize the NB groups at the α-chain ends of NB-PBLAs with the modified Grubbs' catalyst (Figure 4.4). Due to the poor solubility of NB-PBLA and P(NB-*g*-PBLA) in less polar solvent, solvent with high polarity is required for the ROMP, while most of high polar organic solvents, such as DMF and *N,N*-dimethylacetamide (DMAc), will coordinate to the Ruthenium center of the modified Grubbs' catalyst, resulting in the deactivation of the catalyst and termination of ROMP. Ionic liquid is a class of organic compounds consisting of ionic species with melting temperatures less than 100 °C or even at room temperature, when choosing appropriate ion pair, can fulfill the requirement of high polarity and less coordinating ability in the ROMP of polypeptide macromonomer, such as 1-butyl-3-methylimidazolium tetrafluoroborate ([bmim][BF_4]).[144,145] The solvent mixture of [bmim][BF_4] with dichloromethane (DCM) was used in the ROMP of NB-PBLA due to the limited solubility of polypeptide in the neat ionic liquid. During our initial polymerization attempt, 87% conversion of NB-PBLA with controlled structure (PDI = 1.22) of P(NB-*g*-PBLA) was achieved by using 5% [bmim][BF_4] in DCM (Entry 1 in Table 4.2). With the released ring-strain during the polymerization, the peak at *ca.* 6.10 ppm corresponding to the NB methylene protons disappeared in the ^{1}H NMR spectrum (a in Figure 4.3a), while a broad peak at *ca.* 5.20 ppm was observed instead in the ^{1}H NMR spectrum of P(NB-*g*-PBLA) (a in Figure 4.5). As the content of ionic liquid increased in the solvent mixture, the conversion of NB-PBLA was depressed, even with

elongated reaction time (Entry 1 - 4 in Table 4.2). For example, the conversion of NB-PBLA decreased from 87% to 67% when the content of [bmim][BF_4] increased from 5% to 20% in the solvent. With the increased concentration of NB-PBLA during

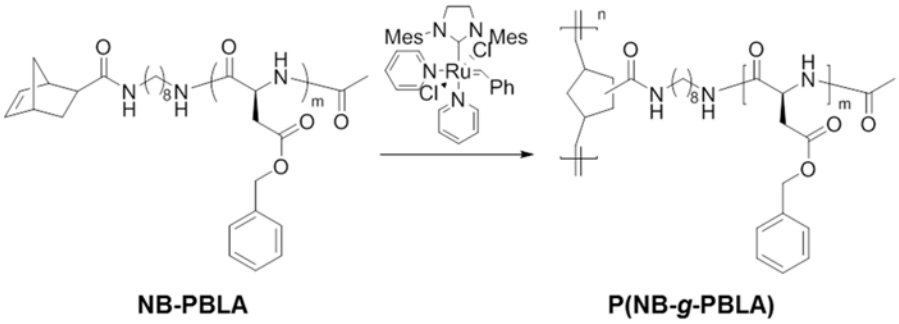

Figure 4.4. Synthesis of P(NB-*g*-PBLA) from ROMP of NB-PBLA with the modified Grubbs' catalyst.

Table 4.2. Reaction condition optimization of ROMP to synthesize P(NB-*g*-PBLA) with different ionic liquid contents and macromonomer concentrations.

Entry[a]	Solvent[b]	Conc. (mg/mL)	Time (h)	Conv. (%)[c]	M_n (kDa)[d]	DP_n (expected)[d]	PDI[d]
1	DCM + 5% IL	40	3	87	117.6	49 (44)	1.22
2	DCM + 10% IL	40	3	82	95.7	40 (41)	1.20
3	DCM + 20% IL	40	5	67	91.2	38 (34)	1.25
4	DCM + 25% IL	20	5	44	88.8	37 (22)	1.22
5	DCM + 10% IL	70	3	91	128.7	54 (46)	1.28
6	DCM + 10% IL	100	3	96	121.5	51 (48)	1.19

[a]All the polymerizations were conducted with monomer to catalyst ratio at 50 at room temperature. [b]IL: ionic liquid. [c]Determined by ^{1}H NMR spectroscopy. [d]Determined by DMF GPC characterization.

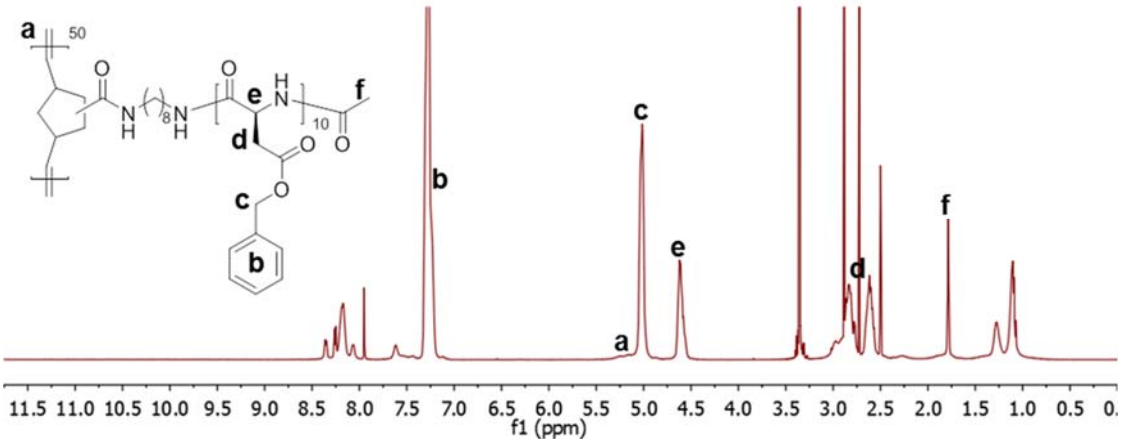

Figure 4.5. ^{1}H NMR spectrum for P(NB-*g*-PBLA$_{10}$)$_{50}$.

the polymerization, the macromonomer conversion was also improved and the molecular structure of the obtained brush polymer was maintained well-defined as indicated by PDI < 1.3 (Entry 2, 5, 6 in Table 4.2). Therefore, the following ROMPs were conducted at the optimized reaction condition by using 10% ionic liquid in DCM with the concentration of NB-PBLA at 100 mg/mL.

With the optimized reaction condition, ROMPs of NB-PBLA with different chain lengths at various monomer to catalyst ratios were performed and the results were summarized in Table 4.3. For each NB-PBLA macromonomer, with the increase of the monomer to catalyst ratio, the NB-PBLA conversion decreased correspondingly, which was determined by measuring the intensity of NB methylene protons in ^{1}H NMR, resulting from the decreased reactivity of propagating chain end. For example, when the ratio of monomer to catalyst increased from 20 to 100, the conversion of NB-PBLA$_{10}$ decreased from 99% to 78% (Entry 1 - 3 in Table 4.3). The well-defined structures of

P(NB-*g*-PBLA) were indicated in Figure 4.6 with the monomodal GPC distribution patterns for all three brush polymers derived from NB-PBLA$_{10}$. With the increased steric hindrance of the polypeptide macromonomer from NB-PBLA$_{10}$ to NB-PBLA$_{50}$, the conversion of NB-PBLA dropped remarkably at the same monomer to catalyst ratio, especially for NB-PBLA$_{50}$, which possessed the largest steric hindrance in the three NB-PBLA brush side chains (Entry 1, 4, 8 in Table 4.3).

Table 4.3. Syntheses of P(NB-*g*-PBLA)s from NB-PBLAs with different chain lengths at different macromonomer to catalyst ratios using [bmim][BF$_4$].

Entry[a]	M[a]	M/C[a]	Time (h)	Conv. (%)[b]	M_n (kDa)[c]	DP_n (expected)[c]	PDI[c]
1	NB-PBLA$_{10}$	20	1	99	56.7	23 (20)	1.17
2	NB-PBLA$_{10}$	50	3	96	112.1	47 (48)	1.09
3	NB-PBLA$_{10}$	100	3	78	280.5	117 (78)	1.27
4	NB-PBLA$_{20}$	20	3	92	82.6	22 (19)	1.16
5	NB-PBLA$_{20}$	50	3	83	129.8	38 (42)	1.24
6	NB-PBLA$_{20}$	100	3	64	200.7	59 (64)	1.35
7	NB-PBLA$_{50}$	10	6	85	96.6	8 (8)	1.13
8	NB-PBLA$_{50}$	20	6	74	141.0	12 (15)	1.16
9	NB-PBLA$_{50}$	50	6	34	186.0	16 (17)	1.16

[a]All polymerizations were conducted at the optimized condition with the concentration of macromonomer at 100 mg/mL in the solvent mixture with 10% [bmim][BF$_4$] in DCM, M: macromonomer, C: catalyst. [b]Determined by ^{1}H NMR spectroscopy. [c]Determined by DMF GPC characterization.

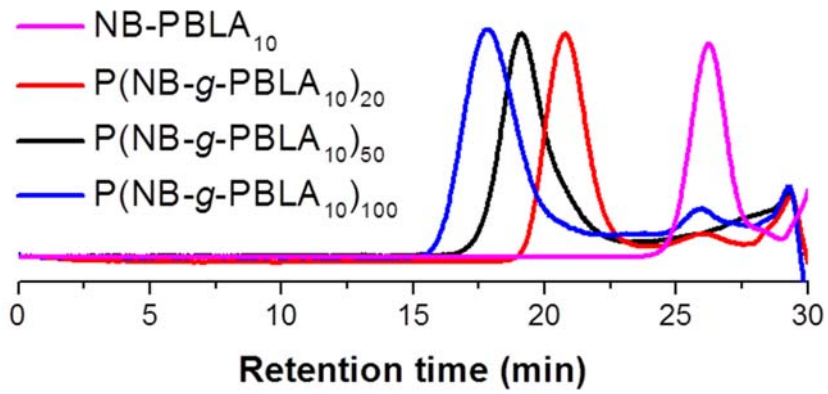

Figure 4.6. GPC traces for P(NB-*g*-PBLA$_{10}$) from ROMPs with macromonomer to catalyst ratio of 20, 50, 100 in comparison with NB-PBLA$_{10}$.

In addition to the steric hindrance from the polypeptide macromonomer that could cause the decreased macromonomer conversion in ROMP, we started to revisit the ionic liquid used in the polymerization. The [bmim] cation was reported to degrade into a carbene species *via* the proton abstraction at 2-position, and this carbene compound could coordinate to the center metal to deactivate the catalyst.[144-146] In order to avoid this potential negative effect from [bmim][BF$_4$] on the modified Grubbs' catalyst used in the ROMP, another ionic liquid compound, 1-butyl-2,3-dimethylimidazolium tetrafluoroborate ([bdmim][BF$_4$]) by replacing the proton at 2-position with a methyl group, was investigated in the ROMP of NB-PBLA. Due to the melting temperature at 37 °C, the polymerizations were conducted at 40 °C while the other reaction conditions were maintained the same as previously described (Table 4.4). For both NB-PBLA$_{10}$ and NB-PBLA$_{20}$, the conversions of polypeptide macromonomers were improved above 80%, in which a 16% increase was achieved for NB-PBLA$_{20}$ at the monomer to catalyst

ratio of 100 (Entry 6 in Table 4.4). With the improved conversion, the largest molecular weight of P(NB-*g*-PBLA) reached *ca.* 380.5 kDa, which was 40% increase in comparison with the brushes synthesized with [bmim][BF_4]. Therefore, the ROMP of NB-PBLA in a mixture of DCM and ionic liquid provided the second-dimensional control over the brush molecular architecture by building the brush backbone with desirable segment length.

Table 4.4. Syntheses of P(NB-*g*-PBLA)s from NB-PBLAs with different chain lengths at different macromonomer to catalyst ratios using [bdmim][BF_4].

Entry[a]	M[a]	M/C[a]	Time (h)	Conv. (%)[b]	M_n (kDa)[c]	DP_n (expected)[c]	PDI[c]
1	NB-$PBLA_{10}$	20	1	99	58.7	24 (20)	1.09
2	NB-$PBLA_{10}$	50	3	99	138.7	57 (49)	1.23
3	NB-$PBLA_{10}$	100	3	92	251.5	105 (92)	1.36
4	NB-$PBLA_{20}$	20	3	99	89.2	23 (20)	1.14
5	NB-$PBLA_{20}$	50	3	85	166.3	44 (43)	1.26
6	NB-$PBLA_{20}$	100	3	80	385.4	101 (80)	1.32

[a]All polymerizations were conducted at the optimized condition with the concentration of macromonomer at 100 mg/mL in the solvent mixture with 10% [bdmim][BF_4] in DCM at 40 °C, M: macromonomer, C: catalyst. [b]Determined by ^{1}H NMR spectroscopy. [c]Determined by DMF GPC characterization.

The aminolysis of PBLA is a facile and efficient approach to attach functional moieties onto the backbone of PBLA without undesired side reactions, such as cleavage of the amide linkages along the polypeptide backbone.[147,148] This reaction is found to

proceed *via* the formation of a succinimide intermediate in the polymer backbone, which is converted to polyaspartamide, accompanying the α,β isomerization of the backbone. In order to investigate the efficiency of the aminolysis of PBLA in the more densely-packed brush structure of P(NB-*g*-PBLA), a total amount of 50 equivalents of *N*-Boc-ethylenediamine to the benzyl ester groups was used to avoid crosslinking and ensure high efficiency (Figure 4.7). The obtained polyaspartamide product, P(NB-*g*-PABEDA), was characterized by ^{1}H NMR spectroscopy (Figure 4.8a), in which the disappearance of methylene protons of benzyl ester groups and phenyl protons (b and c in Figure 4.5), together with the observation of other functional groups (e, g, and h in Figure 4.8a), demonstrated the high efficiency (> 95%) of the aminolysis of PBLA as a post-polymerization modification approach for P(NB-*g*-PBLA) brush. In addition, the well-controlled brush structure was maintained during the modification, which was indicated from the monomodal GPC pattern with PDI = 1.23 of the obtained product (Figure 4.8b).

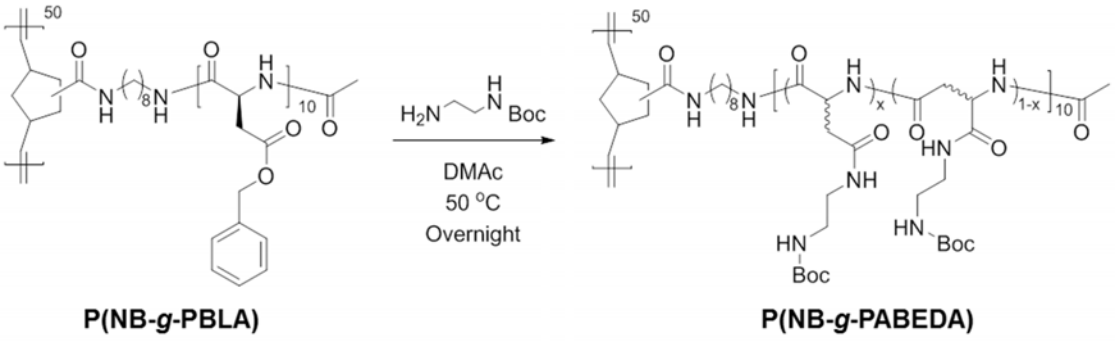

Figure 4.7. Aminolysis of PBLA side chain of P(NB-*g*-PBLA) molecular brush.

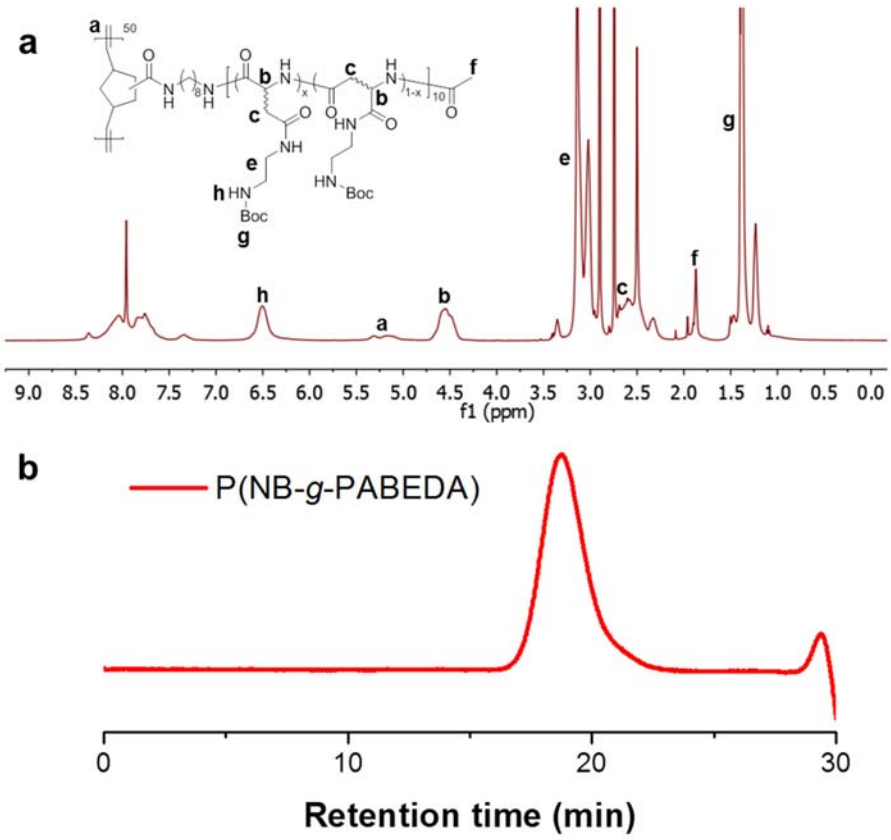

Figure 4.8. (a) ^{1}H NMR spectrum and (b) GPC trace of P(NB-*g*-PABEDA) from the aminolysis product of P(NB-*g*-PBLA).

4.4 Conclusions

In summary, a "grafting through" synthetic approach integrating NCA ROP and ROMP was investigated to build well-defined brush-like polymers bearing polypeptides as brush side chains with two-dimensional control over the brush molecular architectures. Polypeptide side chains with desirable segment lengths were synthesized by the N_2 flow accelerated NCA ROPs, which provided the first-dimensional control over the brush side

chains. By using the solvent mixture of ionic liquid with DCM, which fulfilled the requirement of high polarity and weak coordinating tendency, the second-dimensional control was achieved *via* the ROMPs of polypeptide macromonomers to construct brush backbones with well-controlled structures. The aminolysis of PBLA side chain was demonstrated as a facile and efficient post-polymerization modification method to further install functional groups onto the densely-packed brush-like structure. With this two-dimensional control strategy, a library of polypeptide molecular brushes with varying segment lengths of both side chain and brush backbone can be prepared and utilized to explore the effect of molecular architecture on polymer properties. Given the numerous types of NCA monomers and NB-incorporated materials, this novel synthetic approach can also be expanded to build various hybrid materials with broad applications.

CHAPTER V

TUNABLE MECHANO-RESPONSIVE ORGANOGELS BY RING-OPENING COPOLYMERIZATIONS OF *N*-CARBOXYANHYDRIDES*

5.1 Introduction

Stimuli-responsive materials have attracted significant attention in the last decades for their potential applications in the construction of adaptive materials, art conservation, sensor design, and controlled release systems.[149-155] Light,[156-158] temperature,[19,159,160] pH,[161-163] magnetic flux,[164] and oxidation-reduction[165] are commonly used stimuli to trigger the reorganization of self-assembled nano- or microstructures. These triggers often focus on controlling supramolecular noncovalent interactions, such as hydrogen-bonding, π-π stacking and van der Waals interactions. Recently, it has been found that sonication can be a novel stimulus to tune the self-assembly behavior and aggregate morphology[166] within organogel systems, by disrupting hydrogen-bonding and π-π stacking interactions, resulting in sol-to-gel,[167-170] gel-to-sol,[171] and gel-to-gel[172] transitions. However, elaborate designs having precise control on the molecular level and, consequently, tedious multi-step syntheses are required to obtain these subtle transitions. Thus, sonication-responsive organogels remain limited to primarily low-molecular-weight gelators (LMWGs),[166] few studies of

* Reproduced (adapted) "Tunable mechano-responsive organogels by ring-opening copolymerizations of *N*-carboxyanhydrides" by Fan, J.; Zou, J.; He, X.; Zhang, F.; Zhang, S.; Raymond, J. E.; Wooley, K. L., *Chem. Sci.* **2014**, *5*, 141-150 with permission from The Royal Society of Chemistry.

systems developed from macromolecular hydrogelators and organogelators have been performed.[173,174]

Polypeptide-based materials have been widely used in supramolecularly-assembled hydrogels[16,51,70,175] and organogels.[64-66,176] Their broad applicability is due to the precisely-defined nano- and microstructures derived from supramolecular hierarchical assemblies of polypeptides and the variety of stimuli responses available to natural and synthetic polypeptides, which are often unobtainable from non-polypeptide-based materials. Secondary structures from the self-assembly of polypeptides, especially α-helix and β-sheet conformations, have been proposed as driving forces for the construction of organogels. For example, Kim *et al.* reported poly(ferrocenysilane)-*block*-poly(γ-benzyl-L-glutamate) (PFS-*b*-PBLG) as an organogelator in toluene with thermosreversible gel-to-sol behavior, originating from the monolayer one-dimensional stacking of the α-helical polypeptide segments (PBLG) into nanoribbons.[64] In 2008, Cameron and co-worker reported thermoreversible organogelators, poly(*O*-benzyl-L-threonine)-*block*-poly(γ-benzyl-L-glutamate) (PBnT-*b*-BnE) and poly(*O*-benzyl-L-threonine)-*block*-poly(ε-*N*-Boc-L-lysine) (PBnT-*b*-BocK); both of which contained one α-helix- and one β-sheet-producing polypeptide segment.[66] The gelation was found to be driven by β-sheet formation and stacking into nanotapes by the PBnT segments. At the same time the α-helical structure from the PBnE or PBocK block, in an energetically-unfavorable parallel configuration, triggered twisting of the nanotapes in order to minimize these interactions. At present, tunable sonication-responsive organogels from polypeptides have not been explored, and

we were interested in investigating such systems, including the self-assembly and gelation behavior of hybrid statistical copolypeptides.

Recently, our group reported a chemically-reactive polypeptide-based organogelator, poly(ethylene glycol)-*block*-poly(DL-allylglycine) (PEG-*b*-PDLAG), containing a racemic PDLAG homopolypeptide block.[67] Gel formation was driven by supramolecular assembly of β-sheet secondary structures into nanofibrils in the nanodomain, and which underwent gel-to-sol transition when subjected to sonication stimulus. To explore the effect of constituency control of the secondary structures formed, particularly α-helix and β-sheet configurations, on the physical and mechanical properties, this current work involves a new type of organogelator, methoxy poly(ethylene glycol)-*block*-poly(γ-benzyl-L-glutamate-*co*-glycine) (mPEG-*b*-P(BLG-*co*-Gly)) These organogel systems exhibited tunable sonication-responsive properties by variation of the secondary structures from the hybrid copolypeptide without the need of elaborate design and multi-step syntheses. Secondary structures were modified by systematically altering the ratios of BLG to Gly, which, respectively, have preferences for α-helix and β-sheet configurations.[33] The organogels from α-helix-rich diblock copolymers showed higher stability against sonication and instantaneous gel-to-gel transitions were observed. However, the β-sheet-rich organogel formulations exhibited immediate gel-to-sol transition when sonication was applied. Further, the injectability and self-healing abilities of these organogel systems were directly observed through assessment of the bulk macroscopic self-healing responses.

5.2 Experimental section

5.2.1 Materials

Ethyl acetate, *n*-hexane, tetrahydrofuran (THF), diethyl ether, *N,N*-dimethylformamide (DMF, anhydrous, ≥ 99.8%), γ-benzyl-L-glutamate (≥ 99%), bis(trichloromethyl) carbonate (≥ 98%), glycine (≥ 99%), trichloromethyl chloroformate (≥ 97%) and Alizarin Red S were purchased from Sigma-Aldrich company (USA). Monomethoxy-monoamino-terminated poly(ethylene glycol) ($mPEG_{45}$-NH_2, M_n = 2000 g/mol) was purchased from Rapp Polymere (Germany). All chemicals were used without further purification, unless otherwise noted.

5.2.2 Instrumentation

^1H and ^{13}C NMR spectra were recorded on Varian Inova 300 MHz spectrometers interfaced to a UNIX computer using VnmrJ software. Chemical shifts were referenced to the solvent resonance signals. Attenuated total reflectance-Fourier transform infrared spectroscopy (ATR-FTIR) spectra were recorded on an IR Prestige 21 system (Shimadzu Corp.) and analyzed using IRsolution v. 1.40 software.

Thermogravimetric analysis (TGA) was performed under Argon atmosphere using a Mettler-Toledo model TGA/SDTA851^e (Mettler-Toledo, Inc., Columbus, OH), with a heating rate of 10 °C/min. Measurements were analyzed using Mettler-Toledo STAR^e v. 7.01 software. Glass transition temperatures (T_g) were measured by differential scanning calorimetry (DSC) on a Mettler-Toredo DSC822®, with a heating rate of 10 °C/min. Measurements were analyzed using Mettler-Toledo STAR^e v. 7.01

software. The T_g was taken as the midpoint of the inflection tangent, upon the second heating scan.

Wide-angle X-ray scattering (WAXS) was performed on a Bruker D8 Bragg-Brentano X-ray powder diffractometer. The sample was placed in the sample holder of a two circle goniometer, enclosed in a radiation safety enclosure. The X-ray source was a 2.2 kW Cu X-ray tube, maintained at an operating current of 40 kV and 40 mA. The X-ray optics was the standard Bragg-Brentano para-focusing mode with the X-ray diverging from a DS slit (1 mm) at the tube to strike the sample and then converging at a position sensitive X-ray Detector (Lynx-Eye, Bruker-AXS). The two-circle 250 mm diameter goniometer was computer controlled with independent stepper motors and optical encoders for the θ and 2θ circles with the smallest angular step size of 0.0001° 2θ. The software suit for data collection and evaluation was window based. Data collection was automated COMMANDER program by employing a DQL file and analyzed by the program EVA.

Transmission electron microscopy (TEM) images were collected on a JEOL 1200 EX operating at 100 kV and micrographs were recorded at calibrated magnifications using a SLA-15C CCD camera. The final pixel size was 0.42 nm/pixel. Samples for TEM measurements were prepared as follows: 10 μL of the dilute solution (with a polymer concentration of 1 mg/mL) was deposited onto a carbon-coated copper grid, and after 2 min, the excess of the solution was quickly wicked away by a piece of filter paper. The samples were then negatively stained with 1 wt % phosphotungstic acid

(PTA) aqueous solution. After 30 s, the excess staining solution was quickly wicked away by a piece of filter paper and the samples were left to dry under vacuum overnight.

Sonication responsive experiments were performed in an ultrasonic homogenizer (maximum power, 150W, 20KHz, Model 150 V/T, Biologics, Inc.) equipped with a micro tip with a diameter of 3.81 mm, employing the power outlet of 45 W in the frequency of 20 KHz at room temperature.

Dynamic mechanical analysis (DMA) was performed on a Mettler Toledo TT-DMA system. DMA of 5 wt % samples in DMF were performed over 3 h in compression on a 3.2 mm thick, 10 mm diameter cylinder. Dynamic measurements were recorded over a range of 0.1 to 10 Hz at room temperature with static stress modulated to 2% compression and a dynamic force applied to provide ±1% deformation. Kinetic data presented were obtained as a single exponential decay using Origin Pro 8.1 software. The gel stiffness was quantified by the evaluation of the compression storage modulus (E′).[177]

Confocal images were taken using a FV 1000 system (Olympus) with a 10× objective (Olympus) and a 543 nm He-Ne laser excitation source. Emission was collected using a monochrometer set to a 100 nm band pass (560 – 660 nm) and a photomultiplier tube. Image analysis was performed in Fluoviow software (Olympus) and a 1.1 gamma correction was used to enhance feature contrast after scaling image contrast intensity to minimum and maximum threshold set points of 1% above dark count and 1% below maximum counts for both fluorescence and differential imaging

contrast (DIC) images. Slides were generated by lightly compressing the gels between a cleaned glass microscope slide and a cleaned glass cover slip after dye addition.

5.2.3 Experimental procedures

Synthesis of γ-benzyl-L-glutamate *N*-carboxyanhydride (BLG NCA) monomer 1

In a 500 mL three-necked round bottom flask equipped with a magnetic stir bar, condenser and N_2 inlet, γ-benzyl-L-glutamate (10.0 g, 42 mmol, 3 equiv) and bis(trichloromethyl) carbonate (4.2 g, 14 mmol, 1 equiv) were added and suspended in 300 mL ethyl acetate at 65 °C under N_2 bubbling for 4 h.[81] After cooling to 5 °C, the crude product was extracted with nanopure water (100 mL, 5 °C) and 0.5 wt % sodium bicarbonate solution (100 mL, 5 °C), respectively. The organic layer was dried over $MgSO_4$, filtrated and concentrated. The resulting solid was recrystallized three times from ethyl acetate/*n*-hexane 1:1 (v/v), and dried in vacuum to obtain a white crystal (2.6 g, yield: 70%). ^{1}H NMR (300 MHz, DMSO-D_6, ppm): δ 1.99 (m, 2H, C*H*$_2$CH$_2$COOCH$_2$), 2.52 (t, *J* = 6.8 Hz, 2H, CH$_2$C*H*$_2$COOCH$_2$), 4.47 (m, 1H, COC*H*NH), 5.10 (s, 2H, COOC*H*$_2$Ar), 7.37 (m, 5H, Ar*H*), 9.10 (br, 1H, COCHN*H*). ^{13}C NMR (75 MHz, DMSO-D_6, ppm): δ 26.4, 29.1, 56.2, 65.7, 128.0, 128.1, 128.4, 136.0, 151.9, 171.3, 171.7. FTIR (cm^{-1}): 3331, 3251, 2931, 1859, 1773, 1703, 1250, 1185, 1112, 930. HRMS: calculated [M-H]$^-$ for $C_{13}H_{13}NO_5$: 262.0715, found: 262.0710.

Synthesis of glycine NCA (Gly NCA) monomer 2

In a 250 mL three-necked round bottom flask equipped with a magnetic stir bar, condenser and N_2 inlet, glycine (5.0 g, 67 mmol, 3 equiv) was suspended in 100 mL THF and heated to 50 °C. Trichloromethyl chloroformate (4.4 g, 22 mmol, 1 equiv) was

added into the reaction solution by syringe and the reaction mixture was refluxed for another 4 h under N_2 atmosphere. The reaction mixture was filtered before cooling to room temperature. The filtrate was concentrated, recrystallized three times from THF/*n*-hexane 2:1 (v/v) and dried in vacuum to obtain a white crystal (1.5 g, yield: 67%). The product was stored in -20 °C freezer under N_2 atmosphere. ^{1}H NMR (300 MHz, DMSO-D_6, ppm): δ 4.18 (s, 2H, COC*H*$_2$NH), 8.83 (br, 1H, COCH$_2$N*H*). ^{13}C NMR (75 MHz, DMSO-D_6, ppm): δ 46.3, 153.0, 169.4. FTIR (cm^{-1}): 3500-3100, 2955, 1876, 1740, 1275, 1113, 1061, 925. HRMS: calculated $[M-H]^-$ for $C_3H_3NO_3$: 100.0035, found: 100.0039.

Synthesis of mPEG-*b*-P(BLG-*co*-Gly) diblock copolymer

As a representative example, the synthesis of mPEG$_{45}$-*b*-P(BLG$_{16}$-*co*-Gly$_{16}$) was described. In a 10 mL flame dried Schlenk flask equipped with a magnetic stir bar, mPEG$_{45}$-NH$_2$ (53.3 mg, 0.027 mmol, 1 equiv) was added into a solution of BLG NCA (105.3 mg, 0.4 mmol, 15 equiv) and Gly NCA (40.4 mg, 0.4 mmol, 15 equiv) in 5.8 ml anhydrous DMF solution. The reaction mixture was stirred with a stir rate of 400 rpm under continuous N_2 flow (100 mL/min) at room temperature for 72 h. The quantitative consumption of monomers was confirmed by measuring the intensity of the NCA anhydride peak at 1788 cm^{-1} using ATR-FTIR. The Schlenk flask was capped with a rubber stopper with a needle outlet connected with a drying tube. The polymerization gelled generally after 24 h polymerization. The gel was precipitated into diethyl ether under vigorous stirring and a white powder was obtained after centrifuged and dried in vacuum at room temperature (122.6 mg, yield: 75%). ^{1}H (300 MHz, TFA-D, ppm): δ

2.04 (br, 32H, C*H*$_2$CH$_2$COOCH$_2$), 2.48 (br, 32H, CH$_2$C*H*$_2$COOCH$_2$), 3.50 (s, 3H, C*H*$_3$O), 3.83 (s, 180H, C*H*$_2$C*H*$_2$O), 4.15 (br, 30H, NHC*H*$_2$CO), 4.65 (br, 16H, NHC*H*CO), 5.07 (br, 32H, COOC*H*$_2$), 7.22 (m, 80H, Ar*H*). ^{13}C NMR (75 MHz, TFA-D, ppm): δ 26.7, 30.0, 42.5, 53.2, 68.4, 69.5, 127.9, 128.3, 128.5, 134.1, 173.3, 175.7, 176.1. FTIR (cm^{-1}): 3289, 2870, 1732, 1701, 1649, 1626, 1545, 1510, 1452, 1437, 1387, 1248, 1159, 1098, 849, 737, 696. DSC: T_g = 18 °C, T_g = 103 °C. TGA in N$_2$: 20-325 °C, 32% mass loss; 325-422 °C, 30% mass loss; 422-500 °C, 6% mass loss; 32% mass remaining above 500 °C.

5.3 Results and discussions

With our general interest in the creation of polymer-based stimuli-responsive materials with simple molecular design and synthetic feasibility, for fundamental studies and future applications, we began investigation into the preparation of hybrid diblock copolymers having statistical copolypeptides as one of the block segments, to incorporate the potential for stimuli-triggered supramolecular assembly of secondary structures within the polypeptide segments. In order to understand the relationship between the polypeptide composition and the secondary structure in the resulting self-assembled organogels, the methoxy poly(ethylene glycol)-*block*-poly(γ-benzyl-L-glutamate-*co*-glycine) (mPEG-*b*-P(BLG-*co*-Gly)) diblock copolymers were synthesized *via* facile statistical ring-opening copolymerizations (ROPs) of BLG (**1**) and Gly (**2**) *N*-carboxyanhydrides (NCAs) by using mPEG$_{45}$-NH$_2$ as the macroinitiator (Figure 5.1). ROPs of amino acid NCAs have been demonstrated to be a convenient and efficient

technique for the preparation of high molecular weight synthetic polypeptides in large quantity, while maintaining the capability of self-assembly into organogels.[22,34] In fact, NCA ROPs can be conducted under normal Schlenk techniques, with the rate of polymerization being controlled by a straightforward N_2 flow method. A series of mPEG-*b*-P(BLG-*co*-Gly) diblock copolymers with altered compositions in the polypeptide segments was synthesized by systematically varying the feed ratio of BLG and Gly NCAs during the copolymerizations (Table 5.1). For each copolymerization, the required amounts of monomers and macroinitiator were dissolved in anhydrous *N,N*-dimethylformamide (DMF) and the ROP was allowed to proceed for 72 h at room temperature, under a continuous N_2 flow (flow rate = 100 mL/min). When Gly NCA occupied a mol % higher than 15% in the monomer mixture, spontaneous gelation occurred during the polymerization (**6** – **12** in Table 5.1) within 24 h. With the mol % of Gly NCA less than 15%, the reaction mixtures remained in the solution state throughout the polymerizations (**4** and **5** in Table 5.1). Each reaction mixture was precipitated into diethyl ether and dried under vacuum to yield the targeted diblock copolymer as a white powder. This processing capability of the mPEG-*b*-P(BLG-*co*-Gly) diblock copolymer

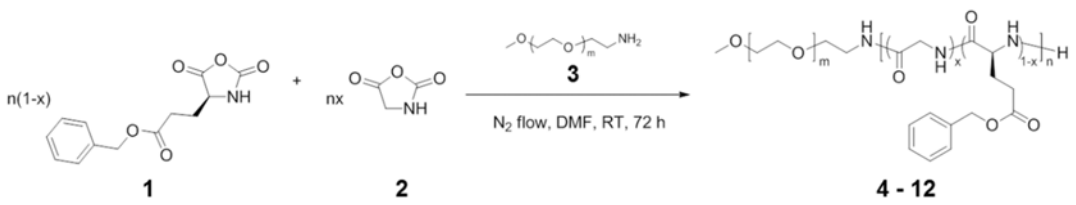

Figure 5.1. Synthetic approach of mPEG-*b*-P(BLG-*co*-Gly) diblock copolymer.

materials, in the form of either gels or powders, allowed further exploration of the compositions, structures and properties.

Table 5.1. Average degree of polymerization (DP_n), number of repeat unit, mole fraction of Gly (χ_{Gly}) in the polypeptide segment, number-average molecular weight (M_n) and critical gelation concentration (CGC) for the mPEG-*b*-P(BLG-*co*-Gly) diblock copolymers synthesized with different monomer feed ratios.

Polymer	**1** : **2**[a]	DP_n[b]	Number of repeat unit[b]		χ_{Gly}	M_n	CGC
			1, BLG	**2, Gly**	(%)[b]	(kDa)[b]	(wt %)[c]
4	1 : 0	33	33	0	0	9.2	-[d]
5	6 : 1	33	29	4	12	8.6	-[d]
6	3 : 1	31	25	6	19	7.8	2.5
7	2 : 1	31	22	9	29	7.3	1.5
8	1.5 : 1	30	19	11	37	6.8	1.2
9	1.2 : 1	30	17	13	43	6.5	0.9
10	1 : 1	32	16	16	50	6.4	0.6
11	1 : 4	32	6	26	81	4.8	0.8
12	0 : 1	33	0	33	100	3.9	2.0

[a]The $mPEG_{45}$-NH_2 (**3**) were used as macroinitiators in all polymerizations with monomer : initiator = 30 : 1. [b]Calculated by ^1H NMR spectroscopy. [c]CGCs of organogels in DMF were determined by the test tube inversion method at room temperature. [d]No gelation was observed with the concentration of polymer up to 10 wt %.

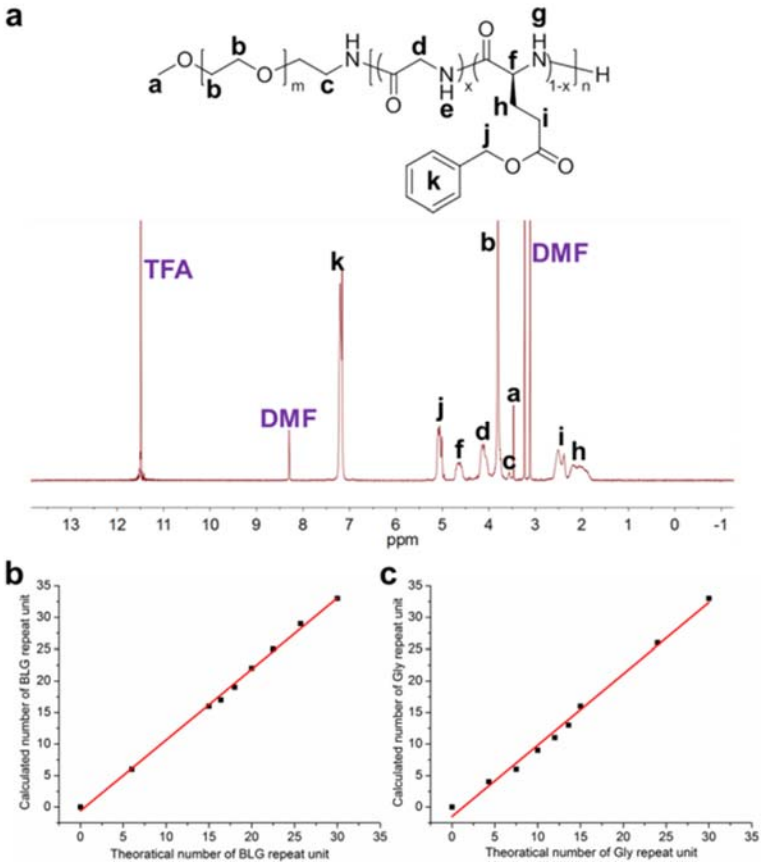

Figure 5.2. (a) ^{1}H NMR spectrum of polymer **10** dissolved in TFA-D. Calculated numbers of (b) BLG and (c) Gly repeat units as a function of theoretical numbers of repeat units in the polymers **4** – **12**.

To investigate the incorporated ratios of the two monomers in the copolymers under different feed ratios, ^{1}H NMR spectroscopy characterization was employed using deuterated trifluoroacetic acid (TFA-D) as the solvent, which was capable of breaking the strong hydrogen-bonding in these systems and maintaining the polymers in the solution state (Figure 5.2). The average degrees of polymerization, numbers of repeat units for BLG and Gly, mole fractions of Gly in the polypeptide segments, and number-average molecular weights of the block copolymers were determined by

comparison of the methylene proton intensities of the mPEG chain resonating at *ca.* 3.83 ppm (b in Figure 5.2a) with the intensities of the PBLG benzyl methylene protons resonating at *ca.* 5.07 ppm (j in Figure 5.2a), the PBLG methine proton at *ca.* 4.65 ppm (f in Figure 5.2a), and the PBLG phenyl protons at *ca.* 7.22 ppm (k in Figure 5.2a), and the integration of the Gly methylene protons at *ca.* 4.15 ppm (d in Figure 5.2a), and were found to be in agreement with the stoichiometry used in the polymer syntheses (Table 5.1). For both BLG (Figure 5.2b) and Gly (Figure 5.2c), the calculated numbers of repeat units from ^{1}H NMR spectroscopy showed linear correlations with the theoretical numbers of repeat units, which were obtained according to the feed ratios of the two monomers and the ratios of monomers to macroinitiator, indicating that BLG and Gly NCA monomers had similar reactivities and were fully consumed during the polymerizations.[178,179]

The ability of mPEG-*b*-P(BLG-*co*-Gly) diblock copolymer to form organogels in different solvents was investigated and the properties of DMF gels were studied comprehensively. To prepare the organogel systems, the denoted weight fractions of polymer and DMF were mixed and stable organogels were generated after standing at room temperature for up to 3 days. To investigate the solvent effect in the gel formation, several organic solvents were screened. The polymers could not be dissolved into non-polar or low-polar organic solvents, such as hexane, dichloromethane (DCM), chloroform and tetrahydrofuran (THF), while gelation was observed in relatively high-polarity organic solvents, such as dioxane and dimethyl sulfoxide (DMSO). The critical gel concentrations (CGCs, Table 5.1) were obtained by preparing different

polymer concentrations in DMF and measured by the test tube inversion method at room temperature.[180] By comparing polymer **11** (0.8 wt %) with polymer **10** (0.6 wt %), it could be concluded that the CGC decreased with increased Gly content in the polypeptide segment when the Gly content was less than 50 mol %, while this trend reversed with Gly at greater than 50 mol %. The turbidities of the organogels at 2.5 wt % also changed from being transparent to opaque with increased Gly content in the polypeptide segments (Figure 5.3).

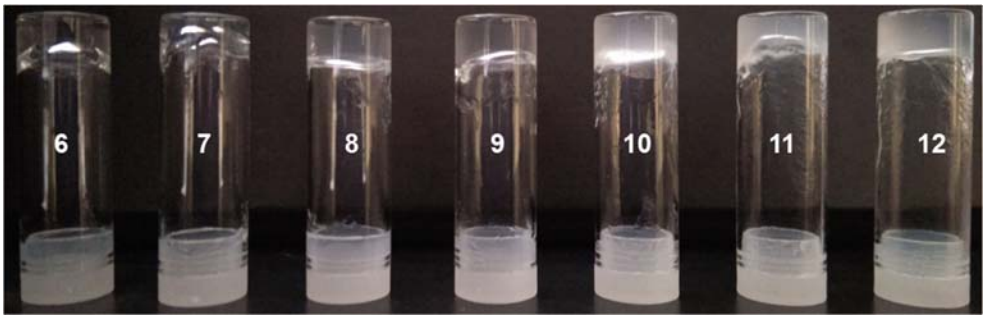

Figure 5.3. Images of organogels from polymers **6**, **7**, **8**, **9**, **10**, **11** and **12** in DMF (2.5 wt %).

In order to further understand the properties of these organogel systems, the supramolecular structures of the dried gels from polymers **4** – **12** were investigated by attenuated total reflectance-Fourier transform infrared spectroscopy (ATR-FTIR) (Figure 5.4a). The characteristic absorbances of secondary structures were clearly observed in the FTIR spectra, especially in the region of amide I band (1700 – 1600 cm^{-1}). The absorbances at 1650 cm^{-1} (amide I) and at 1547 cm^{-1} (amide II) were attributed to α-helical conformations.[120] The β-sheet secondary structure was observed at 1675 cm^{-1}

and 1626 cm^{-1} (both in amide I), in combination with a peak at 1520 cm^{-1} (amide II).[181] Other secondary structure populations, such as random coils or turns, showed absorbances at 1600 – 1620 cm^{-1}, 1640 – 1650 cm^{-1}, 1660 – 1670 cm^{-1} and 1680 – 1700 cm^{-1}.[182] The peak at 1728 cm^{-1} corresponded to the C=O stretch of the benzyl ester

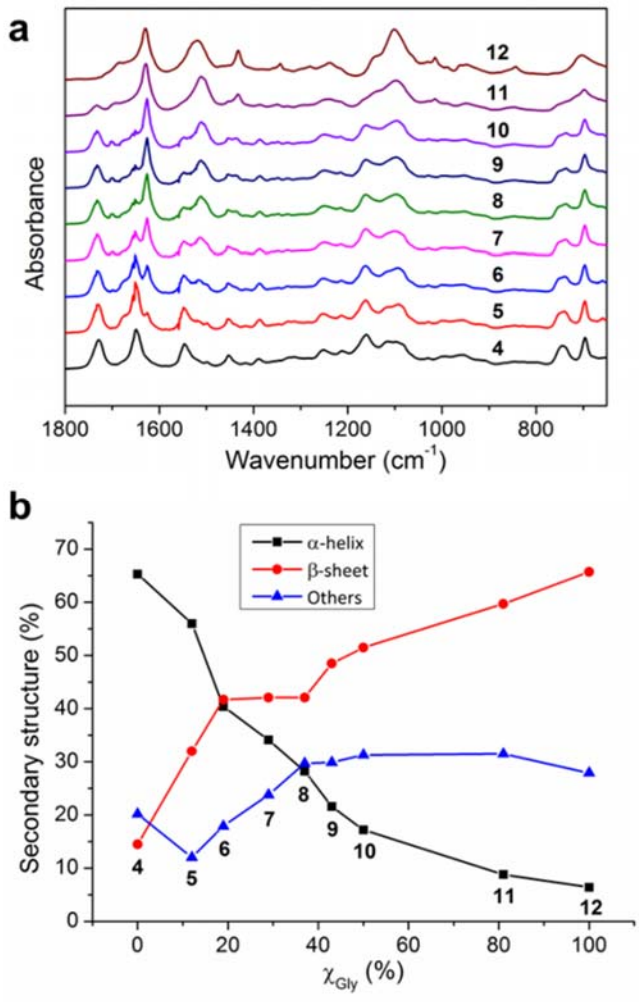

Figure 5.4. (a) ATR-FTIR spectra and (b) secondary structure populations of polymers **4** – **12** in the solid state.

group in the side chain of BLG.[177] Qualitatively, the absorption intensity assigned to the peaks of β-sheet secondary structures increased with higher mole fraction of Gly in the polypeptide segment, while the intensities of peaks of α-helices decreased correspondingly.

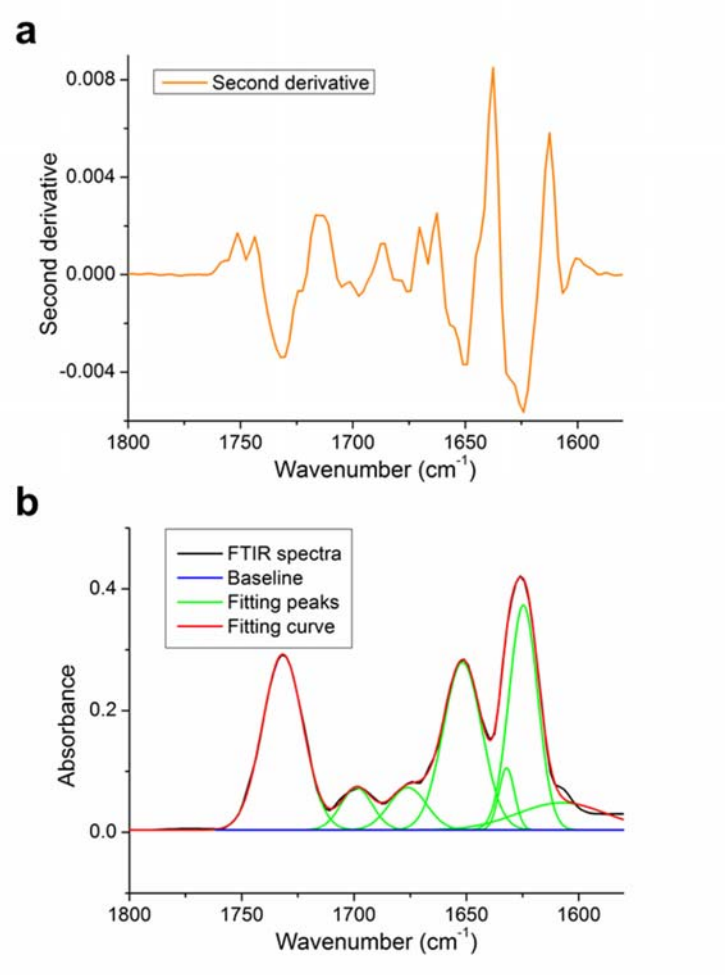

Figure 5.5. (a) Second derivative and (b) ATR-FTIR spectra (black), fitting curve (red), baseline (blue) and fitting peaks (green) for polymer **7** in the solid state.

Further quantitative analyses of secondary structures were conducted by employing second derivative and deconvolution strategies to extract relative peak intensities of individual bands in the ATR-FTIR spectra. These analyses provided extraction of secondary structural components in the heavily populated amide I regions, followed by curve fitting to determine signal amplitude for each band (Figure 5.5), as summarized in Figure 5.4b and Table 5.2.[177,183,184] For each polymer, the supramolecular structures were composed of α-helix, β-sheet and other secondary structures, regardless of the difference in the chemical compositions. As the mole fraction of Gly in the polypeptide segment increased from 0% to 100%, the α-helical content decreased systematically from 65% to 6% of total band intensity and the β-sheet component raised gradually from 14% to 66%. The β-sheet contribution to secondary structure became dominant over the α-helix contribution with Gly mole fraction greater than 19% in the polypeptide segment. Other secondary structure band intensities remained relatively constant for all formulations.

The higher-order self-assembled structures of the dried gels from mPEG-*b*-P(BLG-*co*-Gly) diblock copolymers were also investigated by wide-angle X-ray scattering (WAXS). The WAXS pattern for gel from polymer **12** (Figure 5.6) gave a *d* spacing of 4.4 Å with stronger signals for PEG crystallization reflection, which was also demonstrated by the melting and crystallizing peaks in the differential scanning calorimetry (DSC) trace of polymer **12** (Figure 5.7b). This *d* spacing of 4.4 Å has been observed and assigned to antiparallel β-sheet formation in poly(L-alanylglycine)[185] and the self-assembled PEG-*b*-β-strand-peptides.[186] The WAXS patterns for gels from

polymers **7**, **10** and **11** had similar *d* spacings at 4.6 Å, 4.6 Å and 4.5 Å, respectively. These slightly increased *d* spacings suggested higher α-helix content in the secondary structures, which could enlarge the distance between adjacent polypeptide chains. The presence of α-helical content also appeared to have disrupted PEG chain order, observed as a lack of PEG crystallization peaks in the WAXS patterns of the gels from polymers **7**, **10** and **11** and a lack of melting transition in the DSC trace of polymer **11** (Figure 5.7a).

Transmission electron microscopy (TEM) was employed to study the nanostructures of the organogels as related to the copolypeptide composition. The TEM samples were prepared with a polymer concentration of 1.0 mg/mL in DMF and stained

Table 5.2. Quantitative analyses of secondary structure populations of polymers **4** – **12** in the solid state.

Polymer	α-Helix	β-Sheet	Others
4	65	15	20
5	56	32	12
6	40	42	18
7	34	42	24
8	28	42	30
9	22	49	29
10	17	52	31
11	9	60	31
12	6	66	28

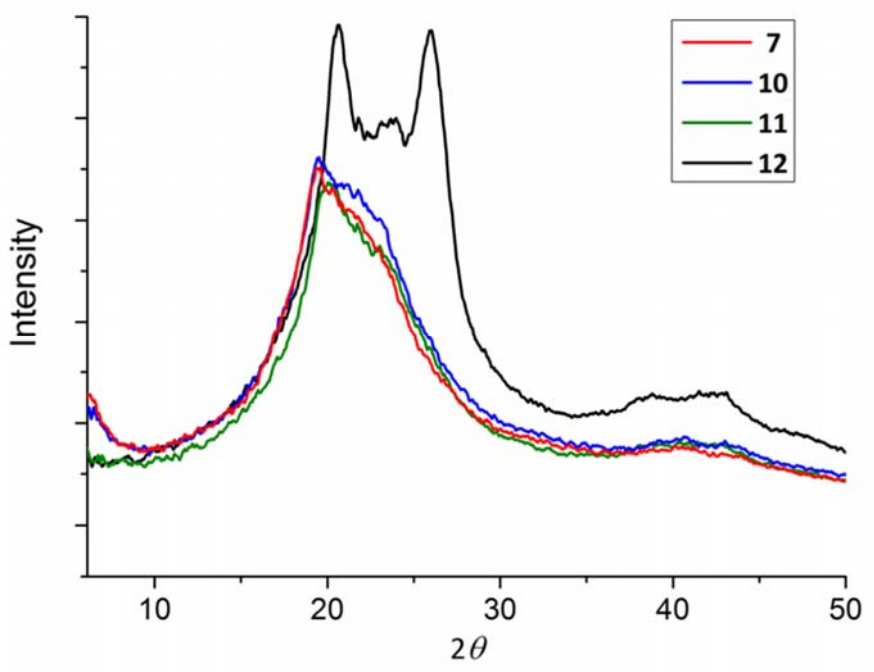

Figure 5.6. WAXS patterns for polymers **7**, **10**, **11** and **12** in the solid state.

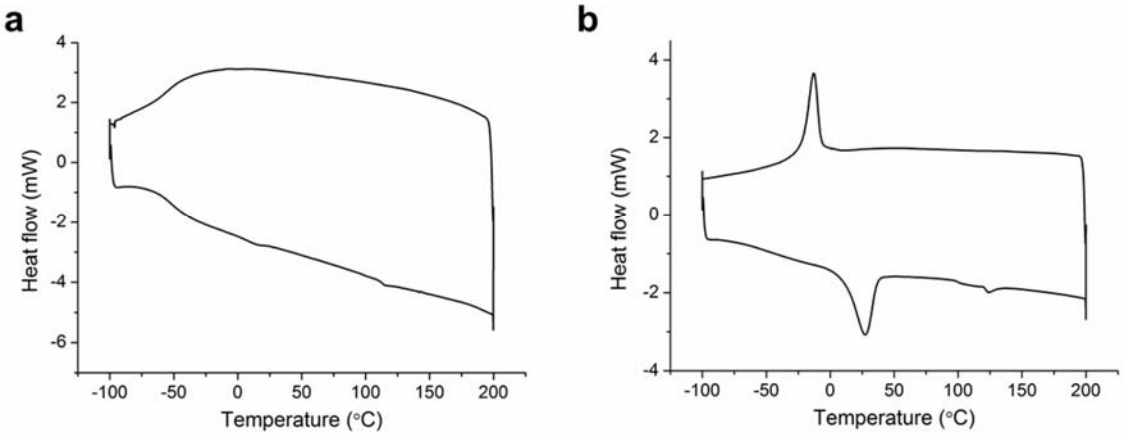

Figure 5.7. DSC traces of polymers (a) **11** and (b) **12** in the solid state. The samples were heated from -100 °C to 200 °C and cooled back to -100 °C, each with a rate of 10 °C/min. The second heating and cooling traces are shown here.

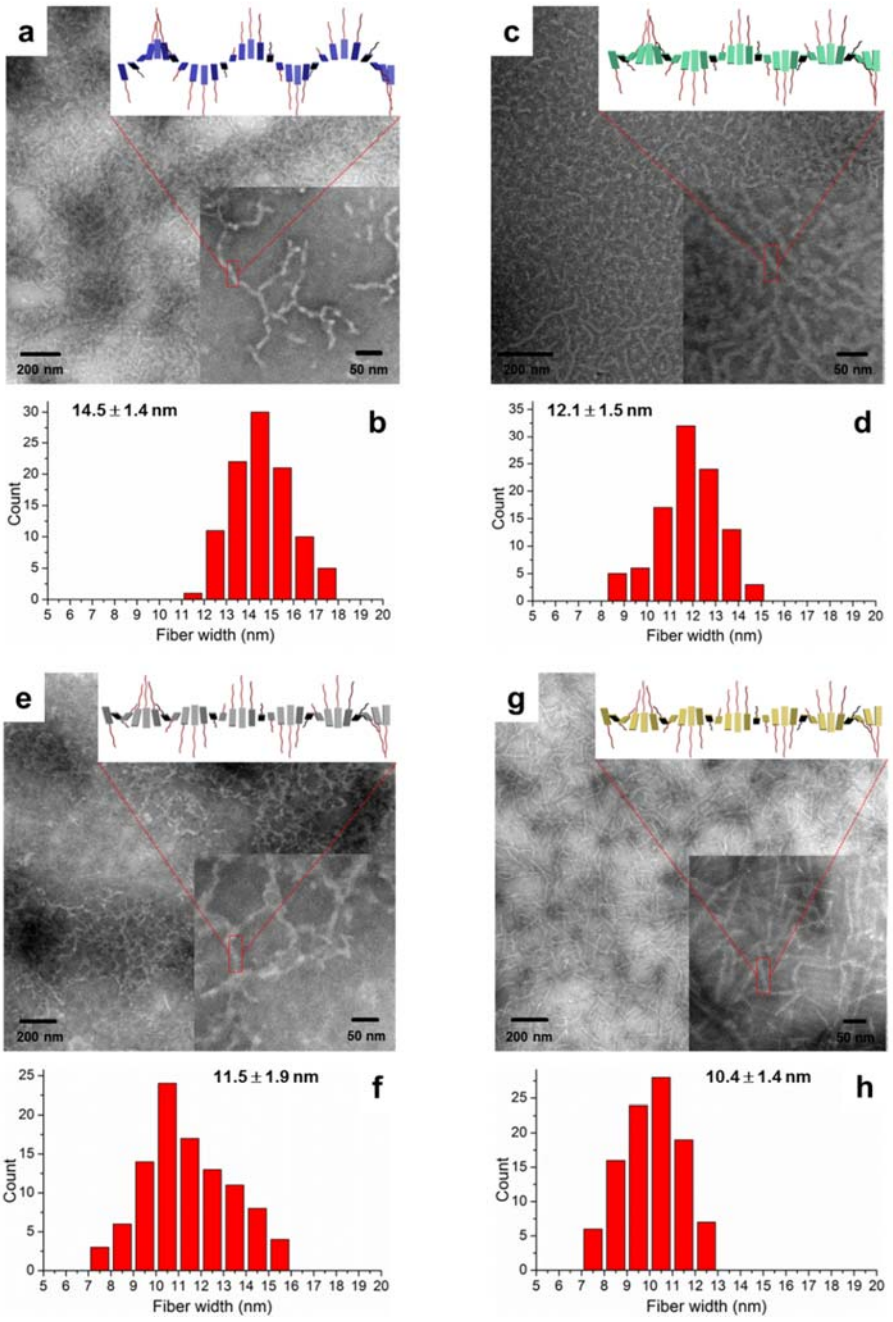

Figure 5.8. TEM images and fiber width distributions of gels from polymers **7**, **10**, **11** and **12**, obtained by counting 100 fibers. (a) TEM image and (b) fiber width distribution of **7**. (c) TEM image and (d) fiber width distribution of **10**. (e) TEM image and (f) fiber width distribution of **11**. (g) TEM image and (h) fiber width distribution of **12**. The inserted images at the upright corners of (a), (c), (e) and (g) are the proposed twisted fibrils.

by phosphotungstic acid (PTA) aqueous solution. Bright-field TEM images of organogels from polymers **7**, **10**, **11** and **12** (Figure 5.8a, 5.8c, 5.8e and 5.8g, respectively) showed fibrillar nanostructures with average widths of 14.5, 12.1, 11.5 and 10.4 nm. The narrow width distributions of nanofibrils from polymers **7**, **10**, **11** and **12** (Figure 5.8b, 5.8d, 5.8f and 5.8h, respectively), obtained by counting 100 nanofibrils in the TEM images, indicated that all of the organogels had well-defined nanofibrillar morphologies. The average diameters of nanofibrils increased with a larger α-helical content in the secondary structures, which might be attributed to the formation of twisted fibrils (Inset images at the upper right corners of Figure 5.8a, 5.8c, 5.8e and 5.8g, respectively), originating from a combination of increased steric hindrance and chirality change with the introduced BLG component.[66,187,188] Furthermore, the β-sheet-rich polymer **12** showed more rigid nanofibrils when compared with the other fibril nanostructures from polymers with increased α-helical components.

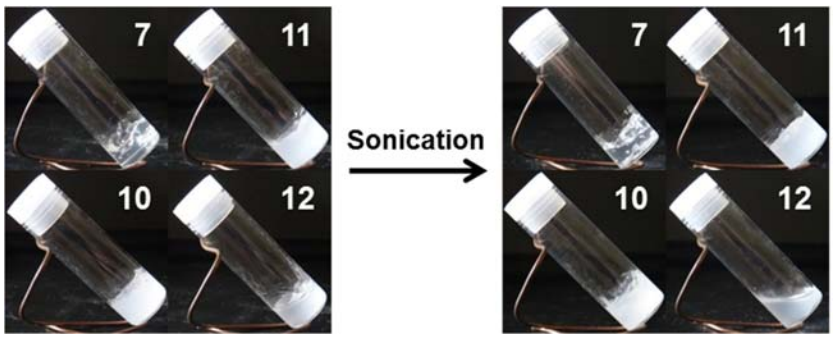

Figure 5.9. Digital images of organogels from polymers **7**, **10**, **11** and **12** in DMF (5.0 wt %) before (left) and after (right) sonication.

Additional studies of the thermal properties and external stimuli-responsive features of the organogel systems from polymers **7**, **10**, **11** and **12** in DMF were also performed. Gels from all four polymers, with a concentration of 5 wt % in DMF, could withstand temperatures of 90 °C over 1 h, however, the four gels behaved quite differently after 30 s sonication at room temperature. The gels from polymers **7**, **10** and **11** remained in the gel state, even with longer sonication time (*ca.* 30 min), while the gel from polymer **12** was transformed to a solution state after 30 s sonication (Figure 5.9). This transition was reversible, with the gel reforming after being placed at room temperature for 3 h. TEM was also used to characterize the changes of nanostructural morphologies within the gels before and after sonication was applied. The gels from polymers **11** and **12**, with an initial concentration of 5 wt % in DMF, were diluted to polymer solutions of 1.0 mg/mL after 30 s sonication, drop deposited, and stained with PTA aqueous solution to prepare the TEM samples. Alterations in the nanostructures for gels from polymers **11** and **12** were observed by comparison of TEM images before (Figure 5.8e and 5.8g) and after (Figure 5.10a and 5.10b) sonication. In the gel from polymer **11**, longer nanofibrils disappeared after sonication and, instead, short nano-rods were observed. The ability of the gel states to reform and for the gel assemblies to undergo toughening was also demonstrated by dynamic mechanical analysis (DMA), in which a 20% increase in storage modulus was detected for the gel after sonication (Figure 5.11). This sonication-promoted gel-to-gel transition with increased modulus implied that a temporary disruption of nanostructures occurred for polymer **11** during sonication and resulted in ordering that was even more stable, akin to an annealing

process. Immediate reassembly of short nano-rods, *in situ* after sonication, facilitated the rebuilding of three-dimensional networks and resulted in a sonication-triggered gel-to-gel transition. However, in the gel produced from polymer **12**, the longer nanofibrils were expressly converted into short nano-rods, which were well-aligned in nanodomians, but lacked longer range connectivity between clusters, ultimately resulting in a gel-to-sol transition. When the solution was maintained at room temperature for 3 h, the one-dimensional growth of nano-rods to longer nanofibrils resulted in reconstruction of the gel.

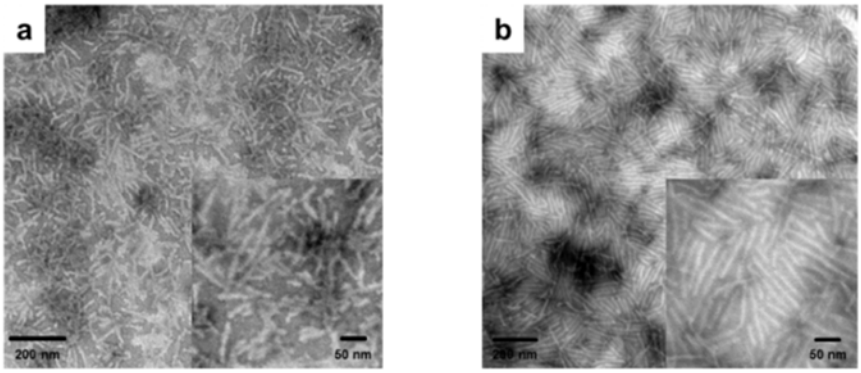

Figure 5.10. TEM images of organogels from polymers (a) **11** and (b) **12** after 30 s sonication.

While the nano- and supramolecular-scale properties could be correlated to the macroscale gel-to-gel and gel-to-sol transitions, it is also important to study the micro- and meso- scale structures of the gels in order to fully understand the gel behavior through all scales of self-interaction. To this effect, dye incubation (1 wt % 0.1 mM Alizarin Red S in DMF) in 5 wt % gels from polymers **11** and **12** were studied by laser

scanning confocal microscopy (Figure 5.12). It was observed that the gel homogeneity on the micro- and meso-scales was much higher in the organogel from polymer **12**, both before and after sonication (Figure 5.12.3 and 5.12.4) when compared to the gel of polymer **11** (Fig. 5.12.1 and 5.12.2). Observing the organogel from polymer **11** in the bulk (Figure 5.12.1a), as well as in isolated regions (Figure 5.12.1b-e), it was evident that both larger mesoscale domains (*ca.* 50 μm) and microscale (*ca.* 1-10 μm) structures could be observed. On sonication of the organogel from polymer **11** (Figure 5.12.2), both types of structures remained on these scales and longer range interactions did not appear to be overtly changed in the gel, correlating well to the tube inversion and DMA findings. Pre-sonication, organogel from polymer **12** possessed a homogeneous background emission with a collection of proximate microdomains (*ca.* <1 to 5 μm). Also of note, the fluorescent image showed diffused (Figure 5.12.3b) structure edges coincident with the differential imaging contrast (DIC) micrograph, but significantly broader than those in the gels from polymer **11**, indicating extradomain interactions beyond that observed in DIC. Considering organogel from polymer **12** post-sonication (Figure 5.12.4), it was observed that the higher emission regions were smaller and more numerous in the fluorescence channel, while in DIC the majority of microstructures had been eliminated. These findings indicated the generation of isolated, sub-diffraction scale domains, which lacked intrinsic long-range interactions.

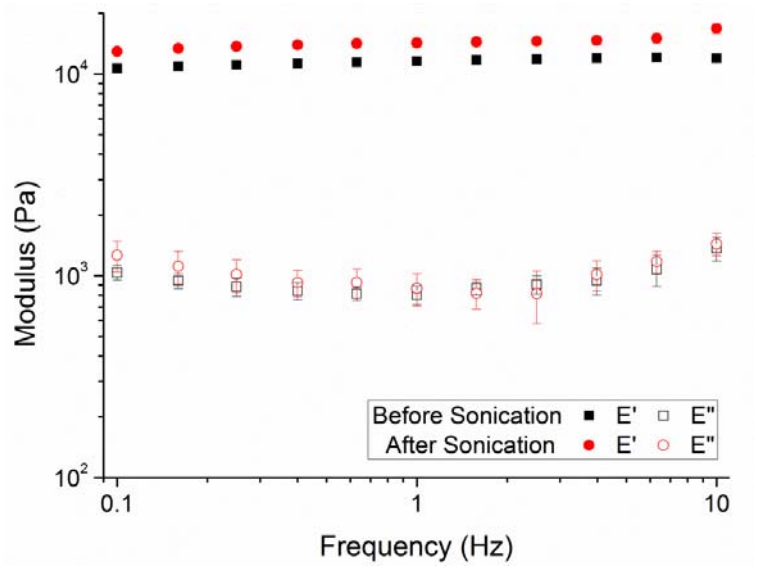

Figure 5.11. Moduli of organogels from polymer **11** in DMF (5 wt %) before and after sonication as a function of frequency conducted by DMA. E′ and E″ indicate storage and loss modulus, respectively.

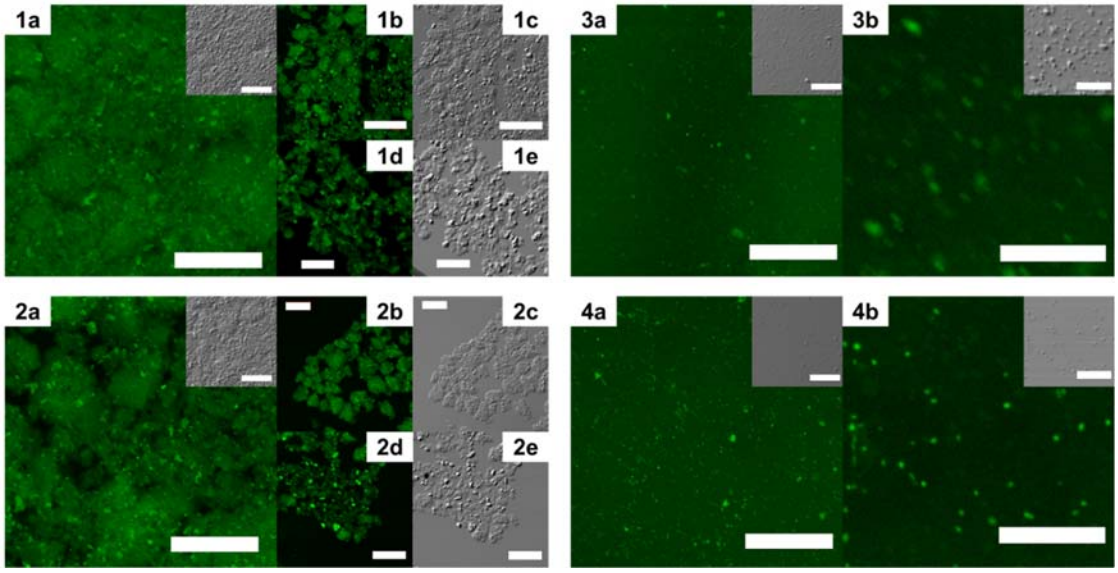

Figure 5.12. Confocal imaging of dyed organogel from polymers **11** in DMF (5 wt %) before (1a-e) and after (2a-e) sonication. Confocal imaging of dyed organogel from polymer **12** in DMF (5 wt %) before (3a-b) and after (4a-b) sonication. Fluorescence images were greenscale and DIC images were greyscale. Scale bars: 100 μm for 1a-c, 2a-c, 3a and 4a; 50 μm for 1d, 1e, 2d, 2e; 20 μm for 3b, 4b.

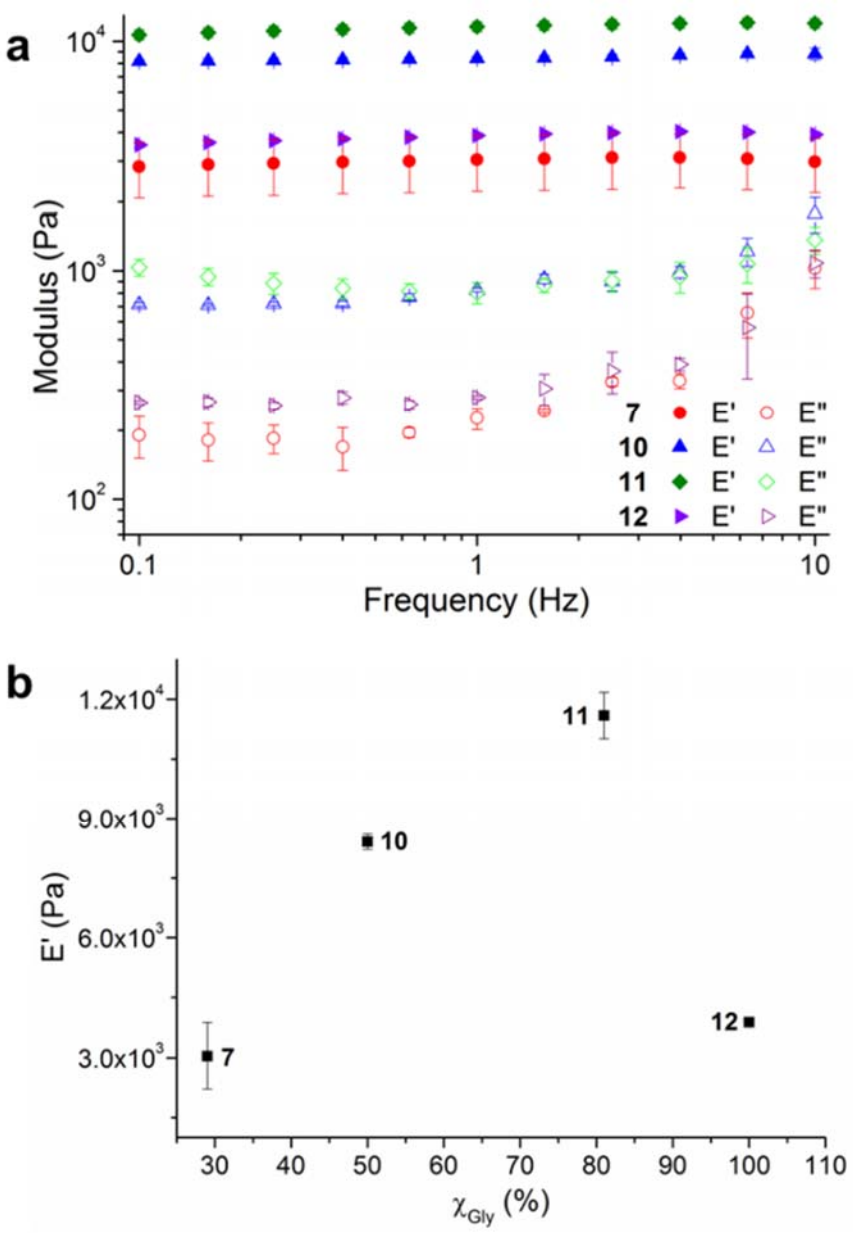

Figure 5.13. (a) Moduli of organogels from polymers **7**, **10**, **11** and **12** in DMF (5 wt %) as a function of frequency conducted by DMA. E′ and E″ indicate storage and loss modulus, respectively. (b) Storage modulus of organogels from polymers **7**, **10**, **11** and **12** in DMF (5 wt %) as a function of mole fraction of Gly (χ_{Gly}) in polypeptide segment under the static frequency of 1 Hz in DMA tests.

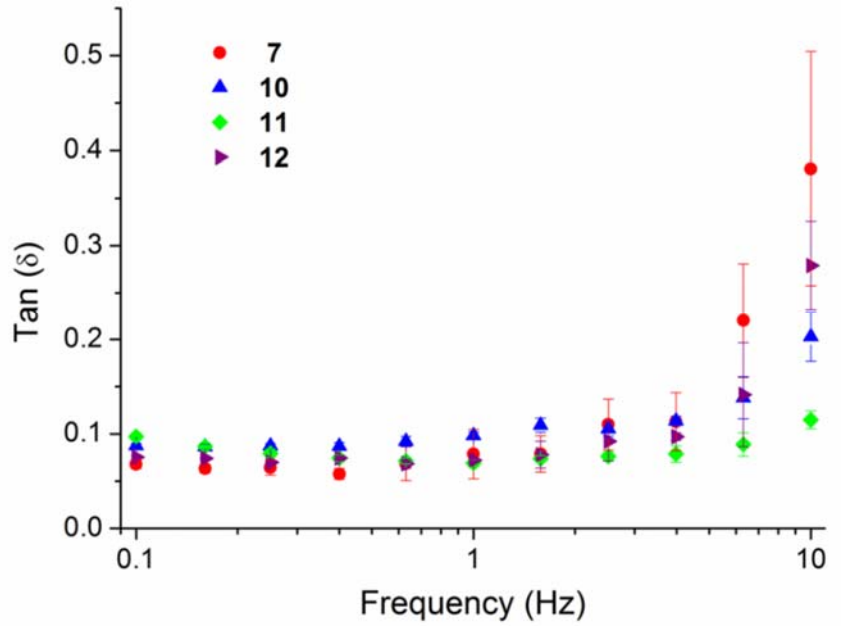

Figure 5.14. Tan (δ) of organogels from polymers **7**, **10**, **11** and **12** in DMF (5 wt %) as a function of frequency, conducted by DMA.

The mechanical properties of the organogel systems were characterized by DMA on polymers **7**, **10**, **11** and **12** in the gel state at a concentration of 5 wt %, which was sufficiently high to produce a robust gel that could withstand high frequency operation. Frequency modulation showed systematic changes in the storage (E′) and loss (E″) moduli of the organogels for polymers **7**, **10**, **11** and **12** (Figure 5.13a). For each polymer, the loss modulus remained smaller than the storage modulus within the frequencies observed (0.1 to 10 Hz), demonstrating no gel-to-sol transition in this frequency range, which was also observed in the tan(δ) data (Figure 5.14). The storage moduli at 1 Hz of the four gels were 3.0, 8.4, 11.6 and 3.9 kPa for the samples **7**, **10**, **11** and **12**. With the mole fraction of Gly changing from 19% to 81%, the gel moduli

increased by a factor of 4, demonstrating an enhancement of the strength of the gel systems. However, the storage modulus dropped significantly for the 100% Gly (polymer **12**) system (Figure 5.13b), in comparison to those copolypeptide block copolymer materials containing proportions of BLG.

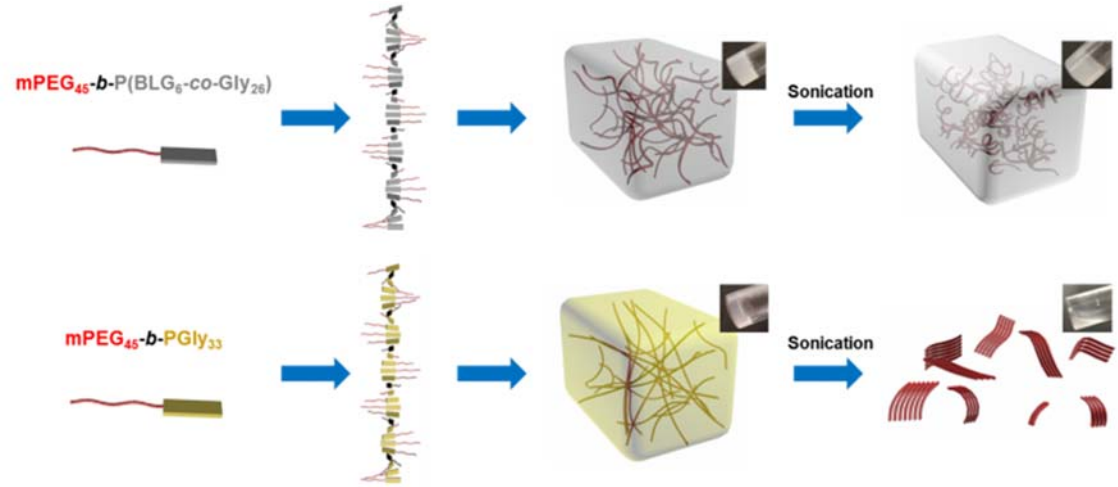

Figure 5.15. A schematic illustration of the nanofibrils formed in the network structure of organogels form polymers **11** (upper) and **12** (lower) and also the gel-to-gel and gel-to-sol transformations after sonication.

Taking together the results of NMR, FTIR, WAXS, DSC, TEM, confocal and DMA analyses, a mechanism for organogel formation from the mPEG-*b*-P(BLG-*co*-Gly) diblock copolymers and the relative stabilities of the matrices to sonication is proposed (Figure 5.15). The supramolecular self-assembly of the polypeptide segments into well-defined nanofibrils was driven by the formation of β-sheet secondary structure, as seen spectrally and microscopically, resulting in the construction of organogels. The presence of α-helical contents in the secondary structures broadened the distance

between the polypeptide chains and the width of nanofibrils. In the gel state, after sonication, the nanofibrillar structures were deconstructed into short nano-rods by cleaving the supramolecular interactions between polypeptide segments. In the α-helix-rich organogels, the reassembly of relatively less locally ordered and more flexible nano-rods,in combination with the maintenance of long-range interactions, resulted in the immediate reconstruction of organogels *in situ* as a sonication-triggered gel-to-gel transition. However, the failure to reconstruct three-dimensional network from more locally aligned and rigid nano-rods, and the disappearance of micro- and meso-scale interactions for the β-sheet-rich polymer, led to a sonication-triggered gel-to-sol transition. Ultimately, the effect on the external sonication-responsive property due to secondary structure control of statistical copolypeptide-based organogels provides a novel and facile method to modify the properties of stimuli-responsive materials by tuning the self-assembled nano- or microstructures without the need of precise control on the molecular level.

With the construction of organogels from mPEG-*b*-P(BLG-*co*-Gly) diblock copolymers being driven by β-sheet formation in the polypeptide segments, a self-healing property of the gel system was expected and demonstrated by a macroscopic self-healing experiment conducted on polymer **11** in DMF at a concentration of 20 wt %.[189,190] Half of the organogel was blended with 0.01 mL of Alizarin Red S DMF solution for visibility (Figure 5.16a). Both of the gel fractions were then loaded into syringes (Figure 5.16b), extruded into a glass petri dish and cut into pieces (Figure

5.16c). Self-healing behavior began immediately after two pieces of organogel were placed into contact on the cut faces (Figure 5.16d). After 3 min, the combined gel was

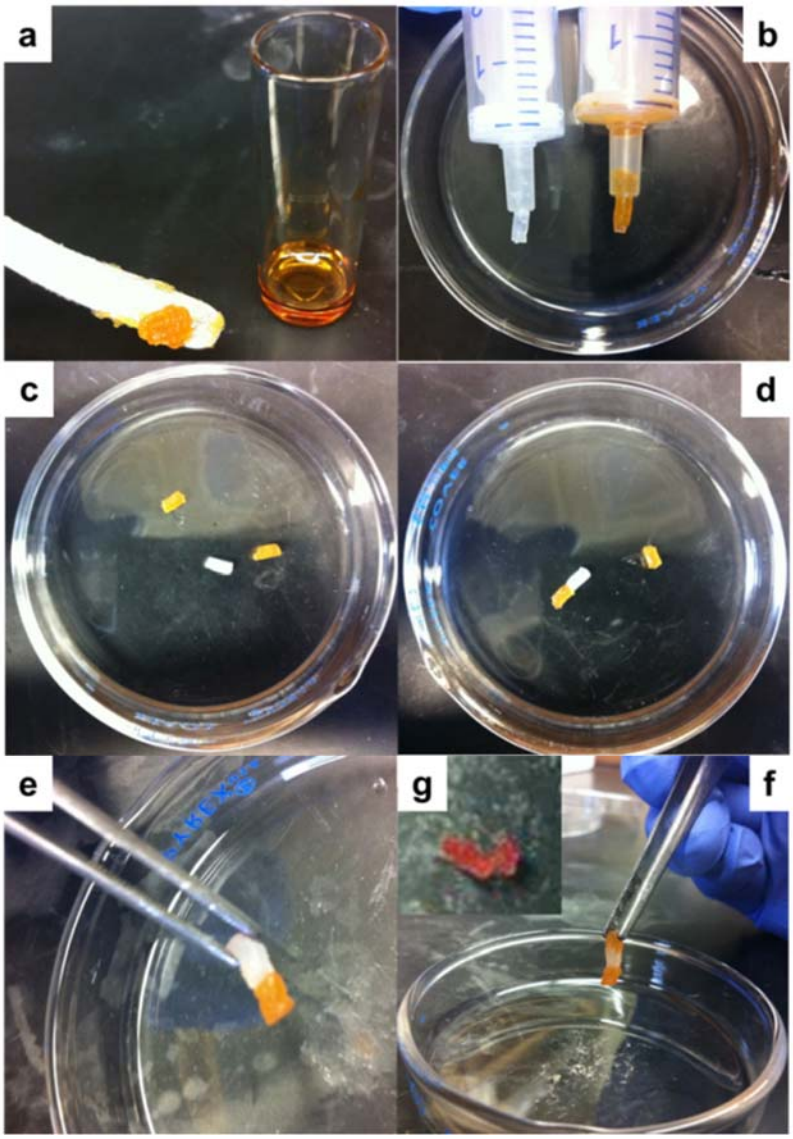

Figure 5.16. Macroscopic self-healing behavior of organogels from polymer **11** in DMF (20 wt %). (a) Gel was mixted with Alizarin Red S DMF solution, (b) loaded into syringe, (c) cut into pieces, (d) attached together, (e) picked up by tweezer, (f) then connected one by one and (g) diffusion of dye complete after 3 days.

sufficiently strong to be picked up by tweezers (Figure 5.16e). Multiple pieces of cut gel could be reconnected together by attaching them one-by-one (Figure 5.16f). The diffusion of Alizarin Red S was observed in the self-healed gel at room temperature, and afforded a single gel matrix with a homogeneous color after 3 days (Figure 5.16g).

5.4 Conclusions

Sonication-responsive macromolecular statistical copolypeptide-based organogels exhibited unique properties that were tuned by secondary structural control that was offered by a series of robust statistical copolymerizations with variation in the copolypeptide feedstock selection. This strategy circumvents the elaborate designs and multi-step syntheses. The effect of the self-assembled secondary structures, especially α-helix and β-sheet configurations, on the properties of organogels were explored by using a serious of mPEG-*b*-P(BLG-*co*-Gly) diblock copolymers with varied chemical compositions in the polypeptide segments. Detailed characterization studies revealed that gelation in DMF was driven by supramolecular assembly of β-sheets into well-defined fiber-like nanostructures, further generating a three-dimensional network through longer-range interactions. The sonication-triggered gel-to-gel transition observed in the case of organogels from α-helix-rich systems was shown to originate from an immediate reconstruction into a three-dimensional network of nano-rods. However, for the β-sheet-rich polymer, a gel-to-sol transition resulted from the failure of network rebuilding, instead showing reorganization of nano-rods into locally-aligned nanodomains with a small amount of interactions between them. The CGC and stiffness

of these organogels could be tuned by simply varying the ratios of α-helix to β-sheet in the secondary structures, which was in-turn, modulated by the feed ratios of BLG and Gly NCA monomers during the polymerization. These results illustrate the influence of secondary structures on supramolecular assembly of hybrid diblock synthetic polypeptides in the gel state and demonstrate a novel, facile approach to fabricate nanostructures with stimuli-responsive properties. Moreover, the sonication-responsive properties, the injectability and self-healing capabilities of the organogels enable further study and potential applications in sensor design, construction of adaptive materials and controlled release systems.

CHAPTER VI

POLYPEPTIDE-BASED CONTROLLED RELEASE HYDROGEL WITH MULTI-RESPONSIVENESS BY RING-OPENING COPOLYMERIZATION OF *N*-CARBOXYANHYDRIDES*

6.1 Introduction

Nonsteroidal anti-inflammatory drugs (NSAIDs) have been widely used in the clinical treatments of acute or chronic pains, or inflammations by inhibiting cyclooxygenases (COXs), which exist in two isoforms: COX-1 and COX-2.[191] Despite their widely systematic usage, NSAIDs are usually ingested orally in high dosage. However, the high dosages of NSAIDs can cause some undesirable side effects, such as adverse gastrointestinal effects and cardiovascular risks.[191,192] To overcome these undesirable side effects, NSAIDs can be incubated in a controlled release system, which will be directly injected into the target sites.[193,194] After injection of this drug-loaded complex, the NSAIDs will be released under some external stimuli or internal enzyme degradations to minimize the systematical dosages and undesirable side effects of NSAIDs.[195,196] Therefore, it is clinically beneficial to develop a biocompatible controlled release system with external stimuli-responsiveness as a localized delivery agent for topical inflammations, such as osteoarthritis.

---

* In collaboration with Sarosh Khan, Xun He, Richen Li, Hai Wang, Jiong Zou, Karen L. Wooley, Departments of Chemistry, Chemical Engineering, Materials Science and Engineering, and Laboratory for Synthetic-Biologic Interactions, Texas A&M University.

Hydrogels have attracted significant attention in the last decades for their potential applications as scaffolds for tissue engineering, matrices for controlled drug release and absorbents for aqueous pollutant capture and removal.[197,198] Hydrogels are a class of materials comprising polymeric or low-molecular-weight crosslinked hydrogelators that can entrap substantial amounts of water or aqueous solutions and maintain distinct three-dimensional networks.[60] The high water content and tunable properties of these materials render them as attractive candidates for mimicking soft tissue microenvironments as well as promising media for localized storage and delivery of therapeutic agents.[199] In addition, hydrogels with various stimuli-responsive properties, which are triggered by physical, chemical or biological stimuli, can be constructed by controlling supramolecular noncovalent interactions and chemically covalent linkages of hydrogelators.[19,200] The regulated reorganizations within the three-dimensional structures as well as transitions between sol and gel states provide tunable release rates of small molecules, which enable stimuli-responsive hydrogels as potential controlled release systems for NSAIDs.[175] Recently, Cao *et al.* reported that one kind of NSAIDs, naproxen (Npx), can be released in a controlled manner from a γ-ray-responsive hydrogel, consisted of a diselenide-containing polymer and Npx-conjugated dipeptide, by UV radiation.[196] At present, Npx-loaded controlled release hydrogels remain limited to primarily low-molecular-weight hydrogelators, few studies of systems developed from polymeric hydrogelators have been performed.

Among biodegradable polymers, polypeptide-based materials have significant advantages including biological compatibility, low toxicity and tunable secondary

structures.[59,75] Polypeptide-based materials have been widely used in the construction of supramolecularly assembled hydrogels.[16,51,70,175] Their broad applicability is due to the precisely-defined nano- and microstructures derived from hierarchical assemblies of polypeptides and the variety of stimuli responses available to natural and synthetic polypeptides. Secondary structures, especially α-helix and β-sheet confirmations, can serve as the driving forces to form well-defined fibrous structures, which self-assemble into noncovalently crosslinked three-dimensional networks and encapsulate water to form hydrogels.[16] Recently, Chen and coworkers reported a biocompatible polypeptide-based hydrogelator, poly(ethylene glycol)-*block*-poly(γ-propargyl-L-glutamate) (PEG-*b*-PPLG), that has a temperature-triggered sol-to-gel transition driven by the formation of β-sheet secondary structures.[70] Herein, we report a thermo-, mechano-, and enzyme-responsive polypeptide-based hydrogelator, methoxy poly(ethylene glycol)-*block*-poly(L-alanine-*co*-glycine-*co*-L-isoleucine) (mPEG-*b*-P(A-G-I)), which was facilely synthesized from the statistical copolymerization of three different α-amino acid *N*-carboxyanhydride (NCA) monomers. In contrast to most of polypeptide-based hydrogelators undergoing gel melting with increased temperature, a reserve thermal gelation profile and sonication-triggered gel-to-sol transition were observed in our report. Detailed characterizations and analyses were performed to investigate the driving force for the heat-induced hydrogelation behavior and understand the correlation between nanostructural morphologies and stimuli-responsive sol-gel transitions. This multi-responsive hydrogel system is very promising as a controlled release system of Npx for the treatments of topical inflammations.

6.2 Experimental section

6.2.1 Materials

Ethyl acetate, *n*-hexane, tetrahydrofuran (THF), diethyl ether, *N,N*-dimethylformamide (DMF, anhydrous, ≥ 99.8%), L-alanine (≥ 99.5%), L-isoleucine (≥ 99.5%), bis(trichloromethyl) carbonate (≥ 98%), glycine (≥ 99%), trichloromethyl chloroformate (≥ 97%), Proteinase K, Trypsin and Naproxen (Npx) were purchased from Sigma-Aldrich company (USA). Monomethoxy-monoamino-terminated poly(ethylene glycol) ($mPEG_{45}$-NH_2, M_n = 2000 g/mol) was purchased from Rapp Polymere (Germany). All chemicals were used without further purification, unless otherwise noted. Nanopure water (18.2 MΩ·cm) was acquired by means of a Milli-Q water filtration system, Millipore Corp. (St. Charles, MO). Tris-HCl buffered saline and phosphoate buffered saline (PBS) were purchased from Sigma-Aldrich company (USA) as dry powders and were dissolved into 1.0 L deionized water to acquire desired buffer solution, respectively.

6.2.2 Instrumentation

^1H and ^{13}C NMR spectra were recorded on Varian Inova 300 MHz spectrometers interfaced to a UNIX computer using VnmrJ software. Chemical shifts were referenced to the solvent resonance signals. Attenuated total reflectance-Fourier transform infrared spectroscopy (ATR-FTIR) spectra were recorded on an IR Prestige 21 system (Shimadzu Corp.) and analyzed using IRsolution v. 1.40 software. Circular dichroism (CD) spectra were recorded on a Chirascan CD spectrometer from Applied Photophysics, Ltd. (Leatherhead, UK) equipped with a 150 watt xenon arc lamp. The polymer solution

samples for CD measurements were prepared at the desired concentration in nanopure water. The samples were placed in a quartz cell with a path length of 1.0 mm and analyzed between 180 and 280 nm with a wavelength step of 1.0 nm. Measurements were analyzed using Pro-Data Version 5 software.

Thermogravimetric analysis (TGA) was performed under Argon atmosphere using a Mettler-Toledo model TGA/SDTA851^e (Mettler-Toledo, Inc., Columbus, OH), with a heating rate of 10 °C/min. Measurements were analyzed using Mettler-Toledo STAR^e v. 7.01 software. Glass transition temperatures (T_g) were measured by differential scanning calorimetry (DSC) on a Mettler-Toredo DSC822®, with a heating rate of 10 °C/min. Measurements were analyzed using Mettler-Toledo STAR^e v. 7.01 software. The T_g was taken as the midpoint of the inflection tangent, upon the second heating scan.

Wide-angle X-ray scattering (WAXS) was performed on a Bruker D8 Bragg-Brentano X-ray powder diffractometer. The sample was placed in the sample holder of a two circle goniometer, enclosed in a radiation safety enclosure. The X-ray source was a 2.2 kW Cu X-ray tube, maintained at an operating current of 40 kV and 40 mA. The X-ray optics was the standard Bragg-Brentano para-focusing mode with the X-ray diverging from a DS slit (1 mm) at the tube to strike the sample and then converging at a position sensitive X-ray Detector (Lynx-Eye, Bruker-AXS). The two-circle 250 mm diameter goniometer was computer controlled with independent stepper motors and optical encoders for the θ and 2θ circles with the smallest angular step size of 0.0001° 2θ. The software suit for data collection and evaluation was

window based. Data collection was automated COMMANDER program by employing a DQL file and analyzed by the program EVA.

Transmission electron microscopy (TEM) images were collected on a JEOL 1200 EX operating at 100 kV and micrographs were recorded at calibrated magnifications using a SLA-15C CCD camera. The final pixel size was 0.42 nm/pixel. Samples for TEM measurements were prepared as follows: 10 μL of the dilute solution (with a polymer concentration of 1 mg/mL) was deposited onto a carbon-coated copper grid, and after 2 min, the excess of the solution was quickly wicked away by a piece of filter paper. The samples were then negatively stained with 1 wt % phosphotungstic acid (PTA) aqueous solution. After 30 s, the excess staining solution was quickly wicked away by a piece of filter paper and the samples were left to dry under vacuum overnight.

Scanning electron microscopy (SEM) imaging was performed in JOEL JSM-6400 SEM operated at an acceleration voltage of 15 kV. The preparation of samples for SEM involved placing 100 μL hydrogel on a carbon thin film. The gel was then subjected to immediate freezing by liquid nitrogen, followed by lyophilization for 3 days. The surface of the gel was sputter coated with gold for 3 min under argon before imaging.

Sonication responsive experiments were performed in an ultrasonic homogenizer (maximum power, 150W, 20KHz, Model 150 V/T, Biologics, Inc.) equipped with a micro tip with a diameter of 3.81 mm, employing the power outlet of 45 W in the frequency of 20 KHz at room temperature.

Dynamic rheological experiments were conducted on an ARES-G2 rheometer (TA Instruments). The rheological study of 4 wt % hydrogel sample was performed over 3 h in compression on a 2.5 mm thick, 1.0 mm diameter cylinder. The measurements of storage modules (G′) and loss modulus (G″) with gelation was recorded as a function of temperature over a range of 25 to 45 °C by a heating rate of 1.0 °C/min at a frequency of 1.0 Hz and at a constant strain of 2%. The data presented were obtained as a single exponential decay using Origin Pro 8.1 software.

6.2.3 Experimental procedures

Synthesis of L-alanine *N*-carboxyanhydride (Ala NCA) monomer

In a 250 mL three-necked round bottom flask equipped with a magnetic stir bar, condenser and N_2 inlet, L-alanine (5.0 g, 56 mmol, 3 equiv) and bis(trichloromethyl) carbonate (5.6 g, 19 mmol, 1 equiv) were added and suspended in 100 mL dry tetrahydrofuran (THF) at 50 °C under N_2 bubbling for 4 h. The reaction solution was cooled to room temperature and any unreacted L-alanine was removed by filtration. The filtrate was concentrated and the resulting brown oil material was further purified by three times recrystallization from THF/*n*-hexane 2:1 (v/v), and dried in vacuum to obtain a white crystal (1.4 g, yield: 63%). The product stored in -20 °C freezer under N_2 protection. ^{1}H NMR (DMSO-D_6, 300 MHz, ppm): δ 1.33 (d, 3H, J = 7.0 Hz, COCH(C*H*$_3$)NH), 4.48 (q, 1H, J = 7.0 Hz, COC*H*(CH$_3$)NH), 9.00 (br, 1H, COCH(CH$_3$)N*H*). ^{13}C NMR (DMSO-D_6, 75 MHz, ppm): δ 18.8, 52.8, 151.7, 172.4. FTIR (cm^{-1}): 3500-3100, 2838, 1840, 1760, 1280, 1139, 1023, 925. HRMS: calculated [M-H]$^-$ for $C_4H_5NO_3$: 114.0191, found: 114.0193.

Synthesis of glycine (Gly) NCA monomer

In a 250 mL three-necked round bottom flask equipped with a magnetic stir bar, condenser and N_2 inlet, glycine (5.0 g, 67 mmol, 3 equiv) was suspended in 100 mL THF and heated to 50 °C. Trichloromethyl chloroformate (4.4 g, 22 mmol, 1 equiv) was added into the reaction solution by syringe and the reaction mixture was refluxed for another 4 h under N_2 atmosphere. The reaction mixture was filtered before cooling to room temperature. The filtrate was concentrated, recrystallized three times from THF/*n*-hexane 2:1 (v/v) and dried in vacuum to obtain a white crystal (1.5 g, yield: 67%). The product was stored in -20 °C freezer under N_2 atmosphere. ^{1}H NMR (300 MHz, DMSO-D_6, ppm): δ 4.18 (s, 2H, COC*H*$_2$NH), 8.83 (br, 1H, COCH$_2$N*H*). ^{13}C NMR (75 MHz, DMSO-D_6, ppm): δ 46.3, 153.0, 169.4. FTIR (cm^{-1}): 3500-3100, 2955, 1876, 1740, 1275, 1113, 1061, 925. HRMS: calculated $[M-H]^-$ for $C_3H_3NO_3$: 100.0035, found: 100.0039.

Synthesis of L-isoleucine (Ile) NCA monomer

In a 250 mL three-necked round bottom flask equipped with a magnetic stir bar, condenser and N_2 inlet, L-isoleucine (5.0 g, 42 mmol, 3 equiv) and bis(trichloromethyl) carbonate (4.6 g, 14 mmol, 1 equiv) were added and suspended in 100 mL dry tetrahydrofuran at 50 °C under N_2 bubbling for 4.5 h. The reaction solution was cooled to room temperature and any unreacted L-isoleucine was removed by filtration. The filtrate was concentrated and the resulting yellow oil material was further purified by three times recrystallization from THF/*n*-hexane 2:1 (v/v), and dried in vacuum to obtain a white crystal (2.2 g, yield: quantitative). The product stored in -20 °C freezer under N_2

protection. ^{1}H NMR (DMSO-D_6, 300 MHz, ppm): δ 0.86 (t, 3H, *J* = 9.0 Hz, $CH_3CHCH_2CH_3$), 0.92 (d, 3H, *J* = 7.0 Hz, $CH_3CHCH_2CH_3$), 1.28 (m, 2H, $CH_3CHCH_2CH_3$), 1.79 (s, 1H, CH_3CHCH_2), 4.39, (s, 1H, COCHNH), 9.09 (br, 1H, COCHNH). ^{13}C NMR (DMSO-D_6, 75 MHz, ppm): δ 11.3, 14.7, 23.8, 36.5, 61.7, 152.2, 170.8. FTIR (cm^{-1}): 3500-3100, 2970, 2881, 1848, 1750, 1215, 1091, 1070, 939. HRMS: calculated $[M-H]^-$ for $C_7H_{11}NO_3$: 156.0661, found: 156.0665.

Synthesis of methoxy poly(ethylene glycol)-*block*-poly(L-alanine-*co*-glycine-*co*-L-isoleucine) (mPEG-*b*-P(A-G-I) diblock copolymer from statistical copolymerization of NCA monomers initiated by mPEG-NH_2

As a representative example, the synthesis of mPEG45-*b*-P(A_5-G_7-I_5) was described. In a 10 mL flame dried Schlenk fask equipped with a magnetic stir bar, mPEG$_{45}$-NH_2 (80.0 mg, 0.04 mmol, 1 equiv) was added into a solution of Ala NCA (23.0 mg, 0.2 mmol, 5 equiv), Gly NCA (20.0 mg, 0.2 mmol, 5 equiv) and Ile NCA (31.4 mg, 0.2 mmol, 5 equiv) were dissolved in 6.4 mL anhydrous DMF solution. The reaction mixture was stirred with a stir rate of 400 rpm under continuous N_2 flow (100 mL/min) at room temperature for 12 h. The quantitative consumption of monomers was confirmed by measuring the intensity of the NCA anhydride peak at 1788 cm^{-1} using ATR-FTIR. The Schlenk flask was capped with a rubber stopper with a needle outlet connected with a drying tube. The polymerization solution was precipitated into diethyl ether under vigorous stirring and a white powder was obtained after centrifuged and dried under vacuum at room temperature (102.2 mg, yield: 80%). ^{1}H (300 MHz, TFA-D, ppm): δ 0.70-1.10 (br, 15H, $CH_3CHCH_2CH_3$; br, 15H, $CH_3CHCH_2CH_3$), 1.46 (br, 10H,

$CH_3CHCH_2CH_3$; br, 15H, CH_3CH), 1.60-2.10 (br, 5H, $CH_3CHCH_2CH_3$), 3.52 (s, 3H, CH_3O), 3.85 (s, 180H, CH_2CH_2O), 4.20 (br, 14H, $NHCH_2CO$), 4.64 (br, 10H, NHCHCO). ^{13}C NMR (75 MHz, TFA-D, ppm): δ 12.9, 13.8, 15.8, 24.0, 36.9, 42.6, 50.1, 57.5, 69.5, 70.7, 172.5, 174.8, 175.6. FTIR (cm^{-1}): 3286, 2868, 1699, 1625, 1515, 1451, 1349, 1249, 1099, 948, 849, 696. DSC: T_g = -17 °C, T_c = -15 °C, T_m = 30 °C, T_g = 126 °C. TGA in N_2: 20-233 °C, 2% mass loss; 233-367 °C, 29% mass loss; 367-430 °C, 46% mass loss; 430-500 °C, 3% mass loss; 20% mass remaining above 500 °C.

Determination of critical gelation temperature (T_{gel}) for polypeptide-based hydrogel

The polymer solutions were prepared by dissolving polypeptide powders in nanopure water at the desired concentrations. The homogeneous solutions were obtained by 2 min sonication with probe sonicator at room temperature. The formation of the hydrogels was determined *via* test tube inversion method. Each sample at a given concentration was dissolved into nanopure water in a 2 mL vial. After equilibrium at room temperature overnight, the vials containing samples were immersed in an oil bath equilibrated at each given temperature for 30 min. The sol-gel transition was determined by the test tube inversion method and stayed for at least 5 min.[180] If no flow was observed, the sample was regarded as gel. For the sol-gel transition temperature measurements, the temperature was raised in a step of 0.5 °C/h. Each measurement was conducted three times and standard derivations were made.

Hydrogel degradation profile

Degradation of the polypeptide-based hydrogel was performed by measuring the weight loss of the hydrogel by mixing the hydrogel with the degradation media during a

period time of 10 days.[16] A 300 μL aliquot of hydrogel with the concentration of 4 wt % polypeptide gelator in nanopure water were placed in a 1.5 mL vial and maintained at 37 °C overnight for gel formation. A 500 μL of Tris-HCl buffer (0.05 M, pH = 8.0, 0.2 wt % NaN_3) was gently added into the vial without disturbing the gel. The vial was then maintained at 37 °C during the whole period of the degradation study. The Tris-HCl buffer solution, together with any accumulated gel debris, was removed at the desired time and the weight of the vial was recorded to assess the change of the hydrogel weight during the degradation study. In the enzymatic degradation study, the enzymes were first dissolved into Tris-HCl buffer solution (0.05M, pH = 8.0, 0.2 wt % NaN_3) with the concentration of 1 mg/mL. The enzyme solutions were kept in frozen state in -20 °C freezer and prewarmed back to 37 °C before adding into the hydrogel vials. Each degradation study was repeated three times and standard derivations were made.

6.3 Results and discussions

With our general interest in the creation of biodegradable stimuli-responsive polymeric materials with simple molecular design and synthetic feasibility, especially for future biomedical applications, we began investigation into the chemical syntheses and physical properties of hybrid diblock copolymers, having statistical copolypeptides as one of the block segments, with the expectation to incorporate responsive properties to multiple external stimuli, including thermal, mechanic and biological triggers. Recently, our group reported a novel approach to tune the stimuli-responsive properties of polypeptide-based gel systems *via* the control of the secondary structures within the

polypeptide segment, which was offered by variation in the copolypeptide feedstock selection during the statistical copolymerization of various *N*-carboxyanhydride (NCA) monomers. Ring-opening polymerizations (ROPs) of amino acid NCAs have been demonstrated to be a convenient and efficient synthetic approach for the preparation of well-defined polypeptide materials in large scale, especially after several controlled NCA ROPs had been reported in the last two decades.[46,50,52-54] In fact, NCA ROPs can be conducted under normal Schlenk techniques, with the enhancement of polymerization rate and retention of controlled features by a straightforward N_2 flow method. Therefore, the methoxy poly(ethylene glycol)-*block*-poly(L-alanine-*co*-glycine-*co*-L-isoleucine) (mPEG-*b*-P(A-G-I)) were synthesized *via* the facile statistical copolymermizations of L-alanine (Ala), glycine (Gly) and L-isoleucine (Ile) NCAs by using monomethoxy-monoamino-terminated poly(ethylene glycol) ($mPEG_{45}$-NH_2, M_n = 2000 g/mol) as the macroinitiator with continues N_2 flow (100 mL/min) over the reaction solutions (Figure 6.1). A series of mPEG-*b*-P(A-G-I) with various lengths of copolypeptide segments were synthesized by varying the ratios of NCA monomers to the macroinitiators with the maintained ratios of three NCA monomers to be 1 : 1 : 1 (Table 6.1). For each polymerization, the required amounts of NCA monomers and macroinitiator were dissolved in anhydrous *N,N*-dimethylformamide (DMF) and the ROP was allowed to proceed for 12 h at room temperature. Spontaneous gelation in DMF were observed in each polymerization within 8 h and the targeted diblock copolymers were obtained as white powder by precipitating the reaction mixtures into diethyl ether, followed by drying under vacuum.

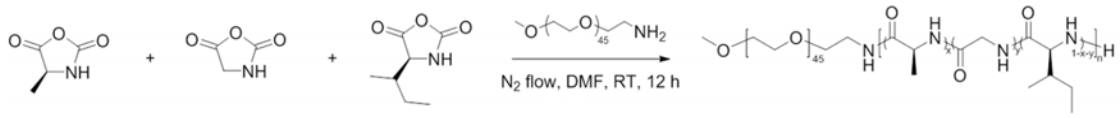

Figure 6.1. Synthetic approach for mPEG-*b*-P(A-G-I) diblock copolymer.

Table 6.1. Average degree of polymerization (DP_n), number-averaged molecular weight (M_n) and chemical structure for the mPEG-*b*-P(A-G-I) diblock copolymers synthesized with different monomer to initiator ratios.

Entry	Monomer : Initiator[a]	DP_n[b]	M_n (kDa)[b]	Polymer[b]
1	15 : 1	17	3.3	$mPEG_{45}$-*b*-Poly(A_5-G_7-I_5)
2	30 : 1	30	4.2	$mPEG_{45}$-*b*-Poly(A_8-G_{13}-I_9)
3	50 : 1	43	5.1	$mPEG_{45}$-*b*-Poly(A_{15}-G_{19}-I_9)
4	80 : 1	63	6.4	$mPEG_{45}$-*b*-Poly(A_{24}-G_{29}-I_{10})
5	100 : 1	72	6.9	$mPEG_{45}$-*b*-Poly(A_{28}-G_{34}-I_{10})

[a]All the polymerizations were conducted using $mPEG_{45}$-NH_2 as the macroinitiator at the concentration of 10 mg/mL and the ratio of Ala : Gly : Ile = 1 : 1 :1. [b]Calculated by ^{1}H NMR spectroscopy.

The molecular weights of the copolymers and the incorporated ratios of three NCA monomers in the polypeptide segments were determined by ^{1}H NMR spectroscopy with the utilization of deuterated trifluoroacetic acid (TFA-D) as the solvent to break the strong hydrogen-bonding within the polypeptide segments and maintain the polymers in the solution state (Figure 6.2a). The chemical structures and molecular weights of the copolymers were measured by comparison of methylene proton intensities of the mPEG

chain resonating at *ca.* 3.85 ppm (b in Figure 6.2a) with the intensities of Gly methylene protons resonating at *ca.* 4.20 ppm (e in Figure 6.2a), the Ile side chain methine proton at *ca.* 1.85 ppm (g in Figure 6.2a), and the integration of the backbone methine protons for both Ile and Ala at *ca.* 4.64 ppm (c+f in Figure 6.2a). For both Ala and Gly, the calculated numbers of repeat units from ^{1}H NMR spectroscopy showed linear correlations with the theoretical numbers of repeat units, while for Ile, the number of repeat unit in the obtained polymer didn't increase with higher ratio of Ile NCA monomer to macroinitiator (Figure 6.2b). These results indicated Gly and Ala NCA monomers had higher reactivities when compared with Ile NCA monomer during the statistical copolymerizations.[178,179]

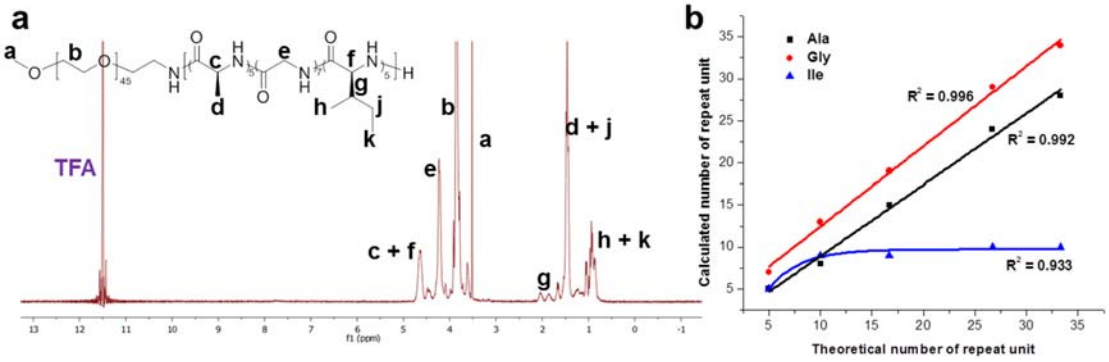

Figure 6.2. (a) ^{1}H NMR spectrum of polymer **1** dissolved in TFA-D. (b) Calculated numbers of repeat units as a function of theoretical numbers of repeat units for Ala, Gly and Ile in the polymers **1 - 5**.

The ability to form hydrogels for copolymers with different block lengths of polypeptide segments were characterized by test tube inversion experiments. To prepare the hydrogel systems, the denoted weight fractions of polymer powder and nanopure

water were mixed at room temperature and hydrogels were generated after the solution been heated to critical gelation temperature (T_{gel}).[180] The obtained hydrogels were stable and no gel-to-sol transitions were observed when they were left undisturbed for at least 3 days at room temperature. In order to explore the effect of the polymer concentration on T_{gel}, the T_{gel} values of a series of copolymers were measured at various concentrations and the results were summarized in Figure 6.3. For each copolymer, T_{gel} decreased with higher concentration of copolymer hydrogelator in nanopure water from the sol-gel phase diagram. For example, T_{gel} of polymer **1** decrease from 84 °C at the concentration of 2 wt % to 22 °C at the concentration of 6 wt %. With the increase of the block length of polypeptide segment, the trend of T_{gel} was complicated from the sol-gel phase diagram. At the concentration of 6 wt %, the T_{gel} value increased from 22 °C (polymer **1**) to 32 °C (polymer **2**), while this trend reversed to decrease to 16 °C (polymer **5**) with longer block length of polypeptide segment. Due to the T_{gel} value (35 °C) close to the physiological temperature of human body with promising potential as a drug delivery system, we would like to focus on the properties of the hydrogel from polymer **1** at the concentration of 4 wt %.

In order to further understand the gelation mechanism of the hydrogel system, the supramolecular structures of the hydrogel in solid state were investigated by attenuated total reflectance-Fourier transform infrared spectroscopy (ATR-FTIR) and wide-angle X-ray scattering (WAXS). The characteristic absorbance of secondary structures were clearly observed in the FTIR spectra, especially in the region of amide I band (1700 - 1600 cm^{-1}) (Figure 6.4a). The absorbances at 1701 cm^{-1} and 1625 cm^{-1} (amide I), in

combination with a peak at 1515 cm^{-1} (amide II) and an amide V band at 694 cm^{-1}, were attributed to β-sheet conformation.[181] Further quantitative analyses of secondary structure populations were conducted by employing secondary derivative and deconvolution strategies to extract relative peak intensities in the heavily populated amide I region (Figure 6.4b).[177,183,184] The β-sheet contribution was calculated to be 63% from the quantitative analyses, which was similar to the content of β-sheet (66%) in the solid state of PEG_{45}-*b*-$PGly_{30}$ in Chapter V. In addition, the WAXS pattern of the dried hydrogel gave a *d* spacing of 4.6 Å with stronger signals for PEG crystallization reflection (Figure 6.5a), which was also demonstrated by the melting and crystallizing peaks in the DSC trace of polymer **1** (Figure 6.5b). This *d* spacing of 4.6 Å has been

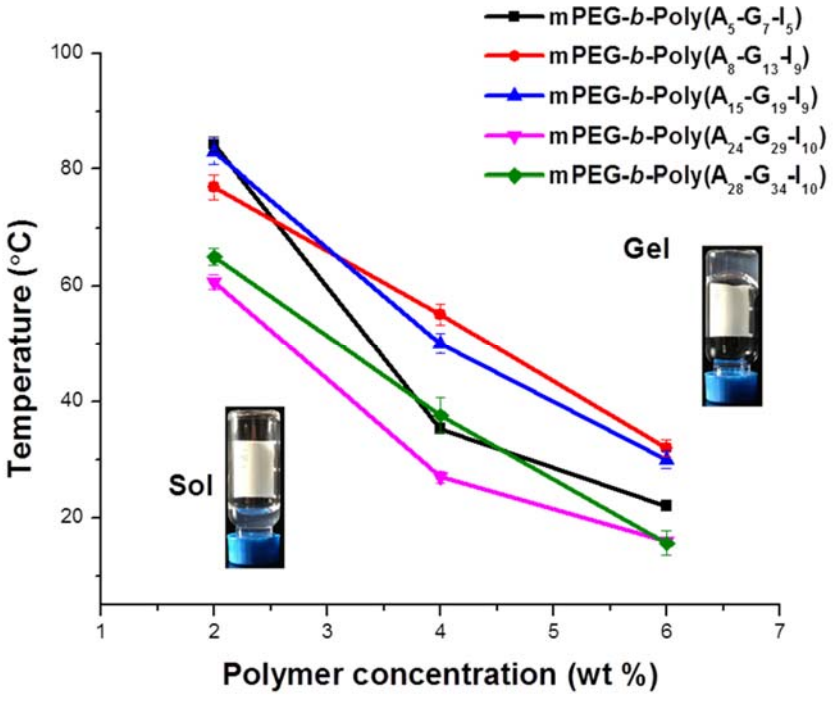

Figure 6.3. T_{gel} of mPEG-*b*-P(A-G-I) hydrogels as a function of polymer concentration.

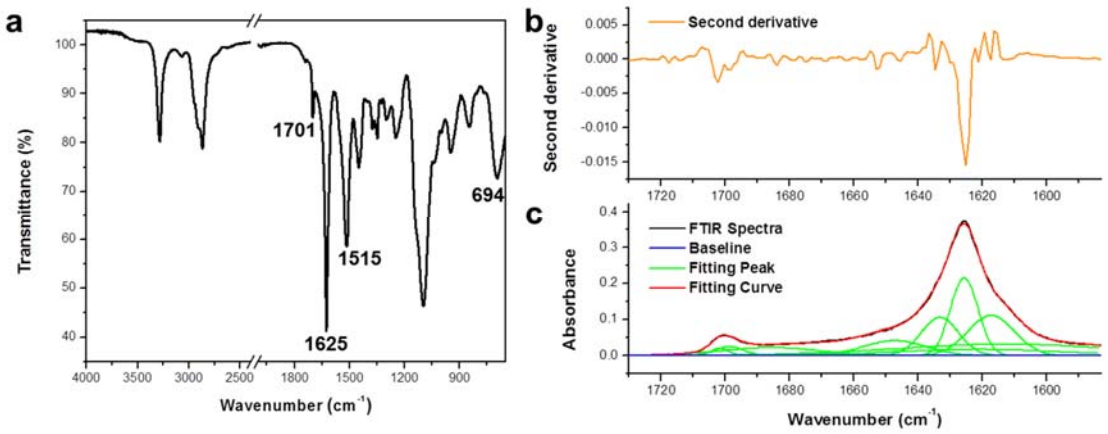

Figure 6.4. (a) ATR-FTIR spectrum of polymer **1** in the solid state. (b) Second derivative and (c) ATR-FTIR spectra (black), fitting curve (red), baseline (blue) and fitting peaks (green) for polymer **1** in the solid state.

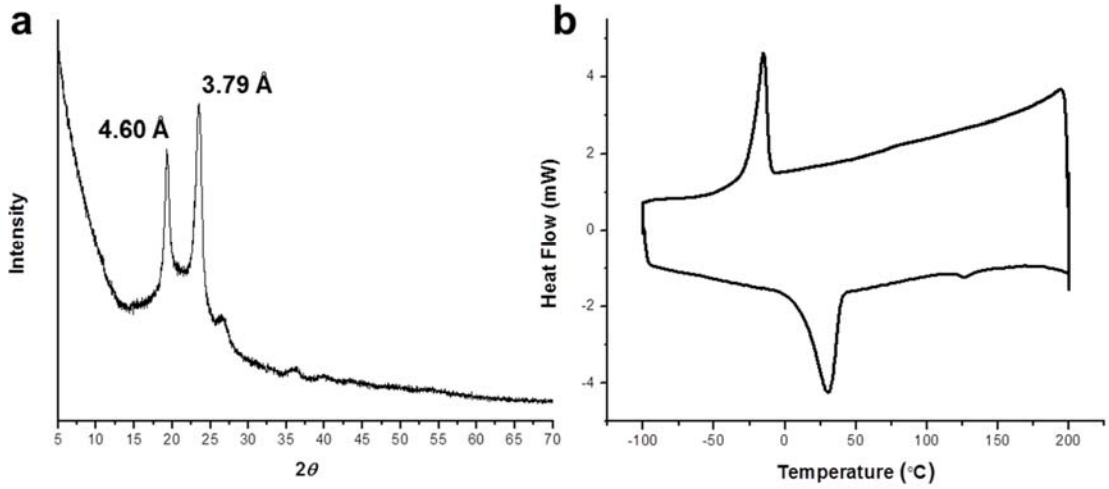

Figure 6.5. (a) WAXS pattern and (b) DSC trace of polymers **1** in the solid state. In the DSC trace, the sample was heated from -100 °C to 200 °C and cooled back to -100 °C, each with a rate of 10 °C/min. The second heating and cooling traces are shown here.

observed and assigned to antiparallel β-sheet conformation in poly(L-alanyglycine)[185] and the self-assembled PEG-*b*-β-strand-peptides.[186] The results from qualitative and quantitative FTIR analyses, together with WXAS characterization, indicated β-sheet conformation dominated in the solid state of the hydrogel system.

Due to the strong absorption of water in the range of amide I (1700-1600 cm^{-1}), it is difficult to analyze the secondary structure population of hydrogel in gel state. While compared to water, the absorption peak of D_2O moved to the range of smaller wavenumber by increasing the molecular weight from H to D (Figure 6.6a), thus *in situ* secondary structure analyses can be performed by replacing water with D_2O in the hydrogel system.[68] The hydrogel sample was prepared by dissolving the polymer powder into D_2O under sonication and the polymer solution was maintained at 37 °C overnight before analyses. With D_2O as the background, the characteristic peak of β-sheet conformation at peak 1625 cm^{-1} (amide I) was observed in the FTIR spectrum (Figure 6.6b), indicating the domination of β-sheet in the secondary structure population in the gel state, which was in agreement with the results from analyses of hydrogel in solid state.

To investigate the conformational changes of copolymer **1** in nanopure water, temperature-dependent circular dichrism (CD) was employed to monitor the changes of the secondary structures as a function of temperature. The copolymer solution samples at the concentration of 0.2 wt % for CD measurements were placed in a quartz cell with a path length of 1.0 mm and analyzed between 180 and 280 nm with a wavelength step of 1.0 nm. As revealed in Figure 6.7a, the negative band at 220 nm gradually increased

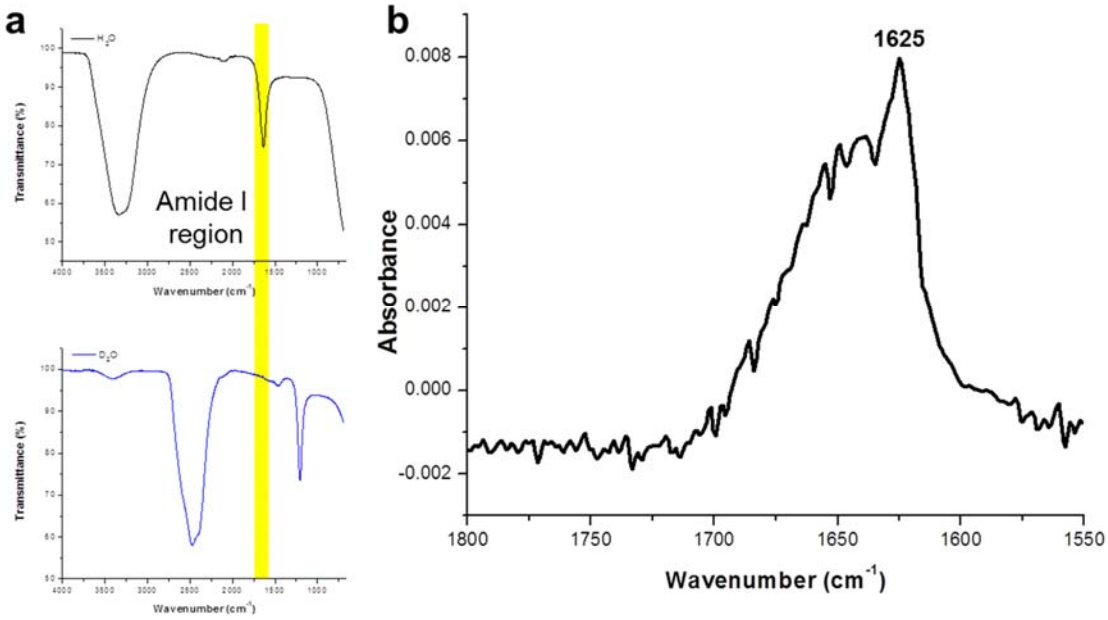

Figure 6.6. (a) FTIR spectra of H_2O and D_2O. (b) *In situ* FTIR spectrum of hydrogel from polymer **1** in the gel state using D_2O as the aqueous medium.

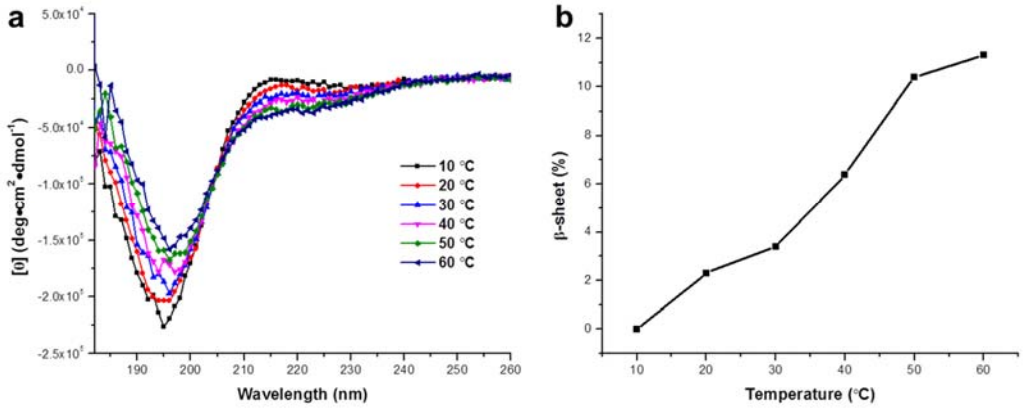

Figure 6.7. (a) CD spectra of polymer **1** in nanopure water at the concentration of 0.2 wt % as a function of temperature from 10 to 60 °C. (b) Estimation the content of β-sheet at each temperature from the CD spectra in the range of 190 – 240 nm by CDPro software with Program CONTILL and SDP48 as the reference sets.

with the increase of temperature from 10 to 60 °C. The β-sheet contents at different temperatures were estimated with CDPro software with Program CONTILL and SDP48 as the reference set and the results were summarized in Figure 6.7b.[201] As the temperature increased from 10 to 60 °C, the content of β-sheet conformation raised from 0% to 12%, indicating the hydrogel system was driven by the temperature-triggered β-sheet formation.

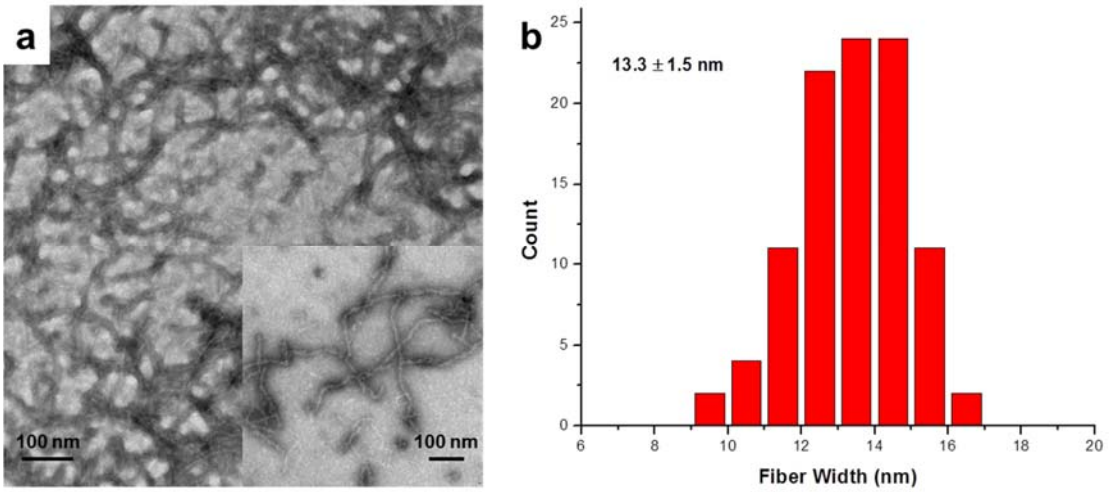

Figure 6.8. (a) TEM image and (b) fiber width distribution of hydrogel from polymers **1**, obtained by counting 100 fibers.

Transmission electron microscopy (TEM) and scanning electron microscopy (SEM) were utilized to study the nano- and microstructures of the hydrogel from polymer **1**. TEM sample was prepared with a polymer concentration of 0.1 wt % in nanopure water and stained by 1 wt % phosphotungstic acid (PTA) aqueous solution. Bright-field TEM image of the hydrogel showed fibrillary nanostructures with average width distribution of 13.3 nm throughout the TEM image (Figure 6.8a). The narrow

width distribution of nanofibrils, obtained by counting 100 nanofibrils in the TEM image, indicated that the hydrogel had well-defined nanofibrillar morphologies (Figure 6.8b). To visualize the microstructure of the hydrogel, SEM samples were prepared by freeze-drying with the aim to maintain the gel networks. From the SEM image (Figure 6.9), interconnected three-dimensional networks and highly porous structure with various sized were observed, which could be potentially utilized to encapsulate and release cargoes such as therapeutic drugs or cells in biomedical applications.

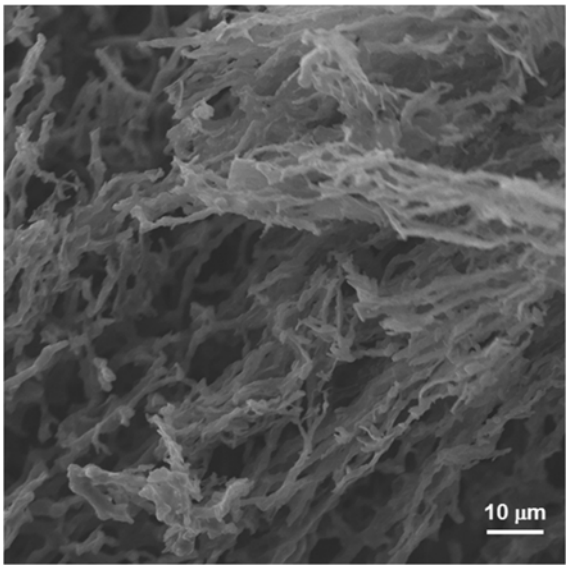

Figure 6.9. SEM image of lyophilized hydrogel from polymer **1**.

Based on the results from NMR, ATR-FTIR, WAXS, CD, SEM and TEM analyses, a mechanism for the hydrogelation of mPEG-*b*-P(A-G-I) was proposed (Figure6.10). The well-defined fibril nanostructures were supramolecular assembled from the one-dimensional stacking of the polypeptide segments in the conformation of

β-sheet secondary structure, as observed spectrally and microscopically. Using hydrogel from polymer **1** as an example, the gyration radius of mPEG with a molecular weight of 2000 Da can be estimated to be 18 Å.[186] The axial distance between adjacent α-amino acid is about 3.5 Å, thus the width of the polypeptide domain can be calculated to be 60 Å in the conformation of β-sheet secondary structure. Therefore, the diameter of the assembled nanofibrils can be estimated to be about 13.2 nm, which is in agreement from the measured width (13.3 nm) of nanofibrils in the TEM image. The hydrophilic mPEG

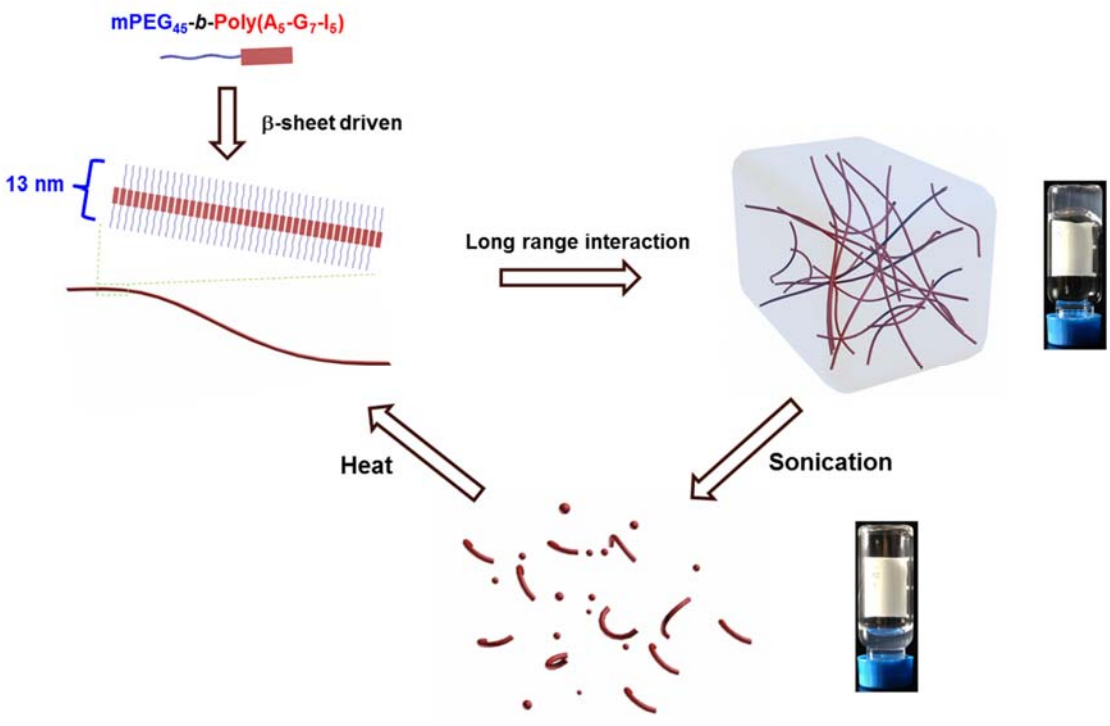

Figure 6.10. An illustrative scheme for reversible sol-gel transitions of hydrogel from polymer **1**, including heat-induced hydrogelation from supramolecular assembled nanofibrils and sonication triggered gel-to-sol transition.

segments can prevent the precipitation of the copolymer *via* increasing aqueous solubility and maintain the hydrogel networks by encapsulating water molecules. The heat-triggered gelation may result from the formation and strengthening of the β-sheet structures and also the dehydration of PEG chain at raised temperature to enhance the hydrophobic interactions. The entanglement of nanofibrils resulting from long range interactions, including peptide-peptide interaction or PEG-PEG association, constructs the three-dimensional networks of the hydrogel system.

The physical properties of the polypeptide-based hydrogel, especially the stimuli-responsive properties, and the correlation between the nanostructure and the physical properties were investigated. As shown in the quantitative ATR-FTIR analyses, the content of β-sheet secondary structure in the hydrogel system was calculated to be 63%, thus mechano-triggered gel-to-sol transition was expected in this hydrogel system based on the conclusion from Chapter V. The sonication-responsiveness of the hydrogel system was tested by applying sonication to the hydrogel for 30s and the gel-to-sol transition was observed in the test tube inversion experiment. This transition was reversible, with the hydrogel reforming after being maintained at T_{gel} (*ca.* 37 °C) over 1 h (Figure 6.11a). Due to the short time in the sonication experiment and also the thermal stability of the hydrogel against heating up to 90 °C in the gelation temperature characterization, mechanical force produced from the sonicator was proposed to break the supramolecular assembled structures of polymer **1**, resulting in the deconstruction of the hydrogel. In order to investigate the secondary structures of the copolymer after sonication, *in situ* FTIR of the hydrogel in the sol state were conducted with D_2O as the

aqueous media. As shown in Figure 6.11b, the FTIR spectrum of the sol state was almost identical to the spectrum of the gel state, indicating no significant change of the secondary structure during the sonication treatment and the β-sheet contribution maintained dominated in the sol state. TEM was also employed to compare the difference of the nanostructural morphologies between the gel and sol states with the aim to further understand the hydrogelation and gel breaking behaviors. In the TEM image of the sol state after applying 1 min sonication, the well-defined nanofribrils in the gel state disappeared (Figure 6.8a), while some short nanofirbrils and spherical aggregates were observed instead (Figure 6.11c). The longer nanofibrils were converted into short-nanofibrils and spherical aggregates, which lacked long range connectivity, resulting in the breakdown of the hydrogel networks. When the sol state was maintained at 37 °C, hydrogel was reconstructed *via* the reformation of the longer nanofibrils with the reconnected hydrogel networks (Figure 6.10).

Enzyme-responsive properties, including enzymatically degrading behaviors, are quite promising for synthetic polypeptide materials to be used in the biomedical applications. The enzyme-responsive properties of this hydrogel were investigated by studying *in vitro* gel weight loss profiles, which was assessed by measuring the weight loss of hydrogels (4 wt %) kept at 37 °C.[16] The enzymatic degradation medium was prepared by dissolving the enzyme (proteinase K or trypsin) in Tris-HCl buffer (0.05 M, pH = 8.0, 0.2 wt % NaN_3) and the hydrogel with Tris-HCl buffer was used as the control experiment. The enzyme solution (500 μL) was added gently into each vial and removed along with accumulated gel debris at the desired time. All the measurements

were repeated three times for each enzyme and control group and the results were summarized in Figure 6.12. According to the weight loss profiles, trypsin, which is targeting lysine and arginine, had no significant effect on the hydrogel degradation, resulting in a similar degradation profile as the control group.[16] While, the hydrogels were subjected to proteinase K showed much faster degradation profile, in which over 90% of the weight loss was observed after 72 h.

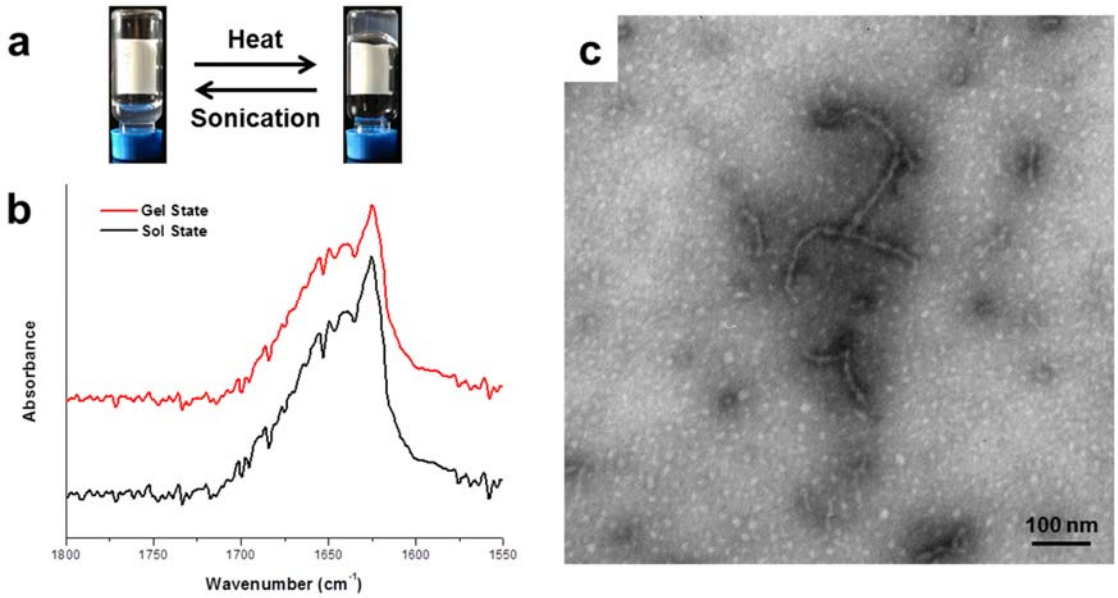

Figure 6.11. (a) Digital photographs showing reversible sol-gel transitions under thermo- and sonication stimuli, respectively. (b) *In situ* FTIR spectra in the gel and sol states when sonication was applied, respectively. (c) TEM image of hydrogel in sol state from polymer **1** after 1 min sonication.

We also explored the use of this hydrogel for the entrapment and the release of small therapeutic drugs, such as naproxen (Npx), with the expectation that the multiple stimuli-responsive properties can be utilized to control the release profile of

encapsulated drug. Npx has very low solubility into nanopure water in the form of acid, but its solubility in phosphoate buffered saline (PBS, 0.01 M, pH = 7.4) can reach 1 mg/mL. Thus the Npx-loaded hydrogel was prepared by mixing the weight fractions of copolymer with the PBS buffer solution of Npx, and transparent hydrogel was generated after the solution was maintained at 37 °C overnight.[196] The obtained hydrogel was stable and neither gel-to-sol transition nor precipitation of Npx was observed for at least one week at room temperature. The sonication-triggered gel-to-sol transition was also observed for this Npx-loaded hydrogel when this hydrogel was applied with sonication for 10 s.

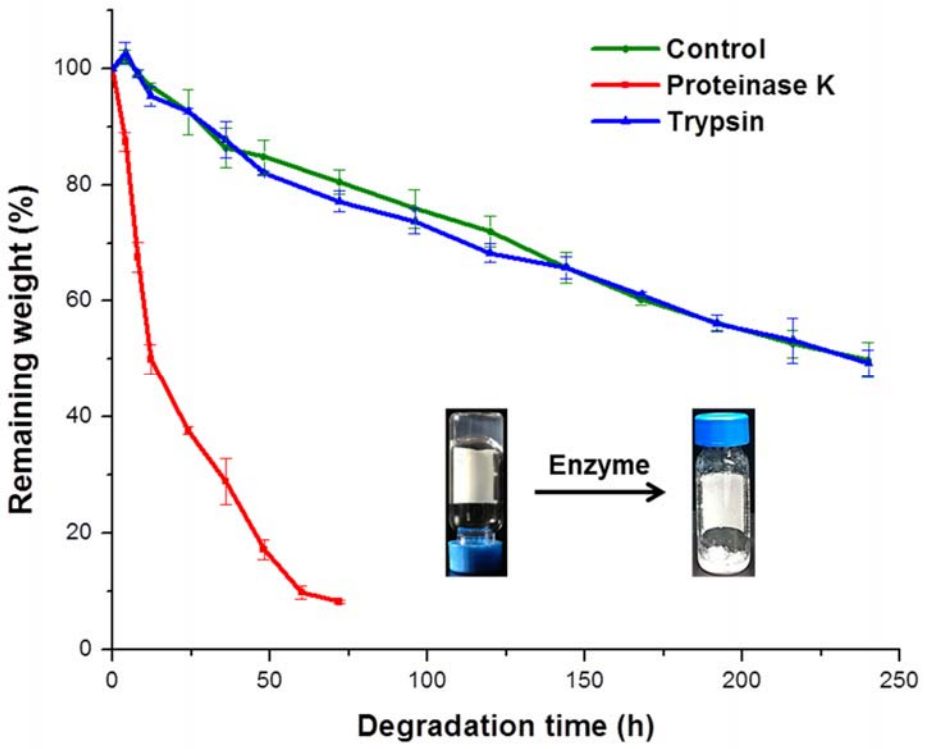

Figure 6.12. Weight loss profiles of hydrogels from polymer **1** with/without enzyme. Measurements were repeated three times for each enzyme and control group.

6.4 Conclusions

In summary, a polypeptide-based hydrogel system, when prepared from a diblock copolymer with polypeptide as one block, exhibited thermo-, mechano- and enzyme-responsive properties, which were capable to tune the release of Npx from the hydrogel in controlled manner. The diblock copolymer, mPEG-*b*-P(A-G-I), was facilely synthesized from the statistical ring-opening copolymerization of Ala, Gly and Ile NCA monomers, with the expectation of G-IAG sequence in polypeptide segments for degradation by protease enzymes, including Proteinase K and Matrix metalloproteinase-2 (MMP-2). Reversible and repeatable sol-gel transitions were observed with heat-induced sol-to-gel transition and sonication-triggered gel-to-sol transition. The gelation temperature was largely dependent on the concentration of copolymer and also the block length of the polypeptide segment, which could be easily tuned into the targeted temperature range. Detailed characterization studies revealed that the hydrogelation was driven by the supramolecular assembly of β-sheets into well-defined fiber-like nanostructures, further generating a three-dimensional network through long range interactions. On the other hand, the mechanical force produced by sonication could deconstruct the supramolecular assembled structures of the hydrogel, resulting in the gel-to-sol transition. In addition, enzymes with capabilities to recognize the built-in sequences in the polypeptide segments, including Proteinase K and MMP-2, could accelerate the breakdown of the hydrogels into sols. Npx could be loaded into the hydrogel at room temperature in the sol state and maintained within the hydrogel after being heated to the gelation temperature, which indicated the potential of this hydrogel

to be utilized as a controlled release system for Npx. The release profiles of Npx from the hydrogel with or without an external stimulus, such as sonication and the characterized enzymes, and also the biological activities of the released Npx are under current investigation.

CHAPTER VII

CONCLUSIONS

Polypeptides have been utilized extensively in the construction of materials for nanomedical applications, such as serving as scaffolds for tissue engineering, matrices for drug and gene delivery, and responsive materials for biosensors, owing to their unique structural characteristics, including innate biocompatibility and biodegradability, multiple functionalities and precisely-defined secondary structures. Especially, in the last two decades, great progress has been achieved to construct well-defined polypeptides with complex structures, versatile functionalities and advanced properties, resulting from advances with synthetic methodology and modification chemistry. In my initial project, polypeptide-based statistical copolymers by ring-opening copolymerization of mixtures of *N*-carboxyanhydride (NCA) monomers derived from natural amino acids were designed and prepared, with the expectation of randomly built-in amino acid sequences for enzyme recognition and cleavage. Further, it was hypothesized that this kind of polymers could be produced as amphiphilic block copolymers to allow for assembly into nanoparticles for nanomedical applications, with enzyme-selective breakdown to facilitate release of drugs and biological clearance. During the development of this project, due to the temporarily inoperable status of glovebox, a new synthetic method for the syntheses of polypeptide materials was required, in which N_2 flow was firstly utilized to keep the moisture out of the reaction setup to maintain the dry condition of NCA polymerization. Surprisingly, accelerated

polymerization rates were observed, which further led into the exploration and development of the straightforward and readily-adoptable N_2 flow method for the preparation of polypeptides with well-defined structures. This synthetic method was then expanded to install functional and charged moieties onto polypeptide backbones for gene delivery and to build complex molecular brushes bearing polypeptides as brush side chains. On the other hand, spontaneous gelation also was observed during the polymerizations of β-sheet-forming amino acid NCA monomers in the development of the initial project, while α-helix-forming NCA monomers could limit the formation of gels, which inspired us to explore the structure-property relationships in polypeptide-based gel systems. After gaining an understanding over stimuli-sensitive gelation behaviors, these materials were further utilized in the construction of controlled release hydrogels from copolymerizations of mixtures of NCA monomers. Enzyme-accelerated breakdown of the hydrogels led the research advances toward the initial target of using randomly built-in amino acid sequence for enzyme recognition and cleavage in the hydrogel platform.

The extensive utilization of polypeptide materials in nanomedical applications originates from the structural characteristics, as well as the synthetic feasibility of polypeptides, especially after controlled ring-opening polymerizations (ROPs) of *N*-carboxyanhydrides (NCAs) has emerged as a practical approach for well-defined polypeptides. Therefore, a straightforward and readily-adoptable synthetic methodology was investigated to synthesize polypeptides, with controllable polymerization rates, targetable molecular weights and narrow molecular weight distributions, by applying

continuous N_2 flow over the reaction mixture during NCA polymerizations. This study involved γ-benzyl-L-glutamate (BLG) NCA as the model NCA monomer, with detailed characterizations to demonstrate the structural differences of obtained polypeptides with/without N_2 flow during the polymerizations. Detailed kinetic studies revealed that N_2 flow could efficiently remove CO_2 from the reaction system to drive the equilibrium toward decarboxylation of the carbamic acid intermediate and generate active amine terminus for further chain propagation, resulting in depression of side reactions and generation of more well-defined polypeptide products. The N_2 flow can be easily tuned to balance the polymerization rate and structure control by applying N_2 flow with different flow rates. This approach is attractive also because most of the primary amine initiators are commercially available and there is no need for removal of a catalyst after polymerization, which diminishes potential toxicity issues that may arise in the use of synthetic polypeptides for nanomedical applications. With enhanced polymerization rates and controlled features, this economical and easily operational method can be expanded to build diblock copolypeptides, install chain-end functionalities, and exert structural control for polypeptide materials.

With this facile synthetic approach, we further constructed a versatile and functional nanoparticle platform with reactive and charged functionalities from the combination of a sequential NCA polymerization and chemical transformation strategy, and the cationic nanoparticle from this amphiphilic diblock copolypeptide was also investigated as a gene delivery carrier by electrostatic complexation. With the enhanced polymerization rate of N_2 flow method, a novel type of diblock copolypeptide,

poly(γ-benzyl-L-glutamate)-*block*-poly(γ-propargyl-L-glutamate) (PBLG-*b*-PPLG) was prepared from the sequential NCA ROPs in a fast (less than 16 h) and atom-efficient manner. The clickable alkynyl groups on the side chains of PPLG block were then modified to install different charges and functionalities onto the polypeptide backbones *via* thiol-yne click-type chemistry. The resulting amphiphilic block copolypeptides were found to self-assemble into nanopure water to obtain globular nanoparticles with distinct surface charges. The stabilized helical structure of polypeptides was achieved, either in the form of free polymer or assembled nanoparticle, resulting from the extended distance between side chain charges and polypeptide backbones. The polypeptide-based cationic nanoparticle exhibited minimum cytotoxicity and complete binding efficiency to small interfering ribonucleic acids (siRNAs) at N^+/P^- ratios higher than 4. High efficient cellular uptake of the delivery complex was evaluated in human ovarian adenocarcinoma (OVCAR-3) cells and RAW 264.7 mouse macrophages, however, low transfection efficiency was observed in OVCAR-3 cells. Therefore, alternate, more complex polymer backbone topologies were explored to enhance the ability of the synthetic polypeptides to serve as effective nucleic acids transfection systems.

After establishment of synthetic methodology for the polypeptides with precisely-controlled structures, more complex molecular architectures, such as molecular brushes, have been demonstrated to improve the efficiency of delivery systems and enhance the protection of therapeutic agents, resulting from the densely-packed brush side chains. Thus, we investigated a “grafting through” synthetic approach to construct well-defined brush-like polymers bearing polypeptides as the brush side chains. By

integrating NCA ROPs with ring-opening metathesis polymerizations (ROMPs), desired segment lengths of polypeptide side chains and brush backbones could be built, independently and respectively, in controlled manners, allowing for two-dimensional control over the brush molecular architectures. A new type of brush-like polymer, poly(norbornene-*graft*-poly(β-benzyl-L-aspartate)) (P(NB-*g*-PBLA)), was synthesized *via* the ROMP of norbornene-terminated polypeptide macromonomers in a mixture of dichloromethane (DCM) and ionic liquid. The solvent mixture of DCM and ionic liquid was employed due to its fulfillment of high polarity for the dissolving of polypeptide macromonomers and brushes, and also weak coordinating ability to maintain the activation of metal catalysts used in ROMPs. The N_2 flow accelerated NCA ROP was utilized to prepare PBLA macromonomers with different lengths by using norbornene-based primary amine as the initiator. High efficient post-polymerization modification (> 95%) was achieved *via* aminolyses of the PBLA side chains, allowing for installment of functional moieties onto the molecular brushes. With this two-dimensional control strategy, a library of polypeptide molecular brushes with varying segment lengths of both side chains and brush backbones can be prepared and utilized to explore the effect of molecular architecture on polymer properties. Given the numerous types of NCA monomers and NB-incorporated materials, this novel synthetic approach can also be expanded to build various hybrid materials with broad applications.

Driven by inter- and intramolecular hydrogen-bonding interactions, supramolecularly assemble of polypeptides into nanofibril and/or nanoribbon structures with one-dimensional stacking of polymers or polymer aggregations, including α-helical

and β-sheet secondary structures, can result in gel formation. In order to explore the effect of constituency control of the secondary structures on the properties of polypeptide-based gel systems, the simple copolymerization of NCA monomers was utilized to generate copolypeptides having a combination of α-helix and β-sheet secondary structures, which were capable of driving mechano-responsive supramolecular gel-to-gel and gel-to-sol transitions reversibly, allowing for injection-based processing and self-healing behaviors. These copolypeptides exhibited tunable secondary structures and resulted in sonication stimulus responsiveness of the organogels with the polypeptide segment variation, controlled by varying the ratio of NCA monomers during the copolymerizations. Detailed characterization studies revealed that gelation in *N,N*-dimethylformamide (DMF) was driven by supramolecular assembly of β-sheets into well-defined fiber-like nanostructures, further generating a three-dimensional network through long range interactions. The presence of α-helical components in the copolypeptides enhanced the stability of the organogels against sonication, and instantaneous gel-to-gel transitions were observed as *in situ* reconstruction of networks occurred within the gelled materials. In marked contrast, the β-sheet-rich gel, exhibited an instant gel-to-sol transition after sonication was applied. The injectability and self-healing capabilities were demonstrated by direct observation of a macroscopic self-healing behavior experiment. These results illustrate the influence of secondary structures on supramolecular assembly of hybrid diblock synthetic polypeptides in the gel state and demonstrate a novel, facile approach to fabricate nanostructures with stimuli-responsive properties. While the utilization of organogels in

nanomedical applications is commonly limited due to the toxic concern of organic solvents, which drove us to further expand the structure-property relationships into polypeptide-based hydrogels for nanomedical applications.

Based on the structure-property relationships between polymer compositions, supramolecular structures and stimuli-responsive properties, a polypeptide-based hydrogel system exhibited thermo-, mechano- and enzyme-responsive properties, which were capable to tune the release of naproxen (Npx) from the hydrogel in controlled manner. The diblock copolymer, methoxy poly(ethylene glycol)-*block*-poly(L-alanine-*co*-glycine-*co*-L-isoleucine) (mPEG-*b*-P(A-G-I)), was facilely synthesized from the statistical ring-opening copolymerization of L-alanine (Ala), glycine (Gly) and L-isoleucine (Ile) NCA monomers, with the expectation of G-IAG sequence in polypeptide segments for degradation by protease enzymes, including Proteinase K and Matrix metalloproteinase-2 (MMP-2). With the dominant component of β-sheet secondary structures within the polypeptide segments, this system exhibited heat-induced sol-to-gel behavior, resulting from supramolecular assembly of β-sheets into nanofibrils for gel formation, and sonication-triggered gel-to-sol transition, which was expected from the structure-property relationships established in the organogel systems. The gelation temperature was largely dependent on the concentration of copolymer and also the block length of the polypeptide segment, which could be easily tuned into the targeted temperature range. In addition, enzymes with capabilities to recognize the built-in sequences in the polypeptide segments, including Proteinase K and MMP-2, could accelerate the breakdown of the hydrogels into sols by investigating *in vitro* gel weight

loss profile. Naproxen (Npx) was loaded into the hydrogel at room temperature in the sol state and maintained within the hydrogel after being heated to the gelation temperature, which indicated the potential of this hydrogel to be utilized as the controlled release system for Npx, when the hydrogel system was applied with mechano- (sonication) or biological (enzymes including Proteinase K or MMP-2) stimuli to break the hydrogel to facilitate the release of Npx.

In summary, polypeptide materials possess great potential to be utilized in nanomedical applications, resulting from their structural characteristics and synthetic feasibility, especially after NCA polymerization has emerged as one practical approach for polypeptide preparation. In this dissertation, the fundamental investigations of polypeptide materials, including the synthetic methodology for well-defined polypeptides with versatile functionalities and complex molecular topologies, as well as the structure-property relationships in polypeptide gel systems, have been used to guide the designs of polypeptide-based materials in nanomedical applications, such as cationic nanoparticles for gene carriers and controlled release hydrogels for Npx. Following these projects in this dissertation, several future investigations can be performed. For example, the N_2 flow method has been demonstrated to significantly accelerate NCA polymerizations, while detailed molecular structural analyses of the intermediates during polymerizations and the obtained polypeptides can provide more information regarding the mechanism of the N_2 flow method and NCA polymerization. Also, the effects of molecular architectures on the properties of materials in nanomedical applications have attracted recent research attention, thus the studies can be conducted between

polypeptide molecular brushes as gene delivery systems in comparison with their linear analogues, relating to the loading capability, cellular uptake, protection of loaded gene, and *in vitro* as well as further *in vivo* transfection efficiencies. Especially, by precisely controlling the chain lengths of brush side chains and backbones, different roles of side chains and brush backbones in the delivery systems can be determined and further utilized to guide the rational design of polypeptide-based delivery system. In addition, our preliminary study has demonstrated the potential capability of polypeptide molecular brushes to construct gel systems, in which the mechanism of gelation will be significantly diverse from the linear polypeptide gelators due to the difference in their molecular structures. The polypeptide segments are hypothesized to be parallel with the extended direction of assembled nanofibrils, enabling the alignment of polypeptides in the liquid crystal-like structures, with the expectation of interesting thermal, optical and electrical properties. And these properties can be further utilized toward nanomedical applications, such as using electronic signal to control the growth and rebuild of neuron cells when the brush polypeptide-based hydrogels serve as reconstruction media for neuron system damage. Clearly, there is more progress to be achieved in both fundamental and application aspects, with this work contributing to the current advancement of polypeptide materials toward nanomedical applications by the rational design and development of simple and easily-controlled preparations of polypeptide-based materials, including full characterization studies of the compositions, structures and properties.

REFERENCES

(1) Freitas, R. A., Jr. *Nanomedicine* **2005**, *1*, 2-9.

(2) Wagner, V.; Dullaart, A.; Bock, A. K.; Zweck, A. *Nat. Biotechnol.* **2006**, *24*, 1211-1217.

(3) Kim, B. Y. S.; Rutka, J. T.; Chan, W. C. W. *N. Engl. J. Med.* **2010**, *363*, 2434-2443.

(4) Osada, K.; Kataoka, K. *Adv. Polym. Sci.* **2006**, *202*, 113-153.

(5) Deming, T. J. *Prog. Polym. Sci.* **2007**, *32*, 858-875.

(6) Deng, C.; Wu, J. T.; Cheng, R.; Meng, F. H.; Klok, H. A.; Zhong, Z. Y. *Prog. Polym. Sci.* **2014**, *39*, 330-364.

(7) Hehir, S.; Cameron, N. R. *Polym. Int.* **2014**, *63*, 943-954.

(8) Lu, H.; Wang, J.; Song, Z. Y.; Yin, L. C.; Zhang, Y. F.; Tang, H. Y.; Tu, C. L.; Lin, Y.; Cheng, J. J. *Chem. Commun.* **2014**, *50*, 139-155.

(9) Li, Y. M.; Osada, K.; Chen, Q. X.; Tockary, T. A.; Dirisala, A.; Takeda, K. M.; Uchida, S.; Nagata, K.; Itaka, K.; Kataoka, K. *Biomacromolecules* **2015**, *16*, 2664-2671.

(10) Deng, J. Z.; Gao, N. N.; Wang, Y. A.; Yi, H. Q.; Fang, S. T.; Ma, Y. F.; Cai, L. T. *Biomacromolecules* **2012**, *13*, 3795-3804.

(11) Hayakawa, K.; Uchida, S.; Ogata, T.; Tanaka, S.; Kataoka, K.; Itaka, K. *J. Controlled Release* **2015**, *197*, 1-9.

(12) Baba, M.; Itaka, K.; Kondo, K.; Yamasoba, T.; Kataoka, K. *J. Controlled Release* **2015**, *201*, 41-48.

(13) Li, J. J.; Chen, Q. X.; Zha, Z. S.; Li, H.; Toh, K.; Dirisala, A.; Matsumoto, Y.; Osada, K.; Kataoka, K.; Ge, Z. S. *J. Controlled Release* **2015**, *209*, 77-87.

(14) Okuda, T.; Suzuki, Y.; Kobayashi, Y.; Ishii, T.; Uchida, S.; Itaka, K.; Kataoka, K.; Okamoto, H. *Pharmaceutics* **2015**, *7*, 233-254.

(15) Matsui, A.; Uchida, S.; Ishii, T.; Itaka, K.; Kataoka, K. *Sci. Rep.* **2015**, 10.1038/Srep15810.

(16) Huang, J.; Hastings, C. L.; Duffy, G. P.; Kelly, H. M.; Raeburn, J.; Adams, D. J.; Heise, A. *Biomacromolecules* **2013**, *14*, 200-206.

(17) He, X.; Fan, J. W.; Zhang, F. W.; Li, R. C.; Pollack, K. A.; Raymond, J. E.; Zou, J.; Wooley, K. L. *J. Mater. Chem. B* **2014**, *2*, 8123-8130.

(18) Jeong, Y.; Joo, M. K.; Bahk, K. H.; Choi, Y. Y.; Kim, H. T.; Kim, W. K.; Lee, H. J.; Sohn, Y. S.; Jeong, B. *J. Controlled Release* **2009**, *137*, 25-30.

(19) Park, M. H.; Joo, M. K.; Choi, B. G.; Jeong, B. *Acc. Chem. Res.* **2012**, *45*, 424-433.

(20) Myung, S.; Yin, P. T.; Kim, C.; Park, J.; Solanki, A.; Reyes, P. I.; Lu, Y.; Kim, K. S.; Lee, K.-B. *Adv. Mater.* **2012**, *24*, 6081-6087.

(21) Deming, T. J. *Chem. Rev.* **2016**, *116*, 786-808.

(22) Huang, J.; Heise, A. *Chem. Soc. Rev.* **2013**, *42*, 7373-7390.

(23) Shen, Y.; Fu, X. H.; Fu, W. X.; Li, Z. B. *Chem. Soc. Rev.* **2015**, *44*, 612-622.

(24) Huang, J.; Bonduelle, C.; Thevenot, J.; Lecommandoux, S.; Heise, A. *J. Am. Chem. Soc.* **2012**, *134*, 119-122.

(25) Holowka, E. P.; Sun, V. Z.; Kamei, D. T.; Deming, T. J. *Nature Mater.* **2007**, *6*, 52-57.

(26) Lu, H.; Wang, J.; Bai, Y. G.; Lang, J. W.; Liu, S. Y.; Lin, Y.; Cheng, J. J. *Nat. Commun.* **2011**, 10.1038/ncomms1209.

(27) Zhang, R.; Song, Z.; Yin, L.; Zheng, N.; Tang, H.; Lu, H.; Gabrielson, N. P.; Lin, Y.; Kim, K.; Cheng, J. *WIREs Nanomed. Nanobiotechnol.* **2015**, *7*, 98-110.

(28) Xiong, M.; Lee, M. W.; Mansbach, R. A.; Song, Z.; Bao, Y.; Peek, R. M.; Yao, C.; Chen, L. F.; Ferguson, A. L.; Wong, G. C. L.; Cheng, J. J. *Proc. Natl. Acad. Sci. U. S. A.* **2015**, *112*, 13155-13160.

(29) He, H.; Zheng, N.; Song, Z.; Kim, K. H.; Yao, C.; Zhang, R.; Zhang, C.; Huang, Y.; Uckun, F. M.; Cheng, J.; Zhang, Y.; Yin, L. *ACS Nano* **2016**, *10*, 1859-1870.

(30) Gabrielson, N. P.; Lu, H.; Yin, L. C.; Li, D.; Wang, F.; Cheng, J. J. *Angew. Chem. Int. Ed.* **2012**, *51*, 1143-1147.

(31) Gabrielson, N. P.; Lu, H.; Yin, L. C.; Kim, K. H.; Cheng, J. J. *Mol. Ther.* **2012**, *20*, 1599-1609.

(32) Yin, L. C.; Tang, H. Y.; Kim, K. H.; Zheng, N.; Song, Z. Y.; Gabrielson, N. P.; Lu, H.; Cheng, J. J. *Angew. Chem. Int. Ed.* **2013**, *52*, 9182-9186.

(33) Kricheldorf, H. R. *Angew. Chem. Int. Ed.* **2006**, *45*, 5752-5784.

(34) Hadjichristidis, N.; Iatrou, H.; Pitsikalis, M.; Sakellariou, G. *Chem. Rev.* **2009**, *109*, 5528-5578.

(35) Habraken, G. J. M.; Heise, A.; Thornton, P. D. *Macromol. Rapid Commun.* **2012**, *33*, 272-286.

(36) Paradis-Bas, M.; Tulla-Puche, J.; Albericio, F. *Chem. Soc. Rev.* **2016**, *45*, 631-654.

(37) Leuchs, H. *Ber. Detsch. Chem. Ges.* **1906**, *39*, 857-861.

(38) Leuchs, H.; Manasse, W. *Ber. Detsch. Chem. Ges.* **1907**, *40*, 3235-3249.

(39) Leuchs, H.; Geiger, W. *Ber. Detsch. Chem. Ges.* **1908**, *41*, 1721-1726.

(40) Cheng, J. J.; Deming, T. J. *Top. Curr. Chem.* **2012**, *310*, 1-26.

(41) Zhao, W.; Gnanou, Y.; Hadjichristidis, N. *Polym. Chem.* **2015**, *6*, 6193-6201.

(42) Lu, Y.; Ngo Ndjock Mbong, G.; Liu, P.; Chan, C.; Cai, Z.; Weinrich, D.; Boyle, A. J.; Reilly, R. M.; Winnik, M. A. *Biomacromolecules* **2014**, *15*, 2027-2037.

(43) Wibowo, S. H.; Sulistio, A.; Wong, E. H. H.; Blencowe, A.; Qiao, G. G. *Adv. Funct. Mater.* **2015**, *25*, 3147-3156.

(44) Ulkoski, D.; Meister, A.; Busse, K.; Kressler, J.; Scholz, C. *Colloid Polym. Sci.* **2015**, *293*, 2147-2155.

(45) Wei, Z.; Zhu, S.; Zhao, H. *Polym. Chem.* **2015**, *6*, 1316-1324.

(46) Aliferis, T.; Iatrou, H.; Hadjichristidis, N. *Biomacromolecules* **2004**, *5*, 1653-1656.

(47) Pickel, D. L.; Politakos, N.; Avgeropoulos, A.; Messman, J. M. *Macromolecules* **2009**, *42*, 7781-7788.

(48) Vayaboury, W.; Giani, O.; Cottet, H.; Deratani, A.; Schue, F. *Macromol. Rapid Commun.* **2004**, *25*, 1221-1224.

(49) Habraken, G. J. M.; Wilsens, K. H. R. M.; Koning, C. E.; Heise, A. *Polym. Chem.* **2011**, *2*, 1322-1330.

(50) Deming, T. J. *Nature* **1997**, *390*, 386-389.

(51) Nowak, A. P.; Breedveld, V.; Pakstis, L.; Ozbas, B.; Pine, D. J.; Pochan, D.; Deming, T. J. *Nature* **2002**, *417*, 424-428.

(52) Dimitrov, I.; Schlaad, H. *Chem. Commun.* **2003**, 2944-2945.

(53) Conejos-Sanchez, I.; Duro-Castano, A.; Birke, A.; Barz, M.; Vicent, M. J. *Polym. Chem.* **2013**, *4*, 3182-3186.

(54) Lu, H.; Cheng, J. *J. Am. Chem. Soc.* **2007**, *129*, 14114-14115.

(55) Lu, H.; Cheng, J. *J. Am. Chem. Soc.* **2008**, *130*, 12562-12563.

(56) Stukenkemper, T.; Dose, A.; Caballo Gonzalez, M.; Groenen, A. J. J.; Hehir, S.; Andrés-Guerrero, V.; Herrero Vanrell, R.; Cameron, N. R. *Macromol. Biosci.* **2015**, *15*, 138-145.

(57) Zhao, W.; Gnanou, Y.; Hadjichristidis, N. *Chem. Commun.* **2015**, *51*, 3663-3666.

(58) Zhao, W.; Gnanou, Y.; Hadjichristidis, N. *Biomacromolecules* **2015**, *16*, 1352-1357.

(59) Deming, T. J. *Nature Mater.* **2010**, *9*, 535-536.

(60) Kopecek, J.; Yang, J. *Angew. Chem. Int. Ed.* **2012**, *51*, 7396-7417.

(61) Babu, S. S.; Prasanthkumar, S.; Ajayaghosh, A. *Angew. Chem. Int. Ed.* **2012**, *51*, 1766-1776.

(62) He, X.; Fan, J. W.; Wooley, K. L. *Chem. Asian J.* **2016**, *11*, 437-447.

(63) Hartgerink, J. D.; Beniash, E.; Stupp, S. I. *Science* **2001**, *294*, 1684-1688.

(64) Kim, K. T.; Park, C.; Vandermeulen, G. W. M.; Rider, D. A.; Kim, C.; Winnik, M. A.; Manners, I. *Angew. Chem. Int. Ed.* **2005**, *44*, 7964-7968.

(65) Jeong, Y.; Joo, M. K.; Sohn, Y. S.; Jeong, B. *Adv. Mater.* **2007**, *19*, 3947-3950.

(66) Gibson, M. I.; Cameron, N. R. *Angew. Chem. Int. Ed.* **2008**, *47*, 5160-5162.

(67) Zou, J.; Zhang, F.; Chen, Y.; Raymond, J. E.; Zhang, S.; Fan, J.; Zhu, J.; Li, A.; Seetho, K.; He, X.; Pochan, D. J.; Wooley, K. L. *Soft Matter* **2013**, *9*, 5951-5958.

(68) Kim, E. H.; Joo, M. K.; Bahk, K. H.; Park, M. H.; Chi, B.; Lee, Y. M.; Jeong, B. *Biomacromolecules* **2009**, *10*, 2476-2481.

(69) Choi, Y. Y.; Jang, J. H.; Park, M. H.; Choi, B. G.; Chi, B.; Jeong, B. *J. Mater. Chem.* **2010**, *20*, 3416-3421.

(70) Cheng, Y.; He, C.; Xiao, C.; Ding, J.; Cui, H.; Zhuang, X.; Chen, X. *Biomacromolecules* **2013**, *14*, 468-475.

(71) Zhang, S.; Fu, W.; Li, Z. *Polym. Chem.* **2014**, *5*, 3346-3351.

(72) Choi, Y. Y.; Joo, M. K.; Sohn, Y. S.; Jeong, B. *Soft Matter* **2008**, *4*, 2383-2387.

(73) Hamley, I. W.; Daniel, C.; Mingvanish, W.; Mai, S. M.; Booth, C.; Messe, L.; Ryan, A. J. *Langmuir* **2000**, *16*, 2508-2514.

(74) Liu, D.-L.; Chang, X.; Dong, C.-M. *Chem. Commun.* **2013**, *49*, 1229-1231.

(75) Lalatsa, A.; Schatzlein, A. G.; Mazza, M.; Thi, B. H. L.; Uchegbu, I. F. *J. Controlled Release* **2012**, *161*, 523-536.

(76) Matson, J. B.; Stupp, S. I. *Chem. Commun.* **2012**, *48*, 26-33.

(77) Hernandez, J. R.; Klok, H. A. *J. Polym. Sci., Part A: Polym. Chem.* **2003**, *41*, 1167-1187.

(78) Curtius, T.; Sieber, W. *Ber. Detsch. Chem. Ges.* **1921**, *54*, 1430-1437.

(79) Kramer, J. R.; Deming, T. J. *Biomacromolecules* **2010**, *11*, 3668-3672.

(80) Thunig, D.; Semen, J.; Elias, H. G. *Makromol. Chem.* **1977**, *178*, 603-607.

(81) Poche, D. S.; Moore, M. J.; Bowles, J. L. *Synth. Commun.* **1999**, *29*, 843-854.

(82) Goodman, M.; Hutchiso.J *J. Am. Chem. Soc.* **1965**, *87*, 3524-3525.

(83) Rinaudo, M.; Domard, A. *Biopolymers* **1976**, *15*, 2185-2199.

(84) Ballard, D. G. H.; Bamford, C. H.; Weymouth, F. J. *Proc. R. Soc. London, Ser. A* **1955**, *227*, 155-183.

(85) Ballard, D. G. H.; Bamford, C. H. *Proc. R. Soc. London, Ser. A* **1954**, *223*, 495-520.

(86) Zhang, X. Q.; Li, J. G.; Li, W.; Zhang, A. *Biomacromolecules* **2007**, *8*, 3557-3567.

(87) Liu, A. H.; Ma, R.; Song, C.; Yang, Z. Z.; Yu, A.; Cai, Y.; He, L. N.; Zhao, Y. N.; Yu, B.; Song, Q. W. *Angew. Chem. Int. Ed.* **2012**, *51*, 11306-11310.

(88) Muzart, J. *Tetrahedron* **2009**, *65*, 8313-8323.

(89) Bumcrot, D.; Manoharan, M.; Koteliansky, V.; Sah, D. W. Y. *Nat. Chem. Biol.* **2006**, *2*, 711-719.

(90) Kurreck, J. *Angew. Chem. Int. Ed.* **2009**, *48*, 1378-1398.

(91) Gaynor, J. W.; Campbell, B. J.; Cosstick, R. *Chem. Soc. Rev.* **2010**, *39*, 4169-4184.

(92) Castanotto, D.; Rossi, J. J. *Nature* **2009**, *457*, 426-433.

(93) Davis, M. E.; Zuckerman, J. E.; Choi, C. H. J.; Seligson, D.; Tolcher, A.; Alabi, C. A.; Yen, Y.; Heidel, J. D.; Ribas, A. *Nature* **2010**, *464*, 1067-1070.

(94) Whitehead, K. A.; Langer, R.; Anderson, D. G. *Nat. Rev. Drug Discovery* **2009**, *8*, 129-138.

(95) Gallas, A.; Alexander, C.; Davies, M. C.; Puri, S.; Allen, S. *Chem. Soc. Rev.* **2013**, *42*, 7983-7997.

(96) Miyata, K.; Nishiyama, N.; Kataoka, K. *Chem. Soc. Rev.* **2012**, *41*, 2562-2574.

(97) Song, E. W.; Zhu, P. C.; Lee, S. K.; Chowdhury, D.; Kussman, S.; Dykxhoorn, D. M.; Feng, Y.; Palliser, D.; Weiner, D. B.; Shankar, P.; Marasco, W. A.; Lieberman, J. *Nat. Biotechnol.* **2005**, *23*, 709-717.

(98) Akinc, A.; Zumbuehl, A.; Goldberg, M.; Leshchiner, E. S.; Busini, V.; Hossain, N.; Bacallado, S. A.; Nguyen, D. N.; Fuller, J.; Alvarez, R.; Borodovsky, A.; Borland, T.; Constien, R.; de Fougerolles, A.; Dorkin, J. R.; Jayaprakash, K. N.; Jayaraman, M.; John, M.; Koteliansky, V.; Manoharan, M.; Nechev, L.; Qin, J.; Racie, T.; Raitcheva, D.; Rajeev, K. G.; Sah, D. W. Y.; Soutschek, J.; Toudjarska, I.; Vornlocher, H. P.; Zimmermann, T. S.; Langer, R.; Anderson, D. G. *Nat. Biotechnol.* **2008**, *26*, 561-569.

(99) Zhou, J. H.; Li, H. T.; Li, S.; Zaia, J.; Rossi, J. J. *Mol. Ther.* **2008**, *16*, 1481-1489.

(100) Kusumoto, K.; Akita, H.; Ishitsuka, T.; Matsumoto, Y.; Nomoto, T.; Furukawa, R.; El-Sayed, A.; Hatakeyama, H.; Kajimoto, K.; Yamada, Y.; Kataoka, K.; Harashima, H. *ACS Nano* **2013**, *7*, 7534-7541.

(101) Yan, Y.; Such, G. K.; Johnston, A. P. R.; Best, J. P.; Caruso, F. *ACS Nano* **2012**, *6*, 3663-3669.

(102) Mout, R.; Moyano, D. F.; Rana, S.; Rotello, V. M. *Chem. Soc. Rev.* **2012**, *41*, 2539-2544.

(103) Zhang, F.; Elsabahy, M.; Zhang, S.; Lin, L. Y.; Zou, J.; Wooley, K. L. *Nanoscale* **2013**, *5*, 3220-3225.

(104) Elsabahy, M.; Wooley, K. L. *Chem. Soc. Rev.* **2012**, *41*, 2545-2561.

(105) Kohane, D. S.; Langer, R. *Chem. Sci.* **2010**, *1*, 441-446.

(106) Robin, M. P.; Mabire, A. B.; Damborsky, J. C.; Thom, E. S.; Winzer-Serhan, U. H.; Raymond, J. E.; O'Reilly, R. K. *J. Am. Chem. Soc.* **2013**, *135*, 9518-9524.

(107) Tempelaar, S.; Mespouille, L.; Coulembier, O.; Dubois, P.; Dove, A. P. *Chem. Soc. Rev.* **2013**, *42*, 1312-1336.

(108) Shen, Y.; Zhang, S.; Zhang, F.; Loftis, A.; Pavía-Sanders, A.; Zou, J.; Fan, J.; Taylor, J.-S. A.; Wooley, K. L. *Adv. Mater.* **2013**, *25*, 5609-5614.

(109) Naik, S. S.; Ray, J. G.; Savin, D. A. *Langmuir* **2011**, *27*, 7231-7240.

(110) Zou, J.; Zhang, F.; Zhang, S.; Pollack, S. F.; Elsabahy, M.; Fan, J.; Wooley, K. L. *Adv. Healthcare Mater.* **2014**, *3*, 441-448.

(111) Zhang, F. W.; Zhang, S. Y.; Pollack, S. F.; Li, R. C.; Gonzalez, A. M.; Fan, J. W.; Zou, J.; Leininger, S. E.; Pavia-Sanders, A.; Johnson, R.; Nelson, L. D.; Raymond, J. E.; Elsabahy, M.; Hughes, D. M. P.; Lenox, M. W.; Gustafson, T. P.; Wooley, K. L. *J. Am. Chem. Soc.* **2015**, *137*, 2056-2066.

(112) Dong, H.; Shu, J. Y.; Dube, N.; Ma, Y. F.; Tirrell, M. V.; Downing, K. H.; Xu, T. *J. Am. Chem. Soc.* **2012**, *134*, 11807-11814.

(113) Tang, H. Y.; Li, Y. C.; Lahasky, S. H.; Sheiko, S. S.; Zhang, D. H. *Macromolecules* **2011**, *44*, 1491-1499.

(114) Quadir, M. A.; Martin, M.; Hammond, P. T. *Chem. Mater.* **2013**, *26*, 461-476.

(115) Engler, A. C.; Lee, H. I.; Hammond, P. T. *Angew. Chem. Int. Ed.* **2009**, *48*, 9334-9338.

(116) Huang, Y. G.; Zeng, Y. H.; Yang, J. W.; Zeng, Z. H.; Zhu, F. M.; Chen, X. D. *Chem. Commun.* **2011**, *47*, 7509-7511.

(117) Obeid, R.; Armstrong, T.; Peng, X.; Busse, K.; Kressler, J.; Scholz, C. *J. Polym. Sci., Part A: Polym. Chem.* **2014**, *52*, 248-257.

(118) Dominguez, A.; Fernandez, A.; Gonzalez, N.; Iglesias, E.; Montenegro, L. *J. Chem. Educ.* **1997**, *74*, 1227-1231.

(119) Xi, W.; Scott, T. F.; Kloxin, C. J.; Bowman, C. N. *Adv. Funct. Mater.* **2014**, *24*, 2572-2590.

(120) Kuo, S. W.; Lee, H. F.; Huang, W. J.; Jeong, K. U.; Chang, F. C. *Macromolecules* **2009**, *42*, 1619-1626.

(121) Greenfield, N. J.; Fasman, G. D. *Biochemistry* **1969**, *8*, 4108-4116.

(122) Verduzco, R.; Li, X. Y.; Peseka, S. L.; Steinc, G. E. *Chem. Soc. Rev.* **2015**, *44*, 2405-2420.

(123) Li, W.; Zhang, X. Q.; Wang, J.; Qiao, X.; Liu, K.; Zhang, A. *J. Polym. Sci., Part A: Polym. Chem.* **2012**, *50*, 4063-4072.

(124) Sun, G. R.; Cho, S. H.; Clark, C.; Verkhoturov, S. V.; Eller, M. J.; Li, A.; Pavia-Jimenez, A.; Schweikert, E. A.; Thackeray, J. W.; Trefonas, P.; Wooley, K. L. *J. Am. Chem. Soc.* **2013**, *135*, 4203-4206.

(125) Lu, X. G.; Tran, T. H.; Jia, F.; Tan, X. Y.; Davis, S.; Krishnan, S.; Amiji, M. M.; Zhang, K. *J. Am. Chem. Soc.* **2015**, *137*, 12466-12469.

(126) Parelkar, S. S.; Chan-Seng, D.; Emrick, T. *Biomaterials* **2011**, *32*, 2432-2444.

(127) Blum, A. P.; Kammeyer, J. K.; Yin, J.; Crystal, D. T.; Rush, A. M.; Gilson, M. K.; Gianneschi, N. C. *J. Am. Chem. Soc.* **2014**, *136*, 15422-15437.

(128) Blum, A. P.; Kammeyer, J. K.; Gianneschi, N. C. *Chem. Sci.* **2016**, *7*, 989-994.

(129) Hadjichristidis, N.; Iatrou, H.; Pitsikalis, M.; Mays, J. *Prog. Polym. Sci.* **2006**, *31*, 1068-1132.

(130) Peleshanko, S.; Tsukruk, V. V. *Prog. Polym. Sci.* **2008**, *33*, 523-580.

(131) Zhang, B.; Fischer, K.; Schmidt, M. *Macromol. Chem. Phys.* **2005**, *206*, 157-162.

(132) Lu, H.; Wang, J.; Lin, Y.; Cheng, J. J. *J. Am. Chem. Soc.* **2009**, *131*, 13582-13583.

(133) Zhang, Y. F.; Yin, Q.; Lu, H.; Xia, H. W.; Lin, Y.; Cheng, J. J. *ACS Macro Lett.* **2013**, *2*, 809-813.

(134) Wang, J.; Lu, H.; Kamat, R.; Pingali, S. V.; Urban, V. S.; Cheng, J. J.; Lin, Y. *J. Am. Chem. Soc.* **2011**, *133*, 12906-12909.

(135) Wang, J.; Lu, H.; Ren, Y.; Zhang, Y. F.; Morton, M.; Cheng, J. J.; Lin, Y. *Macromolecules* **2011**, *44*, 8699-8708.

(136) Liu, Y.; Chen, P.; Li, Z. B. *Macromol. Rapid Commun.* **2012**, *33*, 287-295.

(137) Engler, A. C.; Bonner, D. K.; Buss, H. G.; Cheung, E. Y.; Hammond, P. T. *Soft Matter* **2011**, *7*, 5627-5637.

(138) Rhodes, A. J.; Deming, T. J. *ACS Macro Lett.* **2013**, *2*, 351-354.

(139) Rhodes, A. J.; Deming, T. J. *J. Am. Chem. Soc.* **2012**, *134*, 19463-19467.

(140) Li, Z.; Ma, J.; Lee, N. S.; Wooley, K. L. *J. Am. Chem. Soc.* **2011**, *133*, 1228-1231.

(141) Habraken, G. J. M.; Peeters, M.; Dietz, C. H. J. T.; Koning, C. E.; Heise, A. *Polym. Chem.* **2010**, *1*, 514-524.

(142) Compain, P. *Adv. Synth. Catal.* **2007**, *349*, 1829-1846.

(143) Bielawski, C. W.; Grubbs, R. H. *Prog. Polym. Sci.* **2007**, *32*, 1-29.

(144) Csihony, S.; Fischmeister, C.; Bruneau, C.; Horvath, I. T.; Dixneuf, P. H. *New J. Chem.* **2002**, *26*, 1667-1670.

(145) Vygodskii, Y. S.; Shaplov, A. S.; Lozinskaya, E. I.; Filippov, O. A.; Shubina, E. S.; Bandari, R.; Buchmeiser, M. R. *Macromolecules* **2006**, *39*, 7821-7830.

(146) Trnka, T. M.; Morgan, J. P.; Sanford, M. S.; Wilhelm, T. E.; Scholl, M.; Choi, T. L.; Ding, S.; Day, M. W.; Grubbs, R. H. *J. Am. Chem. Soc.* **2003**, *125*, 2546-2558.

(147) Nakanishi, M.; Park, J. S.; Jang, W. D.; Oba, M.; Kataoka, K. *React. Funct. Polym.* **2007**, *67*, 1361-1372.

(148) Uchida, H.; Itaka, K.; Nomoto, T.; Ishii, T.; Suma, T.; Ikegami, M.; Miyata, K.; Oba, M.; Nishiyama, N.; Kataoka, K. *J. Am. Chem. Soc.* **2014**, *136*, 12396-12405.

(149) Grigoryev, A.; Sa, V.; Gopishetty, V.; Tokarev, I.; Kornev, K. G.; Minko, S. *Adv. Funct. Mater.* **2013**, *23*, 5903-5909.

(150) Randolph, L. M.; Chien, M. P.; Gianneschi, N. C. *Chem. Sci.* **2012**, *3*, 1363-1380.

(151) Carretti, E.; Bonini, M.; Dei, L.; Berrie, B. H.; Angelova, L. V.; Baglioni, P.; Weiss, R. G. *Acc. Chem. Res.* **2010**, *43*, 751-760.

(152) Du, J. Z.; O'Reilly, R. K. *Soft Matter* **2009**, *5*, 3544-3561.

(153) Stuart, M. A. C.; Huck, W. T. S.; Genzer, J.; Muller, M.; Ober, C.; Stamm, M.; Sukhorukov, G. B.; Szleifer, I.; Tsukruk, V. V.; Urban, M.; Winnik, F.; Zauscher, S.; Luzinov, I.; Minko, S. *Nature Mater.* **2010**, *9*, 101-113.

(154) Capadona, J. R.; Shanmuganathan, K.; Tyler, D. J.; Rowan, S. J.; Weder, C. *Science* **2008**, *319*, 1370-1374.

(155) Capito, R. M.; Azevedo, H. S.; Velichko, Y. S.; Mata, A.; Stupp, S. I. *Science* **2008**, *319*, 1812-1816.

(156) Goodwin, A. P.; Mynar, J. L.; Ma, Y. Z.; Fleming, G. R.; Frechet, J. M. J. *J. Am. Chem. Soc.* **2005**, *127*, 9952-9953.

(157) Haines, L. A.; Rajagopal, K.; Ozbas, B.; Salick, D. A.; Pochan, D. J.; Schneider, J. P. *J. Am. Chem. Soc.* **2005**, *127*, 17025-17029.

(158) Liu, X. K.; Jiang, M. *Angew. Chem. Int. Ed.* **2006**, *45*, 3846-3850.

(159) Jiang, Y.; Zeng, F.; Gong, R.; Guo, Z.; Chen, C.-F.; Wan, X. *Soft Matter* **2013**, *9*, 7538-7544.

(160) Pester, C. W.; Konradi, A.; Varnholt, B.; van Rijn, P.; Boker, A. *Adv. Funct. Mater.* **2012**, *22*, 1724-1731.

(161) Zou, J.; Zhang, S. Y.; Shrestha, R.; Seetho, K.; Donley, C. L.; Wooley, K. L. *Polym. Chem.* **2012**, *3*, 3146-3156.

(162) Du, J. Z.; Armes, S. P. *J. Am. Chem. Soc.* **2005**, *127*, 12800-12801.

(163) Gensel, J.; Dewald, I.; Erath, J.; Betthausen, E.; Muller, A. H. E.; Fery, A. *Chem. Sci.* **2013**, *4*, 325-334.

(164) Borase, T.; Ninjbadgar, T.; Kapetanakis, A.; Roche, S.; O'Connor, R.; Kerskens, C.; Heise, A.; Brougham, D. F. *Angew. Chem. Int. Ed.* **2013**, *52*, 3164-3167.

(165) Kramer, J. R.; Deming, T. J. *J. Am. Chem. Soc.* **2012**, *134*, 4112-4115.

(166) Cravotto, G.; Cintas, P. *Chem. Soc. Rev.* **2009**, *38*, 2684-2697.

(167) Naota, T.; Koori, H. *J. Am. Chem. Soc.* **2005**, *127*, 9324-9325.

(168) Isozaki, K.; Takaya, H.; Naota, T. *Angew. Chem. Int. Ed.* **2007**, *46*, 2855-2857.

(169) Wu, J. C.; Yi, T.; Shu, T. M.; Yu, M. X.; Zhou, Z. G.; Xu, M.; Zhou, Y. F.; Zhang, H. J.; Han, J. T.; Li, F. Y.; Huang, C. H. *Angew. Chem. Int. Ed.* **2008**, *47*, 1063-1067.

(170) Afrasiabi, R.; Kraatz, H. B. *Chem. Eur. J.* **2013**, *19*, 1769-1777.

(171) Paulusse, J. M. J.; van Beek, D. J. M.; Sijbesma, R. P. *J. Am. Chem. Soc.* **2007**, *129*, 2392-2397.

(172) Yu, X. D.; Liu, Q. A.; Wu, J. C.; Zhang, M. M.; Cao, X. H.; Zhang, S.; Wang, Q.; Chen, L. M.; Yi, T. *Chem. Eur. J.* **2010**, *16*, 9099-9106.

(173) Wang, X. Q.; Kluge, J. A.; Leisk, G. G.; Kaplan, D. L. *Biomaterials* **2008**, *29*, 1054-1064.

(174) Liu, Z. X.; Feng, Y.; Yan, Z. C.; He, Y. M.; Liu, C. Y.; Fan, Q. H. *Chem. Mater.* **2012**, *24*, 3751-3757.

(175) Chen, Y.; Pang, X. H.; Dong, C. M. *Adv. Funct. Mater.* **2010**, *20*, 579-586.

(176) Tang, H. Y.; Lee, C. U.; Zhang, D. H. *J. Polym. Sci., Part A: Polym. Chem.* **2011**, *49*, 3228-3238.

(177) Kotharangannagari, V. K.; Sanchez-Ferrer, A.; Ruokolainen, J.; Mezzenga, R. *Macromolecules* **2012**, *45*, 1982-1990.

(178) Wamsley, A.; Jasti, B.; Phiasivongsa, P.; Li, X. L. *J. Polym. Sci., Part A: Polym. Chem.* **2004**, *42*, 317-325.

(179) Hayashi, S.; Ohkawa, K.; Yamamoto, H. *Macromol. Biosci.* **2006**, *6*, 228-240.

(180) Yu, L.; Zhang, H.; Ding, J. D. *Angew. Chem. Int. Ed.* **2006**, *45*, 2232-2235.

(181) Aggeli, A.; Bell, M.; Boden, N.; Keen, J. N.; Knowles, P. F.; McLeish, T. C. B.; Pitkeathly, M.; Radford, S. E. *Nature* **1997**, *386*, 259-262.

(182) Miyazawa, T.; Blout, E. R. *J. Am. Chem. Soc.* **1961**, *83*, 712-719.

(183) Kauppinen, J. K.; Moffatt, D. J.; Mantsch, H. H.; Cameron, D. G. *Anal. Chem.* **1981**, *53*, 1454-1457.

(184) Kauppinen, J. K.; Moffatt, D. J.; Mantsch, H. H.; Cameron, D. G. *Appl. Spectrosc.* **1981**, *35*, 271-276.

(185) Panitch, A.; Matsuki, K.; Cantor, E. J.; Cooper, S. J.; Atkins, E. D. T.; Fournier, M. J.; Mason, T. L.; Tirrell, D. A. *Macromolecules* **1997**, *30*, 42-49.

(186) Rosler, A.; Klok, H. A.; Hamley, I. W.; Castelletto, V.; Mykhaylyk, O. O. *Biomacromolecules* **2003**, *4*, 859-863.

(187) Blake, C.; Serpell, L. *Structure* **1996**, *4*, 989-998.

(188) Adamcik, J.; Mezzenga, R. *Macromolecules* **2012**, *45*, 1137-1150.

(189) Liu, D.; Wang, D.; Wang, M.; Zheng, Y.; Koynov, K.; Auernhammer, G. K.; Butt, H.-J.; Ikeda, T. *Macromolecules* **2013**, *46*, 4617-4625.

(190) Phadke, A.; Zhang, C.; Arman, B.; Hsu, C. C.; Mashelkar, R. A.; Lele, A. K.; Tauber, M. J.; Arya, G.; Varghese, S. *Proc. Natl. Acad. Sci. U. S. A.* **2012**, *109*, 4383-4388.

(191) Silverstein, F. E.; Faich, G.; Goldstein, J. L.; Simon, L. S.; Pincus, T.; Whelton, A.; Makuch, R.; Eisen, G.; Agarwal, N. M.; Stenson, W. F.; Burr, A. M.; Zhao, W. W.; Kent, J. D.; Lefkowith, J. B.; Verburg, K. M.; Geis, G. S. *J. Am. Med. Assoc.* **2000**, *284*, 1247-1255.

(192) Bresalier, R. S.; Sandler, R. S.; Quan, H.; Bolognese, J. A.; Oxenius, B.; Horgan, K.; Lines, C.; Riddell, R.; Morton, D.; Lanas, A.; Konstam, M. A.; Baron, J. A.; Investigators, A. T. *N. Engl. J. Med.* **2005**, *352*, 1092-1102.

(193) Li, J. Y.; Kuang, Y.; Gao, Y.; Du, X. W.; Shi, J. F.; Xu, B. *J. Am. Chem. Soc.* **2013**, *135*, 542-545.

(194) Majumder, J.; Das, M. R.; Deb, J.; Jana, S. S.; Dastidar, P. *Langmuir* **2013**, *29*, 10254-10263.

(195) Bhuniya, S.; Seo, Y. J.; Kim, B. H. *Tetrahedron Lett.* **2006**, *47*, 7153-7156.

(196) Cao, W.; Zhang, X. L.; Miao, X. M.; Yang, Z. M.; Xu, H. P. *Angew. Chem. Int. Ed.* **2013**, *52*, 6233-6237.

(197) Estroff, L. A.; Hamilton, A. D. *Chem. Rev.* **2004**, *104*, 1201-1217.

(198) Kiyonaka, S.; Sugiyasu, K.; Shinkai, S.; Hamachi, I. *J. Am. Chem. Soc.* **2002**, *124*, 10954-10955.

(199) Kharkar, P. M.; Kiick, K. L.; Kloxin, A. M. *Chem. Soc. Rev.* **2013**, *42*, 7335-7372.

(200) Appel, E. A.; del Barrio, J.; Loh, X. J.; Scherman, O. A. *Chem. Soc. Rev.* **2012**, *41*, 6195-6214.

(201) Greenfield, N. J. *Nat. Protoc.* **2006**, *1*, 2876-2890.